SUGGESTION OF A NEW MODEL FOR NEWTONIAN THERMAL ANALYSIS OF
SOLIDIFICATION

A THESIS SUBMITTED TO
THE GRADUATE SCHOOL OF NATURAL AND APPLIED SCIENCES
OF
MIDDLE EAST TECHNICAL UNIVERSITY

BY

KADİR CAN ERBAŞ

IN PARTIAL FULFILLMENT OF THE REQUIREMENTS
FOR
THE DEGREE OF DOCTOR OF PHILOSOPHY
IN
PHYSICS

DECEMBER 2013

Approval of the thesis:

SUGGESTION OF A NEW MODEL FOR NEWTONIAN THERMAL ANALYSIS OF SOLIDIFICATION

submitted by **KADİR CAN ERBAŞ** in partial fulfillment of the requirements for the degree of **Doctor of Philosophy in Physics Department, Middle East Technical University** by,

Prof. Dr. Canan Özgen
Dean, Graduate School of **Natural and Applied Sciences**   ——————————

Prof. Dr. Mehmet T. Zeyrek
Head of Department, **Physics**   ——————————

Prof. Dr. Ayşe Karasu
Supervisor, **Physics Department, METU**   ——————————

Examining Committee Members:

Prof. Dr. Şinasi Ellialtıoğlu
Basic Sciences Unit, TEDU   ——————————

Prof. Dr. Ayşe Karasu
Physics Department, METU   ——————————

Prof. Dr. Rıza Gürbüz
Metallurgical and Materials Engineering Department, METU   ——————————

Prof. Dr. Mehmet Parlak
Physics Department, METU   ——————————

Prof. Dr. Tamer Özdemir
Metallurgical and Materials Engineering Department, Gazi University   ——————————

Date: ——————————

I hereby declare that all information in this document has been obtained and presented in accordance with academic rules and ethical conduct. I also declare that, as required by these rules and conduct, I have fully cited and referenced all material and results that are not original to this work.

Name, Last Name: KADİR CAN ERBAŞ

Signature   :

ABSTRACT

SUGGESTION OF A NEW MODEL FOR NEWTONIAN THERMAL ANALYSIS OF
SOLIDIFICATION

Erbaş, Kadir Can
Ph.D., Department of Physics
Supervisor : Prof. Dr. Ayşe Karasu

December 2013, 109 pages

Newtonian thermal analysis (NTA) of solidification is a widely used tool to understand the solidification kinetics of metals. It depends on cooling curve analysis by using heat equations especially Newton's law of cooling. Calculation of the latent heat of solidification and solid fraction evolution are one of the primary goals of NTA. Several mathematical models have been proposed in the literature for this purpose. However, there are many discussions on the reliability of these models.

In this study, latent heats of pure metals, which are calculated from several models, were compared with their literal values. These methods from the literature include Newtonian baseline (NBL), dynamic baseline (DBL), and logarithmic relative temperature baseline (LRTBL), which produced unreliable results for the latent heat values of four types of pure metals (aluminum, lead, tin, and zinc).

The most significant restrictions of NTA were determined as the effect of mold's thermal capacity and variations in the data analysis process. A new model, which was named "two-capacitive system baseline (TCSBL)", was developed in order to take thermal capacity of the mold into account. This model also includes the radiative contributions and other temperature dependent effects by considering Taylor expansion approach. At the end of the application of the model to several experiments, it was seen that TCSBL is the most reliable model among other models in the literature.

Keywords: Thermal analysis, latent heat, solid fraction

ÖZ

KATILAŞMANIN NEWTONSAL ISI ANALİZİ İÇİN YENİ BİR MODEL ÖNERİSİ

Erbaş, Kadir Can
Doktora., Fizik Bölümü
Tez Yöneticisi : Prof. Dr. Ayşe Karasu

Aralık 2013, 109 sayfa

Metal dökümlerinde Newton termal analizi (NTA), metalin katılaşma kinetiklerini anlamak adına, çok sık kullanılan bir araçtır. Özellikle Newton soğuma yasası olmak üzere, ısı denklemlerini kullanarak soğuma eğrisi analizine dayanır. Katılaşma ısısının ve katı kesrin hesaplanması NTA nin en öncelikli hedeflerinden biridir. Bunu yapmak için, literatürde çeşitli matematiksel modeller önerilmiştir. Fakat bu modellerin güvenilirliği hala tartışılmaktadır

Bu çalışmada, çeşitli modellerden hesaplanan saf metallerin katılaşma ısıları literatürdeki değerleriyle kıyaslandı. Bu modeller, 4 tip metalin (alüminyum, kurşun, kalay, çinko) katılaşma ısıları için tutarsız sonuçlar üreten Newton taban eğrisi (NTE), dinamik taban eğrisi (DTE) ve logaritmik bağıl sıcaklık taban eğrisi (LBSTE) dir.

NTA nin en önemli kısıtlamaları kabın ısı kapasitesinin etkisi ve veri analizi sürecindeki varyasyonlar olarak tespit edildi. Kabın termal kapasitesini hesaba katabilmek için, ikili kapasitif sistem taban eğrisi (İKSTE) adı verilen yeni bir model geliştirildi. Bu model radiyatif katkıları ve diğer sıcaklığa bağlı etkileri de Taylor açılımı yaklaşımı kullanarak dâhil etti. Bu modelin çeşitli deneylere uygulanması sonrasında, İKSTE nin literatürdeki diğer modeller arasında en güvenilir model olduğu görüldü.

Anahtar Kelimeler: Termal analiz, erime ısısı, katı kesri

To my family

ACKNOWLEDGMENTS

TABLE OF CONTENTS

LIST OF TABLES

TABLES

LIST OF FIGURES

FIGURES

CHAPTER 1

INTRODUCTION

Thermal analysis searches the thermal properties of a material while its temperature or phase is changing. In metallurgical sciences, it especially provides information about the evolution of solid fraction and thermal characteristics of the material, such as melting temperature, latent heat release, specific heat, thermal diffusivity, and heat transfer coefficient between the material and surrounding media.

1. 1 General Information about Heat Transfer

Applications of thermal analysis for metal casting are based on the examination of the cooling curve. When a material is heated to a higher temperature than its melting point, it begins to lose its heat energy through three different ways: conduction, convection, and radiation.

Conduction is simply the transfer of heat energy through the interaction of particles. It flows from the more energetic particles to the less energetic ones [1]. The heat transfer rate or heat flux per unit area in one-dimension is given by:

$$q = -\frac{\dot{Q}}{A} = -k\frac{dT}{dx} \tag{1.1}$$

where q is heat flux per unit area, $\dot{Q}$ is the total rate of heat flowing through the surface, A is the area of the surface, k is thermal conductivity, and dT/dx is the temperature gradient [1]. The negative sign corresponds to the tendency of heat transfer which flows from the hot to the cold region. In a three-dimensional case, the heat may flow through three dimensions. Then the equation becomes:

$$q = -\frac{d\dot{Q}}{dA} = -k\vec{\nabla}T.\hat{n} \tag{1.2}$$

where ∇ is the gradient operator. For a certain closed surface, the net heat flux of the body can be calculated by a surface integral. With the use of Green's theorem, it gives:

$$\dot{Q} = \oint_S k\vec{\nabla}T \cdot d\vec{A} = \int_V \vec{\nabla} \cdot (k\vec{\nabla}T)dV \tag{1.3}$$

The net heat flux of this portion of the body, enclosed by the closed surface S, is the total heat change of volume V. Therefore, the term $\dot{Q}$ corresponds to the rate of change in heat energy in terms of density (ρ) and specific heat (c_p), so it is given by:

$$\dot{Q} = \int_V \rho c_p \frac{\partial T}{\partial t}dV \tag{1.4}$$

Combining Equations 1.3 and 1.4, it yields

$$\frac{\partial T}{\partial t} = \alpha\nabla^2 T \tag{1.5}$$

where α is the diffusivity ($\alpha = k/\rho c_p$) of the material. Equation 1.5 is known as Fourier heat conduction equation without a heat source in three dimensions. It is widely used by researchers to make thermal analysis of a casting process in the name of Fourier thermal analysis (FTA).

Another heat transfer phenomena is seen when a body is exposed to a fluid whose temperature is different from that of the body. This type of heat transfer is called *convection*. If surface temperature of the body is T_s, and temperature of the fluid is T_∞, then total heat flux through the surface is given by

$$q = -\dot{Q} = hA(T_s - T_\infty) \tag{1.6}$$

where h is overall convective heat transfer coefficient, and A is the total surface area of the body. Fourier's law also gives the total heat flux per unit area through the solid-fluid interface, e.g., hot metal surface in air. Equation 1.7 is a boundary condition for the Fourier heat conduction equation [2].

$$q = -k\vec{\nabla}T \cdot \hat{n}\Big|_{surface} = h(T_s - T_\infty) \tag{1.7}$$

Radiation, unlike conduction and convection, is another heat transfer process which transports the heat energy by electromagnetic waves, so it can occur in the vacuum. An ideal thermal radiator emits heat rate proportional to the fourth power of its absolute

2

temperature. Such a body is called a blackbody. The radiative heat rate transferred from the body is given by

$$q = \sigma A T^4$$

(1.8)

where σ is Stephan-Boltzman constant whose value is 5.67×10^{-8} Wm^{-2}K^{-4}, A is the surface area and T is the absolute temperature of the body [3]. In a special case, if a small grey body with temperature T is surrounded by a large isothermal surface whose temperature is T_{sur}, the net rate of radiation heat transfer is:

$$q_{rad} = \sigma \varepsilon A \left(T^4 - T_{sur}^4 \right)$$

(1.9)

where ε is the emissivity of the object with the values varying from zero to unity [1]. Radiative cooling may be neglected in comparison with convectional cooling in low temperature ranges. Its complicated mathematical formulation prevents frequent use in thermal analysis researches.

The energy of metal with respect to a reference point is named as *enthalpy*. The enthalpy of a metal increases with increasing temperature. However, there is a sudden change in enthalpy when a transformation process occurs. The jump in the enthalpy at the melting temperature is called the latent heat of solidification. In contrast to pure metals, alloys solidify in a temperature interval rather than in a specific temperature [3]. Latent heat of fusion (L_f) is the energy required to melt or solidify unit mass of a material, with the unit of J/kg in SI [4]. If the total phase transformation energy is represented by ΔH, the relationship will be:

$$\Delta H = m L_f$$

(1.10)

where m is the mass of the substance. Evolution of the phase transformational source term in time may be expressed in terms of solid fraction (f_s). Solid fraction is a percentage measure of how much of a metal is solid. It is denoted by f_s, and its value is zero for liquid phase but unity for the solid phase. The value of solid fraction changes in time, from zero to one, while the melt is solidifying [5]. For a typical cooling session, solid fraction can be linearly defined by

$$f_s(t) = \begin{cases} 0, & 0 < t < t_s \\ \dfrac{t - t_s}{t_e - t_s}, & t_s \leq t \leq t_e \\ 1, & t_e < t \end{cases}$$

(1.11)

where t_s and t_e are the start and end times of solidification. During the solidification process, there must be a heat source term in terms of rate of heat due to the phase transformation. Total energy released per unit time by the phase transformation in a material with mass m and latent heat L_f is given by

$$\dot{Q}_{PT} = mL_f \frac{df_s}{dt} \qquad (1.12)$$

If any phase transformation occurs in a given material, the heat equations must be rewritten by regarding the energy source term.

$$\dot{Q}_{net} = \dot{Q}_{loss} + \dot{Q}_{PT} \qquad (1.13)$$

where the $\dot{Q}_{net}$ and $\dot{Q}_{loss}$ terms mean the net rate of heat of a given volume and rate of heat lost by heat transfer. For a unit volume in a substance, the Fourier equation can be rewritten as

$$\rho c_p \frac{\partial T}{\partial t} = k\nabla^2 T + \rho L_f \frac{\partial f_s}{\partial t} \qquad (1.14)$$

When the conductivity of the material is high, the temperature distribution in it may be taken as homogeneous. In this case, the spatial dependence of the temperature may be neglected so that the surface temperature is assumed to spread uniformly throughout the material. Equation 1.6 becomes an expression for the evolution of this uniform temperature in time.

$$\dot{Q} = V\rho c_p \frac{dT}{dt} = -hA(T - T_\infty) \qquad (1.15)$$

This equation is called Newton's law of cooling where T is the uniformly distributed instantaneous temperature, which is a function of time. Not only high thermal conductivity, but also small Biot number is required for the validity of the approximation. Biot number is defined by

$$Bi = \frac{h}{k} L_c << 0.1 \qquad (1.16)$$

where Bi is Biot number, h is convective heat transfer coefficient, k is the conductivity of material, and L_c is the characteristic length, defined by the ratio of the volume to the surface area. If the condition in Equation 1.16 is satisfied, lumped heat capacity model, which assumes uniform temperature distribution, is applicable for the thermal setup [6].

1. 2 Newtonian Thermal Analysis for Casting

Thermal analysis is a group of techniques in which thermal properties of a material is investigated. It is usually divided into three categories: Computer aided cooling curve analysis (CA-CCA), differential scanning calorimetry (DSC), and differential thermal analysis (DTA). CA-CCA techniques depend on analyzing temperature or cooling rate curves with complicated mathematical tools [7]. It involves Newtonian and Fourier thermal analyses according to the thermal gradient. Differential thermal analysis measures the temperature difference between a sample and reference material in an identical heat treatment [8]. Differential scanning calorimetry uses the same principle, but it differs from DTA in that DSC includes a source of heat to balance the temperatures of both sample and reference [9]. Newtonian thermal analysis (NTA) is widely used in the literature, and it is the main interest of this study.

In Newtonian thermal analysis of a casting process, one thermocouple (TC) measures the temperature of the metal at every second, and then the cooling curve is plotted. These cooling data show various information about metal characteristics, such as melting point, the solidification time, undercooling point, latent heat release, and heat transfer coefficient. In a typical Newtonian thermal analysis experiment, one thermocouple (TC) is connected to a thermal scanner (data logger), and then its temperature readings are recorded by a computer in order to measure the temperature of the metal at every second. (Figure 1.1) The output of thermocouple consists of two data column; one is time the other is temperature (Table 1.1). After the data is recorded, the corresponding temperature vs. time graph can be plotted as in Figure 1.2.
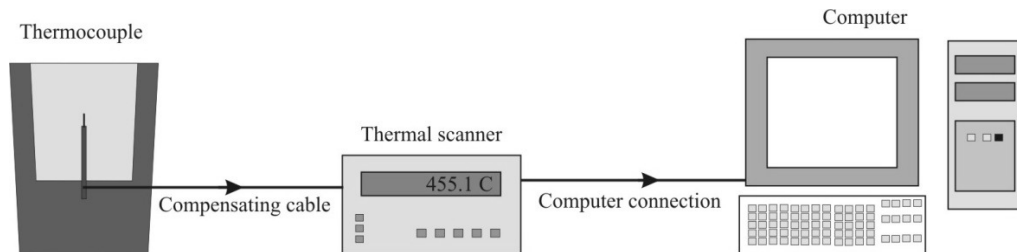
Figure 1.1 : Experimental setup of the Newtonian thermal analysis.

Table 1.1: Sample data for the Newtonian thermal analysis.

Newtonian Analysis	
Time (sec.)	Temperature (C)
1	377.3
2	375.8
3	375.8
4	374.3
5	374.3
6	373.0
7	373.0
8	371.8
9	371.8
⋮	⋮
⋮	⋮
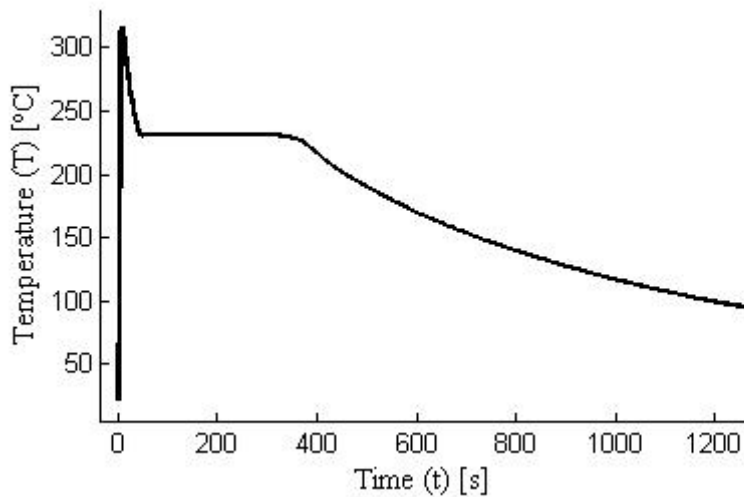
Figure 1.2. Temperature vs. time graph of a pure metal.

For a pure metal, temperature remains constant at the melting temperature during solidification. Some characteristics, such as melting point (T_m), solidification start time (t_s), end time (t_e), and undercooling point can be read from the cooling curve. In the cooling graph, solidification starts when the temperature falls below the melting point. After several steps, such as nucleation, free growth, and impingement; solidification ends when the concavity of the curve has changed. The end of solidification is detected by the help of the derivative of temperature with respect to time. The inflection point in

Figure1.2 (t_e) corresponds to the point where the second derivative is zero, or the first derivative is a local minimum [11, 37].
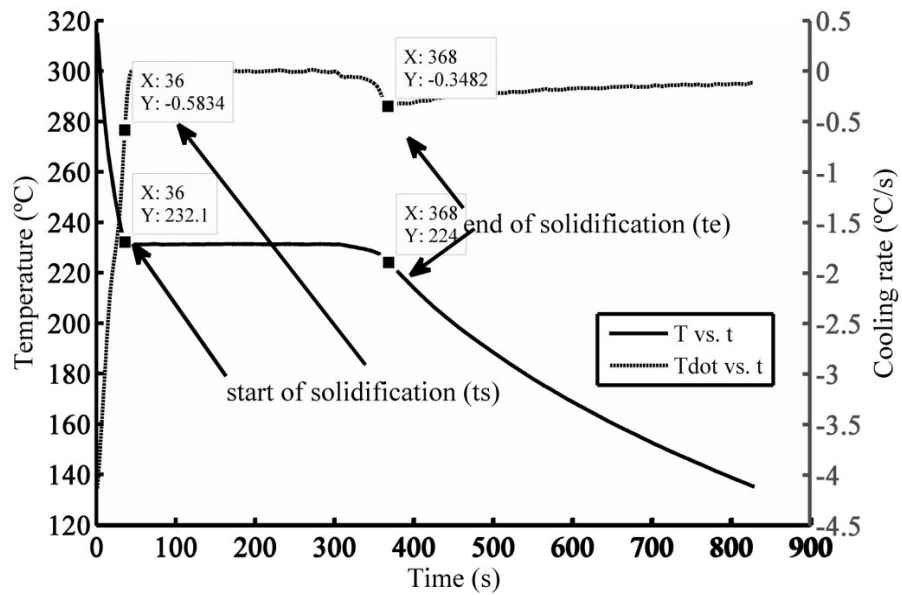
Figure 1.3: Cooling and cooling rate graphs of pure tin. Solidification starts at t=36 s and ends at t=368 s.

The boundary times of solidification, start time (t_s) and end time (t_e), are determined by analyzing Figure 1.3 with respect to the concavity of the curve. It is seen that the temperature curve reaches the arrest point at t=36 second while the dT/dt curve makes a local minimum at t=368 second. It means that start and end time of solidification are 36 and 368 seconds respectively, so the phase transformation process develops between this interval. Time derivative of temperature vs. temperature graph may be useful to find a relation between temperature and heat flux. It is shown in Figure 1.4.
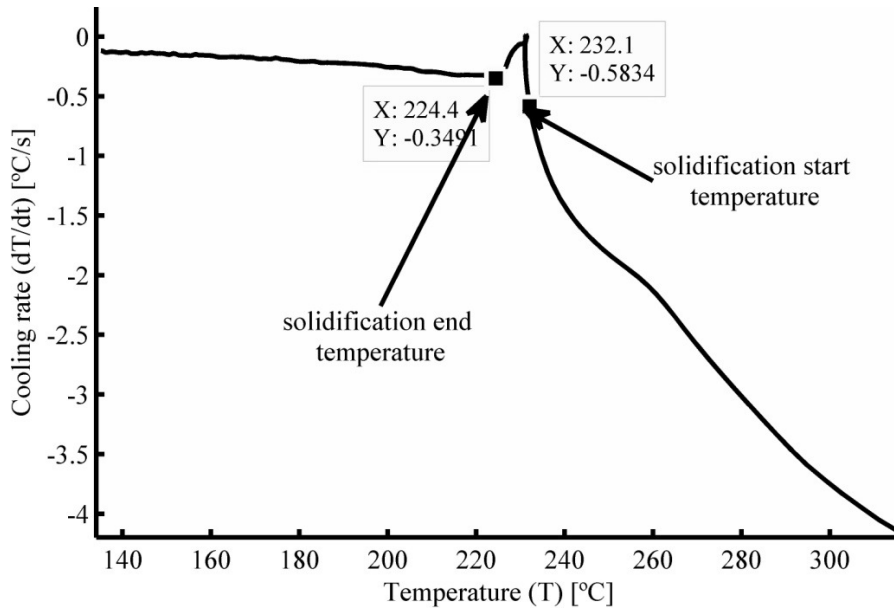
Figure 1.4: Cooling rate vs. temperature graph of Pure Tin.

The main equation used in NTA is Equation 1.15. With the phase transformational source term, it gives:

$$\dot{Q}(t) = V\rho c_p \frac{dT(t)}{dt} = -hA(T(t) - T_\infty) + V\rho L_f \frac{df_s(t)}{dt}$$

(1.17)

The temperature rate can be written for solidification and no-solidification intervals with the initial conditions of solid fraction.

$$\frac{dT}{dt} = \begin{cases} -\dfrac{hA}{V\rho c_p}(T - T_\infty) + \dfrac{L_f}{c_p}\dfrac{df_s}{dt}, & t_s \le t \le t_e \\ -\dfrac{hA}{V\rho c_p}(T - T_\infty) & otherwise \end{cases}$$

(1.18)

$$f_s(t_s) = 0 \quad and \quad f_s(t_e) = 1$$

(1.19)

The solution of temperature for no-phase transformation region (Equation 1.20) is shown in Equation 1.21. The solution for time derivative of temperature is Equation 1.22.

$$\frac{dT}{dt} = -\frac{hA}{V\rho c_p}(T - T_\infty)$$

(1.20)

8

$$T = (T_0 - T_\infty) exp\left(-\frac{hA}{V\rho c_p}t\right) + T_{\infty_s} \qquad (1.21)$$

$$\frac{dT}{dt} = -\frac{hA}{V\rho c_p}(T_0 - T_\infty) exp\left(-\frac{hA}{V\rho c_p}t\right) \qquad (1.22)$$

1. 3 Calculations of NTA for the Latent Heat and Solid Fraction in the Literature

In thermal analysis methods, CCA techniques use a reference state or a comparison line, which is called the *baseline* or *zero curve*. It overlaps the temperature derivative curve in the single-phase region, and then goes a different path through the solidification region. The zero curve or baseline can be linear or polynomial [12]. Newton law of cooling with the assumption of no phase transformation has a solution for temperature rate in terms of time as in Equation 1.23. The solution is called Newtonian zero curve or Newtonian baseline (NBL) in thermal analysis terminology.

Linear Newtonian zero curve has the form of

$$\left(\frac{dT}{dt}\right)_{zc} = ae^{-bt} \qquad (1.23)$$

where a and b are the parameters that may be calculated experimentally. Their expressions are:

$$b = \frac{hA}{V\rho c_p}, \qquad a = -(T_0 - T_\infty)\frac{hA}{V\rho c_p} \qquad (1.24)$$

Experimental cooling rate data, shown in Figure 1.3, is fitted with a function in Equation 1.23 for the no phase transformation interval in order to find the parameters of the zero curve. Figure 1.5 shows the exclusion of curve fitting. A sample of experimental curve and zero curve are plotted in Figure 1.6. The results of curve fitting are in Table 1.2.
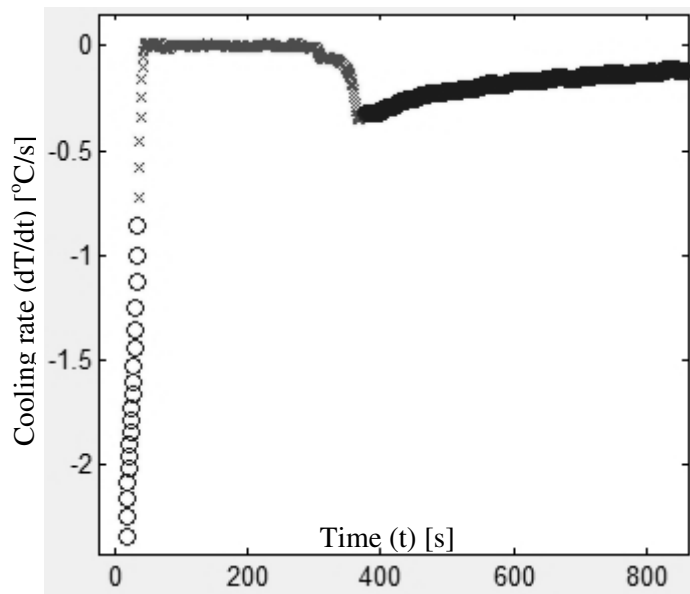
Figure 1.5: Data exclusion for no solidification region of dT/dt vs. t curve. Lighter points, shown with x, are excluded and not accounted by curve fitting tool anymore.
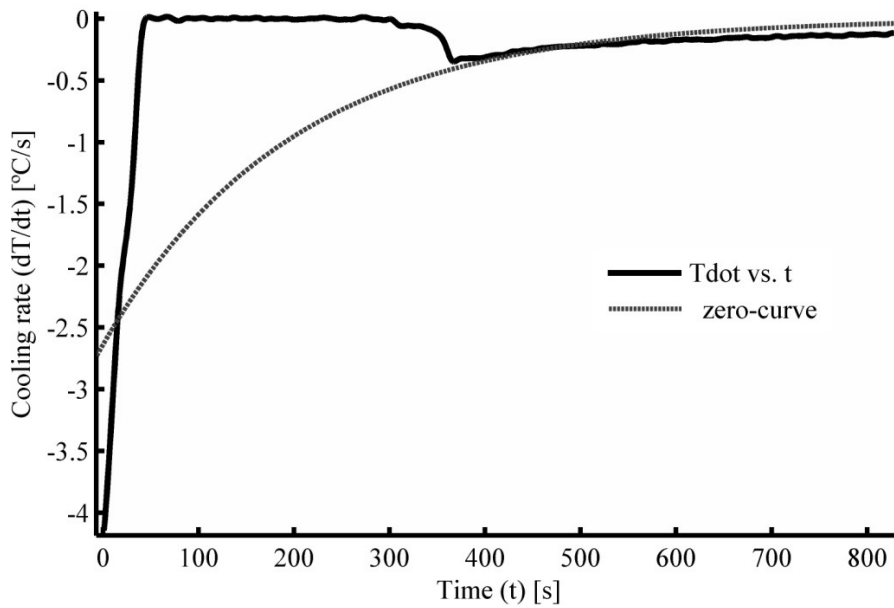
Figure 1.6: Experimental cooling rate curve and Newtonian zero curve (NBL).

Table 1.2: Curve fitting results of zero-curve.

General model Exp1: $\quad$ dT/dt = a*exp(b*t) Coefficients (with 95% confidence bounds): $\quad$ a = $\quad$ -2.637 (-2.725, -2.549) $\quad$ b = -0.005101 (-0.005364, -0.004837)	Goodness of fit: $\quad$ SSE: 26.77 $\quad$ R-square: 0.8568 $\quad$ Adjusted R-square: 0.8565 $\quad$ RMSE: 0.2333

Following the definition of zero curve, Equations 1.25 and 1.26 are written and solved for the solid fraction with the initial conditions of Equation 1.19.

$$\frac{dT}{dt} = \left(\frac{dT}{dt}\right)_{zc} + \frac{L_f}{c_p}\frac{df_s}{dt} \tag{1.25}$$

$$\frac{L_f}{c_p}\frac{df_s}{dt} = \left(\frac{dT}{dt}\right)_{exp} - \left(\frac{dT}{dt}\right)_{zc} \tag{1.26}$$

Integrating Equation 1.26 between t_e and t_s gives:

$$\frac{L_f}{c_p}\int_{t_s}^{t_e}\frac{df_s}{dt}dt = \int_{t_s}^{t_e}\left[\left(\frac{dT}{dt}\right)_{exp} - \left(\frac{dT}{dt}\right)_{zc}\right]dt \tag{1.27}$$

$$\frac{L_f}{c_p} = \int_{t_s}^{t_e}\left[\left(\frac{dT}{dt}\right)_{exp} - \left(\frac{dT}{dt}\right)_{zc}\right]dt \tag{1.28}$$

Latent heat per specific heat is calculated from Equation 1.28. The integral means the area between the experimental cooling rate and zero curves. The cumulative area between these curves gives the solid fraction function. For this purpose, Equation 1.26 is integrated between t and t_s [14].

$$\frac{L_f}{c_p}\int_{t_s}^{t}\frac{df_s}{dt}dt = \int_{t_s}^{t}\left[\left(\frac{dT}{dt}\right)_{exp} - \left(\frac{dT}{dt}\right)_{zc}\right]dt \tag{1.29}$$

$$f_s(t) = \frac{c_p}{L_f}\int_{t_s}^{t}\left[\left(\frac{dT}{dt}\right)_{exp} - \left(\frac{dT}{dt}\right)_{zc}\right]dt \tag{1.30}$$

11

This method of zero curve is called linear Newtonian zero curve or Newtonian baseline (NBL) since it is derived from a linear differential expression of the zero curve [5]. It has a wide range of application in the literature.

Another technique to plot a zero curve is dynamic baseline (DBL). DBL is calculated differently from the Newtonian linear baseline. It uses first time derivative of temperature (dT/dt) vs. temperature (T) data. In order to find DBL, temperature rate (dT/dt) is fitted with a third-degree polynomial in terms of T within the interval of no phase transformation.

$$\left(\frac{dT(t)}{dt}\right)_{zc} = p_1 T^3(t) + p_2 T^2(t) + p_3 T(t) + p_4 \tag{1.31}$$

After the parameters are calculated by computer, DBL is obtained as a function of time [5]. Liang et al. have used the DBL approach, developed by Kierkus and Solowski [5]. They found high correlation coefficient for the polynomial curve fit, which is 0.998 [13]. Figures 1.7-1.9 and Table 1.3 explain the procedure to get a dynamic baseline.
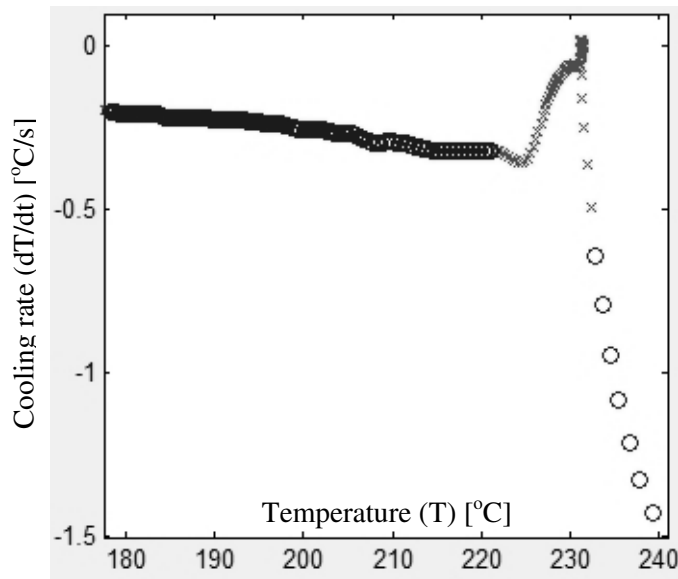
Figure 1.7: Exclusion of Tdot vs. T graph for polynomial curve fitting. Lighter region belongs to the solidification interval ($T_{sol} < T < T_{liq}$); therefore, they are excluded from curve fitting.

12
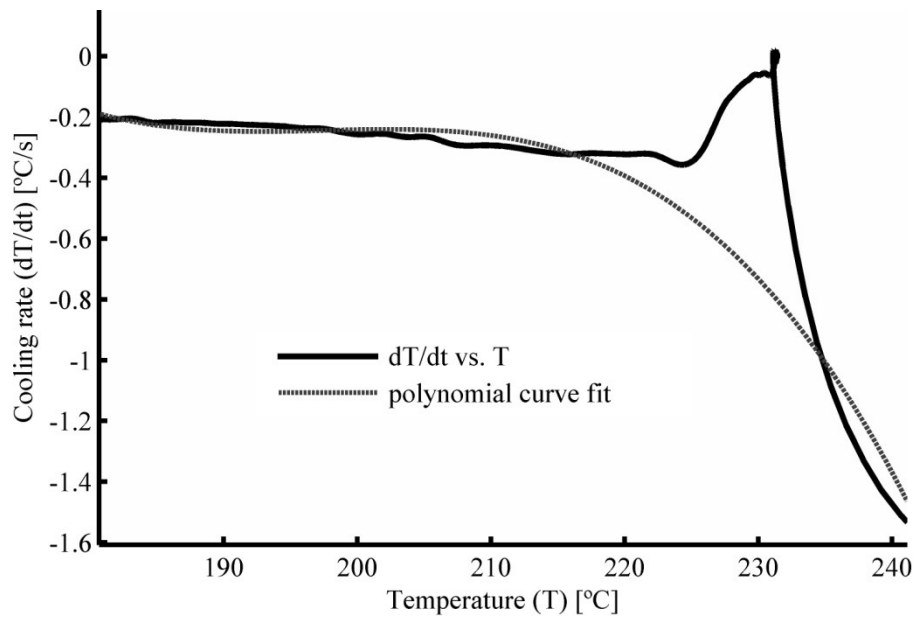
Figure 1.8: Temperature derivative vs. temperature curve and its polynomial curve fit.

Table 1.3: Third degree polynomial curve fitting results of the Tdot vs T graph.

Linear model Poly3:	Goodness of fit:
dT/dt = p1*T^3 + p2*T^2 + p3*T + p4	SSE: 0.2437
Coefficients (with 95% confidence bounds):	R-square: 0.9529
p1 = -1.527e-005 (-1.666e-005,-1.387e-005)	Adjusted R-square: 0.9521
p2 = 0.009045 (0.008178, 0.009912)	RMSE: 0.03742
p3 = -1.785 (-1.964, -1.607)	
p4 = 117.2 (104.9, 129.4)	

Figure 1.9: Experimental temperature derivative vs. time curve and the dynamic baseline obtained from Equation 1.31.

As seen in Figure 1.9, DBL overlaps with the experimental curve better than NBL (Figure 1.6) because NBL contains an integration constant coming from the initial conditions. The integration constant differs in solid and liquid phases, but NBL counts them the same. Since DBL uses the differential equation itself, it does not contain any parameters coming from the initial conditions.

The third baseline conducted from the literature is the Fourier baseline. It necessitates at least two thermocouples in order to include temperature gradient. Among the thermal analysis methods, only Fourier analysis regards the thermal gradient within a sample. Since multi thermocouple usage is required, Fourier thermal analysis can be applied for the dendrite coherency point (DCP) estimation [41, 5]. The derivation of Fourier thermal analysis is based on the Fourier heat conduction law, mentioned in Section 1.1. From Equation 1.14, a non-homogeneous partial differential equation can be obtained by dividing both sides with $\rho.c_p$.

$$\frac{\partial T(\vec{r},t)}{\partial t} = \frac{k}{\rho c_p} \nabla^2 T(\vec{r},t) + \frac{L_f}{c_p} \frac{\partial f_s(\vec{r},t)}{\partial t} \qquad (1.32)$$

where $k/\rho c_p$ is called diffusivity, represented by α, and ∇^2 is Laplacian operator. In this case, the Fourier zero curve corresponds to the temperature Laplacian.

$$Z_F = \alpha \nabla^2 T \qquad (1.33)$$

14

where α is calculated by

$$\alpha = \frac{\dot{T}}{\nabla^2 T} \tag{1.34}$$

$$L_f = c_p \left(\frac{\partial T}{\partial t} - Z_F \right) \tag{1.35}$$

In order to calculate temperature Laplacian, a minimum of three temperature data at different locations seem to be voluntary. However, it can be reduced to two temperature recordings in a symmetric temperature field [9]. In a cylindrical symmetrical experiment, e.g., insulated from top and bottom, the temperature profile depends only on the radial position. Therefore, there is a one-dimensional Laplacian for cylindrical coordinates:

$$\nabla^2 = \frac{\partial^2}{\partial r^2} + \frac{1}{r} \frac{\partial}{\partial r} \tag{1.36}$$

To calculate temperature Laplacian with two thermocouple, one may use thermal symmetry around r=0. Consider there are two thermocouples at $r=r_1$ and $r=r_2$ with temperature records T_1 and T_2 respectively. Temperature distribution can be assigned by a second order polynomial function of r in a small cup. Then, the temperature function satisfying the boundary temperatures (T_1, T_2) at r_1 and r_2 and zero derivative at r=0 is given by

$$T(r) = \frac{T_1 - T_2}{r_1^2 - r_2^2} r^2 + \frac{T_2 r_1^2 - T_1 r_2^2}{r_1^2 - r_2^2} \tag{1.37}$$

Then, the Laplacian can be calculated as follows:

$$\frac{\partial^2 T(r)}{\partial r^2} = 2 \frac{T_1 - T_2}{r_1^2 - r_2^2} \tag{1.38}$$

$$\frac{1}{r} \frac{\partial T(r)}{\partial r} = 2 \frac{T_1 - T_2}{r_1^2 - r_2^2} \tag{1.39}$$

$$\nabla^2 T(r) = 4 \frac{T_1 - T_2}{r_1^2 - r_2^2} \tag{1.40}$$

If T_1 and T_2 are measured by two thermocouples at r_1 and r_2, Fourier zero curve is calculated by Equation 1.33. The detailed explanation of Fourier baseline can be found by the study of Fras et al. [9].

Ekpoom and Heine [7] tried an analysis technique in 1981. They used logarithmic relative temperature as a cooling curve. The cooling parameter of Newton law of cooling was included as time-dependent during cooling process. At the solidification region, the cooling parameter was assumed linear in time. Consider time dependent cooling parameter $\theta(t)$ in Newton law of cooling [7, 38].

$$\dot{T} = -\theta(t)(T - T_\infty) + \frac{L_f}{c_p} \dot{f}_s \tag{1.41}$$

In the non-solidification region, the evolution of θ is defined by:

$$\theta(t) = -\frac{\dot{T}}{(T - T_\infty)} = -\frac{d}{dt}\left(ln\frac{T - T_\infty}{T_0 - T_\infty} \right) \tag{1.42}$$

The term in the logarithm is defined as relative temperature and denoted by Y.

$$Y = \frac{T - T_\infty}{T_0 - T_\infty} \tag{1.43}$$

As a result, the cooling parameter θ can be expressed by the minus slope of the logarithm of relative temperature Y. Figure 1.10 shows an example of -lnY vs. t graph. The tangents of the angles α and β corresponds to the instantaneous cooling parameter θ at t_s and t_e.
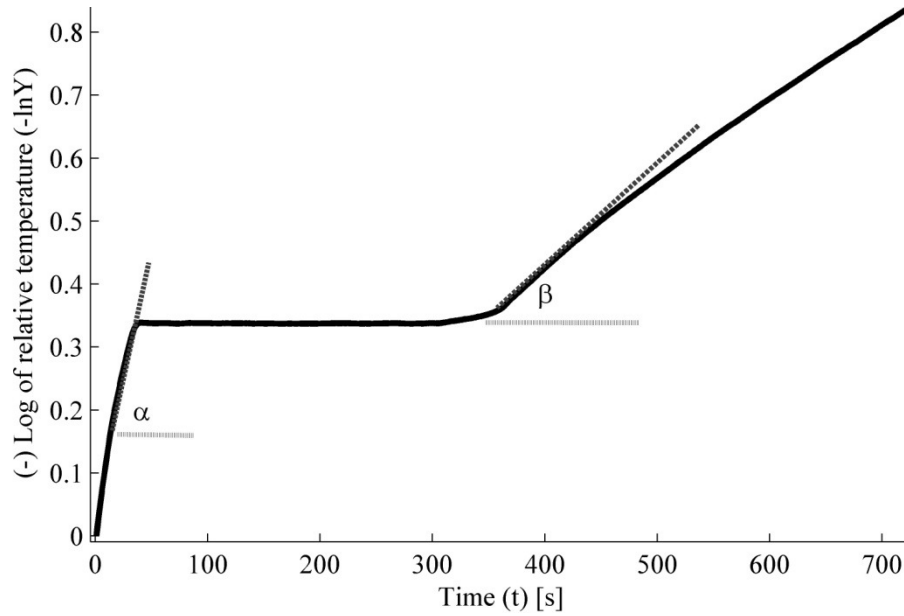
Figure 1.10: Logarithm of relative temperature vs. time for pure tin.

According to Ekpoom and Heine [7], the evolution of θ in the solidification interval is linear in time. The evolution can be expressed as:

$$\theta_{PT}(t) = \frac{\tan\beta - \tan\alpha}{t_e - t_s}t + \frac{t_e\tan\alpha - ts\tan\beta}{t_e - t_s} \qquad t_s < t < t_e \qquad (1.44)$$

Cooling parameter is the derivative of Figure 1.10 (defined in Equation 1.42), so it can be calculated for the solidification region. For the non-solidification region, the definition is Equation 1.44. The calculation of the logarithmic relative temperature baseline (LRTBL) is given by

$$\dot{T}_{zc} = \begin{cases} -\theta_{PT}(t)(T - T_\infty) & t_s < t < t_e \\ -\theta(T - T_\infty) & otherwise \end{cases} \qquad (1.45)$$

A sample zero curve for logarithmic method is shown in Figure 1.11, and the comparison of three baselines is given in Figure 1.12. The area between the experimental cooling rate curve and a baseline in the solidification interval gives the latent hat per specific heat (L_f/c_p) values of the sample. If the normalized cumulative area between t and t_s are calculated, solid fraction evolution can be obtained.

17
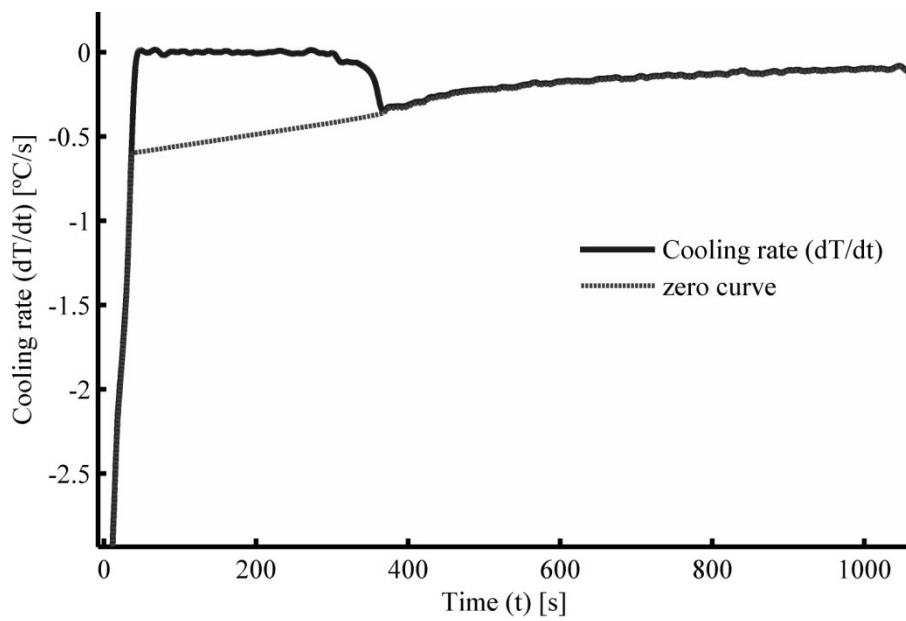
Figure 1.11: Logarithmic relative temperature zero curve.
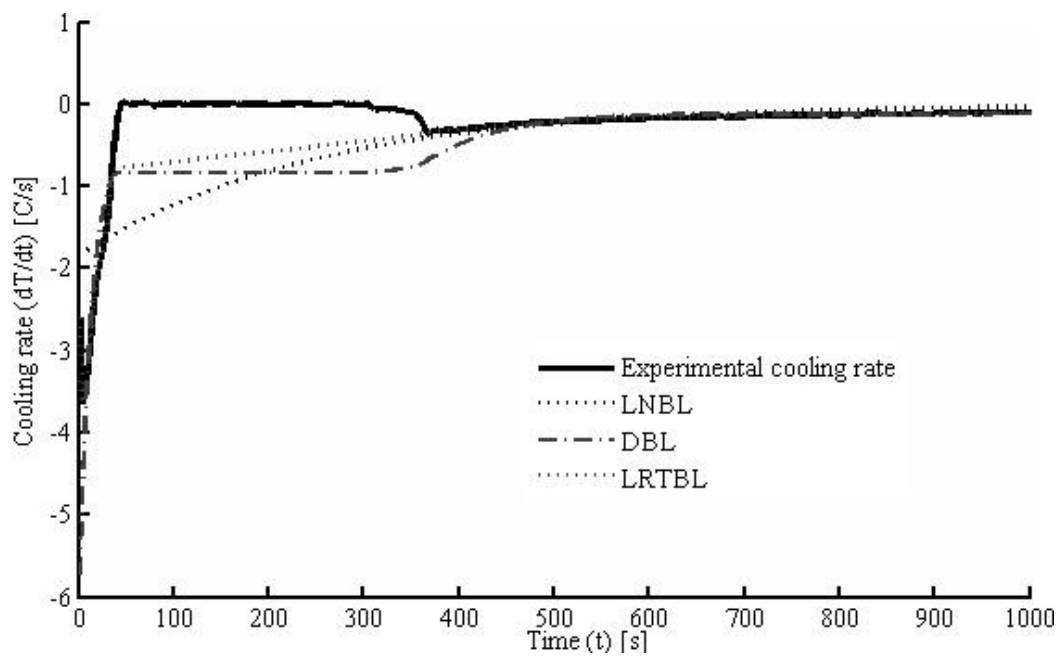
Figure 1.12: Experimental cooling rate curve, linear Newtonian baseline (NBL), dynamic baseline (DBL) and logarithmic relative temperature baseline (LRTBL).

CHAPTER 2

EVALUATION OF NEWTONIAN THERMAL ANALYSIS

2.1 Application of Newtonian Thermal Analysis Methods

Three different Newtonian analysis methods were mentioned in the previous chapter. These methods can be named in terms of their baseline techniques:

1. Linear Newtonian baseline (NBL)
2. Dynamic baseline (DBL)
3. Logarithmic relative temperature baseline (LRTBL)

Each baseline techniques were evaluated in both experimental and theoretical perspective. In addition, some critical studies were reviewed from the literature.

2.1.1 Experimental Results and Its Evaluations

These baselines are applicable to the data from a Newtonian experiment with one thermocouple. They were applied to 12 experiments with 4 types of pure metals with several conditions. The experiments are explained in Table 2.1. In each experiment, the ratio of latent heat to specific heat values (L_f/c_p) was calculated to compare with the literal values of the pure metals. The types of metals used in this study are listed in Table 2.2 with their thermal properties, found in *Perry's Chemical Engineers' Handbook* [16].

Table 2.1: List of the experiments and their explanations.

Experiment	Metal	Type of cup	Insulation
Al 1	Aluminum	Resin-coated sand cup	Without insulation
Al 2			Insulated from base
Al 3			
Pb 1	Lead		
Sn 1	Tin		
Sn 2			
Sn 3			Insulated from mold
Sn 4		Clay bonded graphite crucible	Insulated from outer surface
Sn 5		Resin-coated sand cup	
Zn 1	Zinc		Insulated from base
Zn 2			
Zn 3			

Table 2.2: Thermal properties of selected pure metals [16].

Metal	c_p [cal/deg mol] (Solid phase)	c_p [cal/deg mol] (Liquid phase)	L_f [cal/mol]	Melting Temp. [^{0}C]	L_f/c_p [deg] at melting temp.
Aluminum	4.8+0.00322 T	7.00	2550	660.0	327-364
Lead	5.8+0.00202 T	6.8	1224	327.4	174-180
Tin	5.05+0.0048 T	6.6	1720	231.8	230 - 261
Zinc	5.25+0.0027 T	7.6+0.00055 T	1595	419.5	200 - 224

When these three types of baseline, explained in Section 1.3, were applied the experiments in Table 2.1, the latent heat (L/c) results were obtained, and tabulated in Table 2.3. The percentage errors of the results with respect to literal average value are shown in Table 2.4.

Table 2.3: The results of latent heat per specific heat (L/c) values in ^0C from three baselines. Literal average of L/c values are averaged for 50 ^0C below and above the melting point according to solid and liquid phase specific heat values.

Exp	NBL	DBL	LRTBL	Literal average
Al 1	568.32	482.48	228.07	
Al 2	297.85	435.51	309.32	349
Al 3	327.85	391.11	98.47	
Pb 1	103.53	113.84	16.30	179
Sn 1	278.86	266.44	181.77	
Sn 2	232.73	198.74	167.83	
Sn 3	216.18	214.00	219.09	249
Sn 4	394.68	361.33	109.77	
Sn 5	251.45	191.14	145.84	
Zn 1	260.44	247.27	115.59	
Zn 2	359.23	291.36	117.35	214
Zn 3	289.22	210.66	134.86	

Table 2.4: Percentage errors of the results. Errors smaller than 0.20 are written in italics.

	NBL	DBL	LRTBL
Al 1	0.63	0.38	-0.35
Al 2	*-0.15*	0.25	*-0.11*
Al 3	*-0.06*	*0.12*	-0.72
Pb 1	-0.42	-0.36	-0.91
Sn 1	*0.12*	*0.07*	-0.27
Sn 2	*-0.07*	*-0.20*	-0.33
Sn 3	*-0.13*	*-0.14*	*-0.12*
Sn 4	0.59	0.45	-0.56
Sn 5	*0.01*	*-0.23*	-0.41
Zn 1	0.22	*0.16*	-0.46
Zn 2	0.68	0.36	-0.45
Zn 3	0.35	*-0.02*	-0.37
Absolute average	0.29	0.23	0.43

According to the results of Table 2.4, in general, none of the methods seems reliable for every type of experiment or metal. NBL can be said to be applicable for Al2, Al3, Sn1, Sn2, Sn3 and Sn5. It can be said that NBL is more consistent with Tin than Zinc. DBL

seems to be more reliable than NBL for averaged absolute value of errors. Among the baseline techniques, LRTBL is the least appropriate method for Newtonian thermal analysis research. The reason may be the sensitive dependence of the method to take the derivative of the data, which requires some modifications on the cooling curve. One of the striking results from Table 2.4 is the consistency of Sn 3 for all baselines. This experiment was made in a thermally insulated mold, in which there is an insulating paper in the metal-mold interface. The thermal capacity of the mold is disregarded, so all baselines give proper results for this experiment.

2.1.2 Theoretical Contradictions of Zero Curve Approach

Arbitrary nature of zero curve calculation in NTA makes the qualitative predictions of the latent heat hard. However, it is more reliable on the qualitative identification of solidification kinetics although further studies are required [17]. The nature of zero curve depends on the estimation of cooling rate curve in terms of time or temperature for the non-solidification interval. NBL estimates temperature derivative as a function of time, while DBL makes it in terms of temperature. Therefore, NBL considers the solution of Newton's law of cooling without phase transformation. Newtonian differential equation (Equation 1.18) can be stated by using Heaviside step function for all t.

$$\frac{dT}{dt} = -\frac{hA}{V\rho c_p}\left(T - T_\infty\right) + \frac{L_f}{c_p}\frac{df_s}{dt}\left(\theta(t - t_s) - \theta(t - t_e)\right) \tag{2.1}$$

where θ is Heaviside step function. The solution for the whole interval can be made by linear ordinary differential equation solution method with integration factor. It can be rewritten as:

$$\frac{du}{dt} + bu = g(t) \tag{2.2}$$

where u is the relative temperature (T-T∞), b is the cooling parameter, and g is the source term defined below.

$$g(t) = \frac{L_f}{c_p}\frac{df_s}{dt}\left(\theta(t - t_s) - \theta(t - t_e)\right) \tag{2.3}$$

$$b = \frac{hA}{V\rho c_p} \tag{2.4}$$

Multiplying both sides of Equation 2.2 with integrating factor (exp(bt)), it gives [18]:

$$\frac{du}{dt}e^{bt} + bue^{bt} = g(t)e^{bt} \tag{2.5}$$

It is a derivative of multiplication.

$$\frac{d}{dt}\left(ue^{bt}\right) = g(t)e^{bt} \tag{2.6}$$

Integrating both sides between t=0 and t gives:

$$ue^{bt}\Big|_0^t = \int_0^t dt\, g(t)e^{bt} \tag{2.7}$$

The solution for u(t) is:

$$u(t) = \left[u(0) + \int_0^t g(t)e^{bt}\,dt\right]e^{-bt} \tag{2.8}$$

The solution for temperature T(t) is:

$$T(t) = T_\infty + \left[T(0) - T_\infty + \frac{L_f}{c_p}\int_0^t \frac{df_s}{dt}\left(\theta(t-t_s) - \theta(t-t_e)\right)e^{bt}\,dt\right]e^{-bt} \tag{2.9}$$

If the terms in the square bracket is notated A(t), it yields

$$A(t) = T(0) - T_\infty + \frac{L_f}{c_p}\int_0^t \frac{df_s}{dt}\left(\theta(t-t_s) - \theta(t-t_e)\right)e^{bt}\,dt \tag{2.10}$$

The general solution format of Newton law of cooling is

$$T(t) = T_\infty + A(t)e^{-bt} \tag{2.11}$$

With the existence of the Heaviside function in A(t), it can be stated as a piecewise function in each interval. Three intervals in Equation 2.12 are liquid phase, solidification phase, and solid phase respectively.

23

$$
A(t) = \begin{cases} T(0) - T_\infty & t < t_s \\ T(0) - T_\infty + \dfrac{L_f}{c_p} \displaystyle\int_0^t \dfrac{df_s}{dt} e^{bt} dt & t_s < t < t_s \\ T(0) - T_\infty + \dfrac{L_f}{c_p} \displaystyle\int_{ts}^{te} \dfrac{df_s}{dt} e^{bt} dt & t_e < t \end{cases} \tag{2.12}
$$

Temperature at the cooling region, that is, no-solidification region, is denoted by $T_c(t)$, and it is stated in terms of Heaviside functions because of different integration constant at solid and liquid phase.

$$
T_c(t) = T_\infty + \left(a_L \theta(t_s - t) + a_S \theta(t - t_e) \right) e^{-bt} \tag{2.13}
$$

where a_L and a_S are the integration constants, coming from different initial conditions caused by interference of phase transformations between phases. The time derivative of the temperature at the cooling region, which is also called zero curve, is given by:

$$
\dot{T}_c(t) = -b \left(a_L \theta(t_s - t) + a_S \theta(t - t_e) \right) e^{-bt} \tag{2.14}
$$

Therefore, the zero curve function is actually not a simple exponential. The effect of different coefficients for two phases should be included.

The meaning of zero curve is the curve if there is no phase transformation. The virtual no phase transformation case develops first by cooling in the liquid state, then continues cooling during the solidification interval, and then starts to cool with new initial condition for the solid case (Figures 2.1 and 2.2).
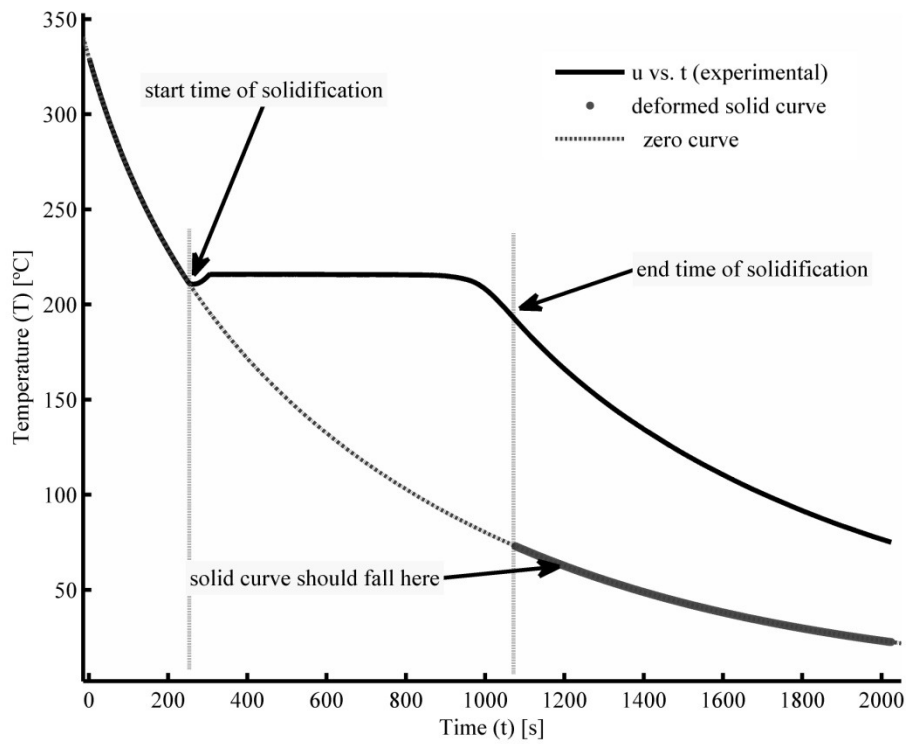
Figure 2.1: Virtual cooling curve data if there were no phase transformation.
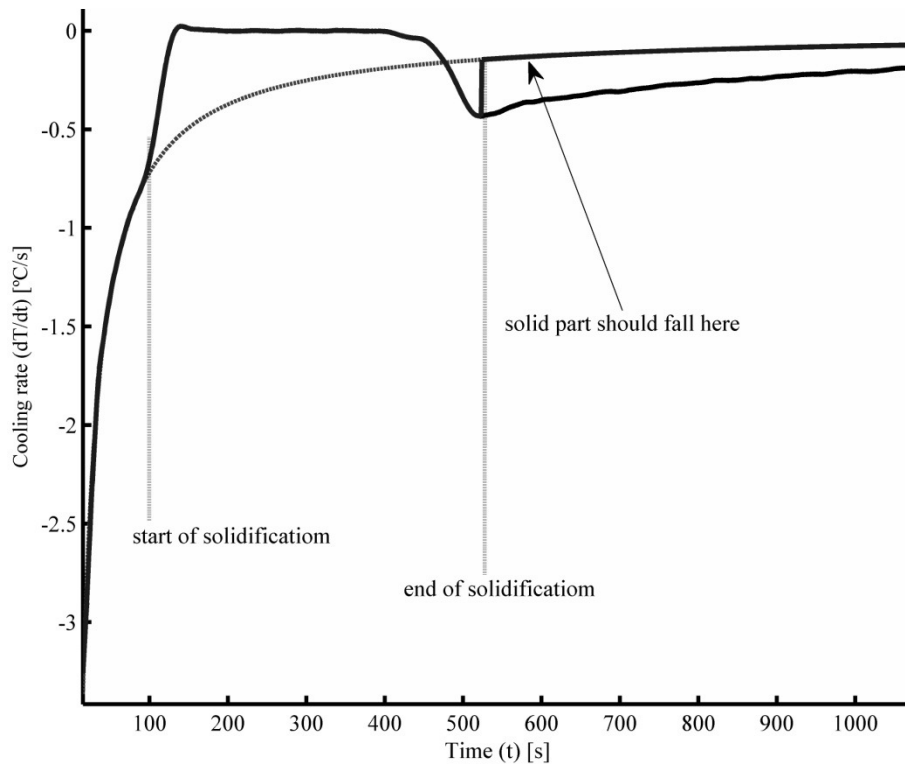
Figure: 2.2: Virtual condition for cooling rate if there were no phase transformation.

A similar approach with the cooling curve can be applied to the cooling rate curve as in Figure 2.2. The solid part of the experimental data should be transformed so that it complements the liquid part, and then curve fit should be done. For this reason, Newtonian baseline method is not appropriate to explain non-transformational case.

Dynamic baseline theory seems to be more reliable than NTA because it considers nonlinearity to include radiative or other temperature dependent contributions. It can be interpreted as a third degree Taylor series expansion of cooling rate in terms of temperature around the melting point. However, Newton's law of cooling is a first degree approximation. The Taylor series expansion of cooling rate is expressed below.

The relation between cooling rate and temperature can be defined by a general function including above restrictions.

$$\dot{T} = F(T)$$
(2.15)

The function F may be very complex function of T including radiation terms, temperature dependence of specific heat ($c_p(T)$) etc. If the temperature interval is narrowed, the Taylor series expansion of F(T) around T_0 may be used for the first and second degree terms.

$$\dot{T} = F(T) = F(T_0) + \frac{\partial F}{\partial T}\bigg|_{T=T_0} (T - T_0) + \frac{1}{2!} \frac{\partial^2 F}{\partial T^2}\bigg|_{T=T_0} (T - T_0)^2 \ldots\ldots$$
(2.16)

The first, second and third degree expansions can be simplified as

$$\dot{T} = a_1 T + a_0$$
(2.17)

$$\dot{T} = a_2 T^2 + a_1 T + a_0$$
(2.18)

$$\dot{T} = a_3 T^3 + a_2 T^2 + a_1 T + a_0$$
(2.19)

The first degree expansion is used in NBL, but the second and third ones are used in DBL techniques. A common property for both of the baselines is the choice of freedom on the ambient temperature. When the baselines are fitted with a function in some interval, they give an ambient temperature output according to the curve fitting interval. Ambient temperature value (T_∞) can be found by the behavior of the function at infinity. Cooling rate and temperature go to zero and ambient temperature when time goes to infinity (Equation 2.20). In order to calculate this unreal ambient temperature, root of the polynomials must be solved for zero temperature rate (Equations 2.21-2.23).

$$\lim_{t \to \infty} \frac{dT(t)}{dt} = 0 \quad and \quad \lim_{t \to \infty} T(t) = T_\infty \tag{2.20}$$

$$0 = a_1 T_\infty + a_0 \tag{2.21}$$

$$0 = a_2 T_\infty^2 + a_1 T_\infty + a_0 \tag{2.22}$$

$$0 = a_3 T_\infty^3 + a_2 T_\infty^2 + a_1 T_\infty + a_0 \tag{2.23}$$
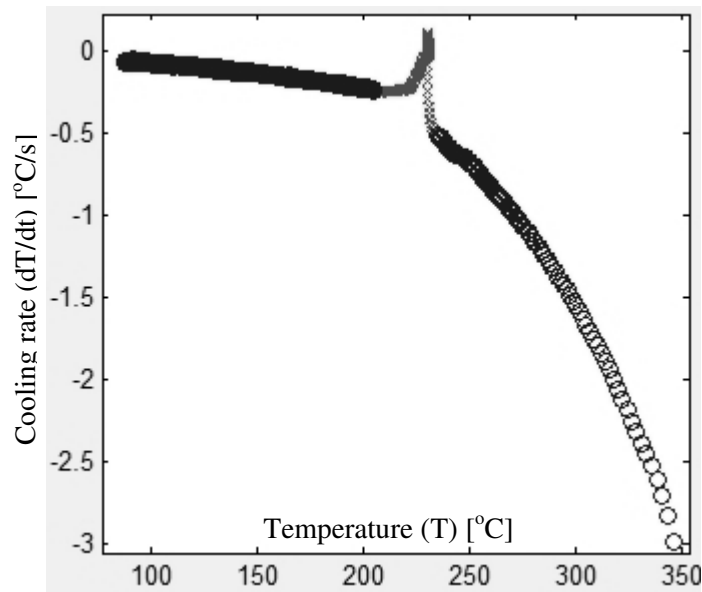
Figure 2.3: Exclusion of dT/dt vs. T data. The full scale of temperature is included except for the solidification temperature range.

Figures 2.3 and 2.4 show the exclusion rules for the curve fitting session of cooling rate in terms of temperature. Two different exclusion intervals were defined for both linear and polynomial fits. One is include the complete cooling range, but the other includes a narrow interval around solidification. The results of fits are shown in Figure 2.5. In the figure, unreal ambient temperatures are the points that the fit curves intersect the T axis. Linear fit in narrow scale has the highest ambient temperature, while the polynomial in narrow scale has no ambient temperature. When the whole scale data is used, the unreal ambient temperature gets closer to the real ambient temperature measured.

27
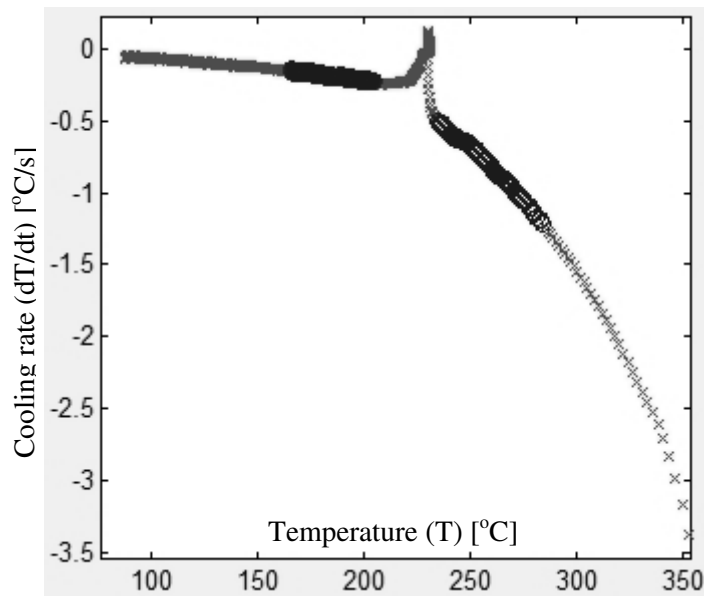
Figure 2.4: Exclusion of dT/dt vs. T data. A narrow scale of temperature is included except for the solidification temperature range.
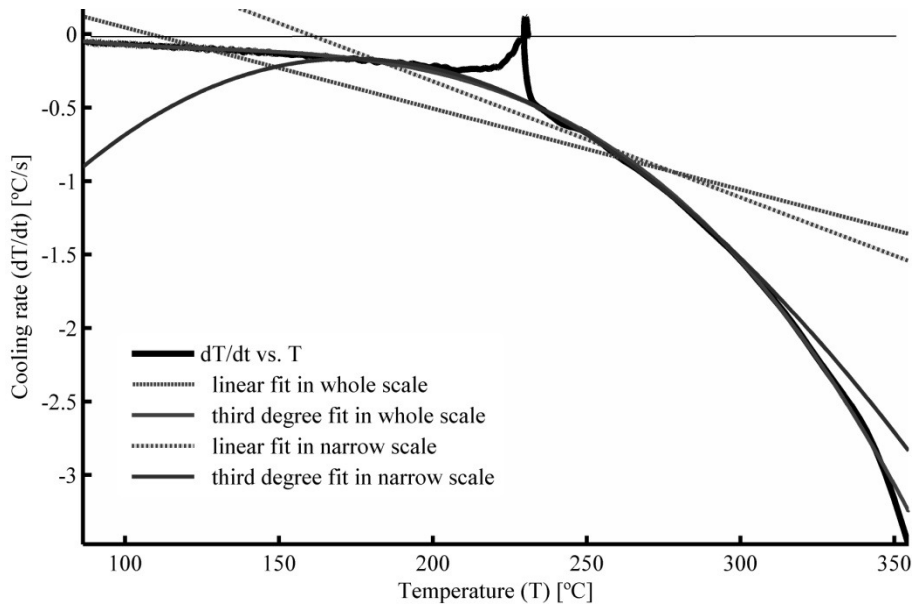
Figure 2.5: Curve fitting results of dT/dt vs. T for the full and narrow scales of both linear and third order polynomial.

DBL has its own unreal ambient temperature coming from the coefficients of Taylor expansion like NBL. The coefficients found by curve fitting do not correspond to the actual coefficients containing heat transfer coefficients or heat capacity. One may say

28

that: heat transfer coefficient and heat capacity cannot be related to the parameters of curve fitting; only the latent heat may give true outcome because of the narrow scale thermal characteristics of the curve fitting around the melting point.

Different from DBL and NBL, LRTBL accounts for the real ambient temperature because it has to measure the ambient temperature to use the logarithmic relative temperature. Therefore, its interval of interest is so wide that it can not be stated by the first degree expansion of the temperature. The unreliable results of LRTBL in Section 2.1 may be caused from this contradiction.

2.2 Evaluations and Comparisons with the Literature

Although the basic idea is common for different thermal analysis baselines, they differ in methods to obtain. Therefore, some comparisons have been made to evaluate the success of these methods. The basic criteria are determination of latent heat and solid fraction evolution. Among the methods, NTA and FTA are the most compared baselines.

In general NTA produces higher solidification rates than FTA at the onset of solidification. A. Çetin reports that the zero curve of FTA exhibits similar trends with the experimental cooling rate curves [15]. According to Fras et al., NTA and FTA methods give great different predictions for volume fractions of solidified phases [9].

Number of thermocouples in a thermal analysis may get the results reliable to some extent. One of the advantages of using two thermocouples is to make thermal distortion less significant. Therefore, FTA with two thermocouples is more consistent than the others [41]. Although FTA gives more reliable outputs than NTA, the exact positions of two thermocouples are difficult to measure because of thermal contradiction of metals [53].

In a study, DBL is compared with the most popular methods, NTA and FTA. In an experiment conducted by Emadi et al., three different methods were studied on the commercial A356 (Al-7%Si) alloys. The results of latent heat from the Newtonian polynomial, Newtonian linear, and Fourier baselines are 172, 170, and 394 J/g respectively. Its DSC method value of the alloy is 432.20 J/g. They also reported that FTA was more reliable than NTA, and the type of sampling cup had less effect in a FTA experiment [19]. In a different article, Emadi et al. measure latent heat of A356 (Al-7%Si) 403, 435, 432 J/g from the Newtonian, Fourier, and DSC methods respectively [4].

Conclusions from the literature, in general, state that NTA is the least reliable one although it is the simplest analysis method. Several papers investigate the possible

29

restrictions. In a study, conducted by Çetin and Kalkanlı, the methodology that uses exponential zero curve is reported as unreliable to predict latent heat of primary solidification. One of the possible sources of errors is the determination of cooling parameters, which is affected by many variables, such as pouring temperatures, metal mold interaction reactions, and the dependence of specific heat to temperature and composition [20].

The procedure of the analysis is based on finding the thermal parameters from curve fitting. However, curve fitting results may vary with the choice of exclusion or the temperature interval of the experiment. According to Emadi et al., "NBL is too dependent upon the fitting method, and therefore, is not a reliable estimate of latent heat." [4]. Moreover, the parameters may differ in the phase of a material. That cooling rate is much lower after solidification than before was reported by Loizaga et al. The authors also stated that this cooling rate difference could not be explained by the different specific heat values of solid and liquid phases [52]. Another limitation of Newtonian thermal analysis is the effect of mold's heat capacity. The capacitive effect of the mold may be responsible for the higher cooling rate at liquid phase. Thermal mass of the crucible should be very small comparing with the sample. In this case, the analysis shows the properties of the sample, not that of crucible-sample system [19].

Heat transfer coefficients assumed constant during the cooling process. Actually, they are affected by temperature or interfacial air gaps between metal and mold. The phase of the sample may be effective for the value of heat transfer coefficients. Lau et al. explain the development of heat transfer coefficient in three stage.Heat transfer coefficient decreases rapidly at the beginning of solidification and then reaches a steady value for a short time. After the steady stage, it increases in the solidification duration. However, for pure aluminum, there is no increase after the steady stage [21].

The junction between the surfaces of metal and mold creates a temperature drop. With the formation of the air gap, the interfacial heat transfer coefficient decreases and solidification rate begins to decelerate. The transient heat transfer coefficients are power functions of time [22]. According to Santos et al. heat transfer through metal and mold surfaces directly affects the solidification process. Because of the good surface conformity between melt and cup, the HTC has high a value at the initial stage of solidification. At the final stage, air gap forms at the interface, and then the HTC decreases rapidly. After a while, relatively constant HTC occurs. The general forms of mold-environment HTC (h_a) and metal-mold HTC (h_i) are:

$$h_a = C_m t^{0.15} \qquad h_i = C_i t^{-n} \tag{2.24}$$

C_m, C_i and n are constants, which depend on alloy composition, chill material (mold) and super heat [23].

Radiation is one of the determinants of solidification and cooling process. Its nonlinear nature makes radiative thermal analysis complex. Some studies show that the effect of radiation can not be ignored. Dombrovsky and Dinh reported that both solidification character and duration depend on radiation. Actually, accurate determination of solidification dynamics require radiative-conductive model [24].

There is no accurate information for the interval of radiation ignorance. For a critical threshold, cooling by radiation is significant if the pure conductive heat transfer coefficient is smaller than 6 Wm-2K-1 [25]. The study of Vollmer gives some limits to the ignorance level of radiation. According to Vollmer, linearization of heat transfer equations with radiative contribution is only reliable on small temperature differences. The constant heat transfer coefficient assumption does sensitively depends on the ratio between convective and radiative heat transfer rates. When convection dominates radiation in an experiment, the permitted temperature difference may be 500 K or higher. But, if radiation dominates, Newton law of cooling can be valid only small temperature differences, e.g. 30 K [26].

2.3 Investigating the Probable Restrictions

In this section, the basic obstacles in front of NTA were examined. Previous sections summarized the probable problems by theoretical evaluation, experimental testing, and literature review. These possible restrictions are:

1. Variations in data analysis, such as curve fitting, taking derivative, and selection of data interval
2. Effect of metal-mold interaction, such as a high heat capacity of mold, formation of air gap, and the variation in interfacial heat transfer coefficient
3. Variations of the thermal properties, such as specific heat and heat transfer coefficients
4. Contribution of radiation to the cooling process

In order to examine these restrictions and determine their priority, two simplified experiments were made. Especially, metal-mold interactions and the effect of mold's thermal capacity were evaluated by the experiments in which there is no thermal contact with mold. The simplest experiment is the hot metal that is left to cool without any conductive contact. The temperature range was tried to keep so low that radiative contributions can be neglected. The second experiment included solidification in a thermally insulated mold to avoid thermal contributions from mold.

2.3.1 Simple Cooling Experiment without Mold

The assumptions for the most ideal and the simplest case are:

1. There is no temperature gradient through solidified metal.

2. There is no phase transformational source or sink term that may emerge.
3. Radiative cooling is assumed to be negligible.
4. Specific heat is assumed to be constant.

A solid pure tin specimen was heated to $180\ ^0C$, and left to cool on an insulator by the convection with air in order to provide the ideal conditions. Newton's law of cooling assumes a linear relationship for a cooling process, so it can be stated as in Equation 2.25. Its solutions in terms of the parameters of the differential equation are in Equation 2.26 and 2.27, where A is the integration constant.

$$\dot{T} = p_1 T + p_2 \tag{2.25}$$

$$T = Ae^{p_1 t} - \frac{p_2}{p_1} \tag{2.26}$$

$$\dot{T} = p_1 Ae^{p_1 t} \tag{2.27}$$

Equations 2.25-2.27 are applied to curve fitting in order to find and compare the parameters. The curve fitting results are shown in Figures 2.6-2.8 and Table 2.5.
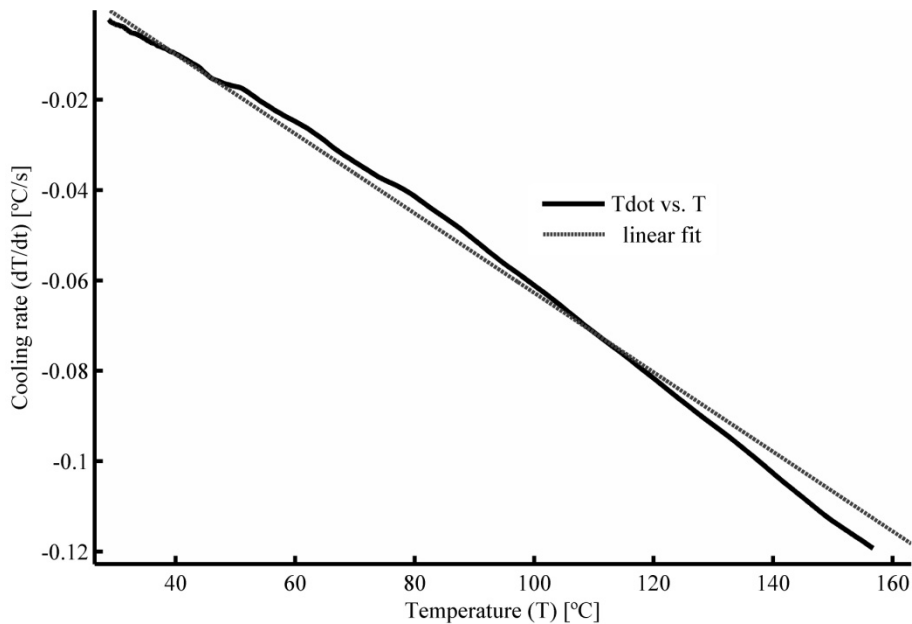
Figure 2.6: Experimental cooling rate vs. temperature curve and linearly fitted curve for pure Sn without mold.
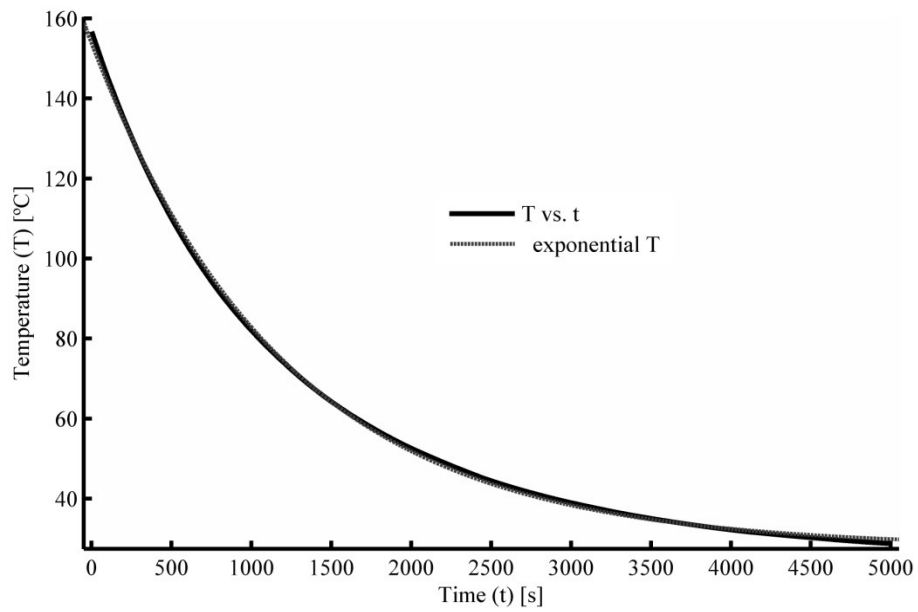
Figure 2.7: Experimental cooling curve and exponentially fitted curve for pure Sn without mold.
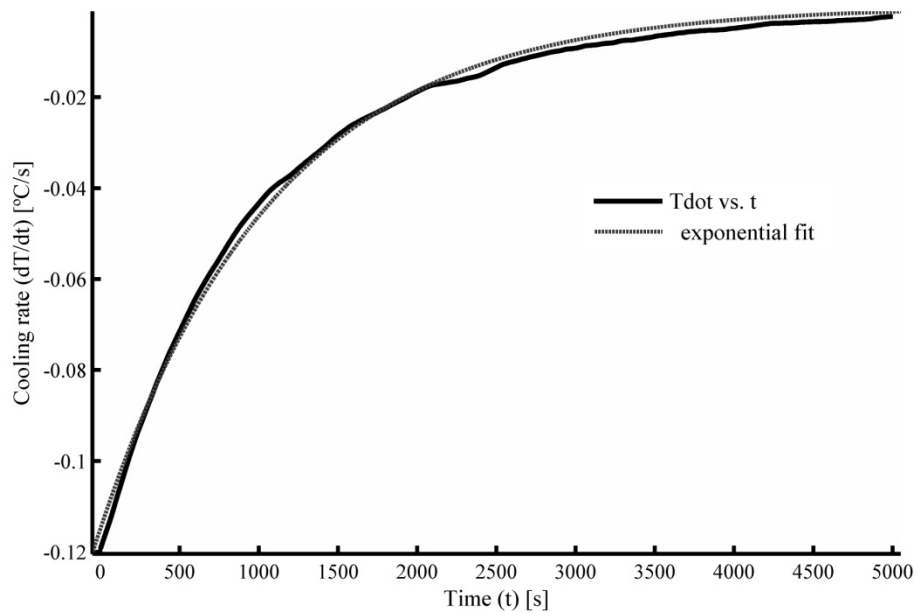
Figure 2.8: Experimental cooling rate vs. time curve and exponentially fitted curve for pure Sn without mold.

33

Table 2.5: Curve fitting results of Equations 2.25-2.27.

	p_1 (10^{-4})	p_2 (10^{-2})	A	R-Square
Linear fit	-8.797	2.523	-	0.9938
Exponential fit of T	-8.296	2.315	126	0.9994
Exponential fit of Tdot	-9.124	-	126	0.9961

The cooling parameter was calculated 0.0008797, 0.0008296, and 0.0009124 from the equations 2.25-2.27 respectively. However, the R-square value is the highest for the curve fit of temperature in terms of time. This may be caused by the deformation of data while its time derivative (Tdot) is being taken because data smoothing deforms the data for the sake of smoothing. Therefore, curve fitting outcomes are more reliable without derivative. It is better to solve the differential equation first and then fit the solution on the original temperature data in order to find the required parameters.

This analysis is the simplest one to find cooling parameter because of its first order and linear differential equation format, but there may be some alternatives to include other effects such as radiation and variable specific heat. The approximation of the equation by Taylor series may get one step further. Dynamic baseline technique advices a second or third degree polynomial fit for Tdot vs. T fit. Equation 2.28 is a quadratic expression of the cooling process [5].

$$\dot{T} = p_1 T^2 + p_2 T + p_3 \tag{2.28}$$

Equation 2.28 is modified so that it ensures the behavior of temperature at infinity (Equation 2.29). When time goes to infinity, rate of temperature must go to zero. Therefore, Equation 2.29 may be suggested as an appropriate 2nd degree differential form of cooling.

$$\dot{T} = -b(T - T_\infty)(T - T_\infty + a) \tag{2.29}$$

where b and a are constants defined below.

$$p_1 = -b, \quad p_2 = -ba, \quad p_3 = b(a - T_\infty)T_\infty \tag{2.30}$$

If relative temperature u is defined for T - T_∞, a nonlinear equation and its solution will be obtained as shown in Equations 2.31 - 2.33.

$$\frac{du}{dt} = -bu(u+a) \tag{2.31}$$

$$u = \frac{a}{ce^{abt} - 1} \tag{2.32}$$

$$T = \frac{a}{ce^{abt} - 1} + T_\infty \tag{2.33}$$

In terms of p_1, p_2 and p_3, Equation 2.33 can be rewritten as:

$$T = \frac{p_2 / p_1}{ce^{-p_2 t} - 1} + \frac{\sqrt{p_2^2 - 4p_1 p_3} - p_2}{2p_1} \tag{2.34}$$

There are two ways to find the thermal parameters of the quadratic relation in Equation 2.28. They may be calculated by the direct curve fitting of Equation 2.28, or 2.33. Figures 2.9 and 2.10 show the curve fitting results. Parameters p_1, p_2, and p_3 were obtained by two ways, and the results were tabulated in Table 2.6.

Table 2.6: Curve fitting results of Equations 2.28 and 2.33.

	p_1 (10^{-6})	p_2 (10^{-4})	p_3 (10^{-2})	c	R-square
Equation 2.28	-2.066	-5.534	1.538	-	0.9998
Equation 2.34	-2.341	-6.335	1.440	3.048	1.0000
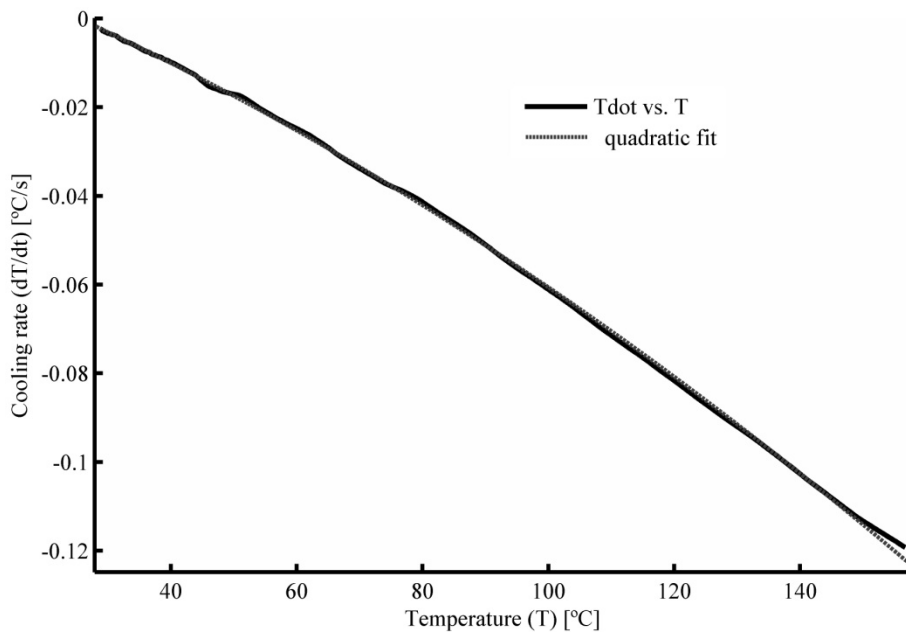
Figure 2.9: Experimental cooling rate vs. temperature curve and quadratically fitted curve for pure Sn without mold.
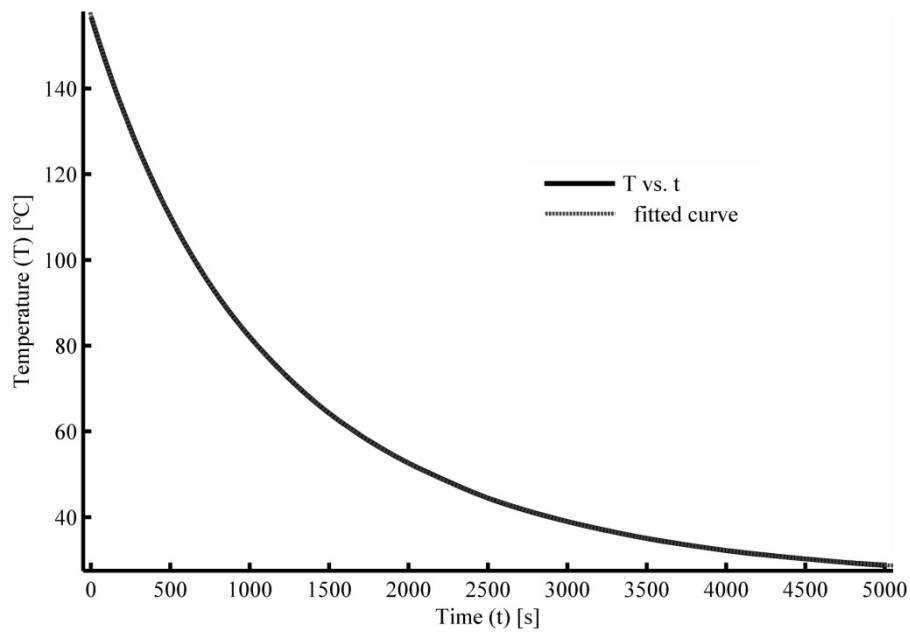
Figure 2.10: Experimental cooling curve and nonlinear exponential fitted curve for pure Sn without mold.

36

The R-square value of the fit by Equation 2.33 is very high, and there is no need to time derivative data to find the parameters of the cooling. It can be concluded that NLC is not perfect even if there is no mold contact. The second degree Taylor series expansion may be expanded to third degree. In this case, third degree of dynamic baseline (DBL) told in the previous chapter is attained.

2.3.2 Solidification in a Thermally Insulated Mold

In the previous section, the quadratic function in terms of temperature gave high correlation with the experimental data. The success of the quadratic function was also examined for the explanation of solidification by a simplified solidification experiment. To exclude the effects of mold, a thermal insulator was placed in the sand mold before the casting process, and then molten tin was poured into the mold at 350 ^{0}C. The photograph of the experiment is in Figure 2.11.
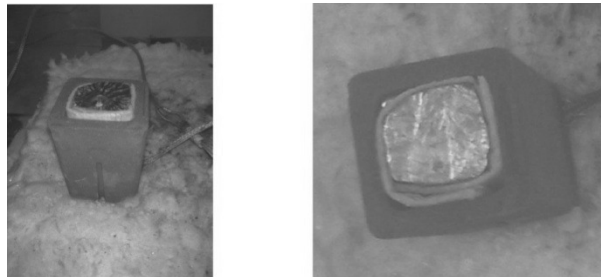
Figure 2.11: Thermally insulated melt from the mold.

Since there is no heat transfer between the cast and mold, the analysis methods explained section 2.3.1 is executed to the pure tin. The temperature and cooling rate with respect to time are seen in Figure 2.12.
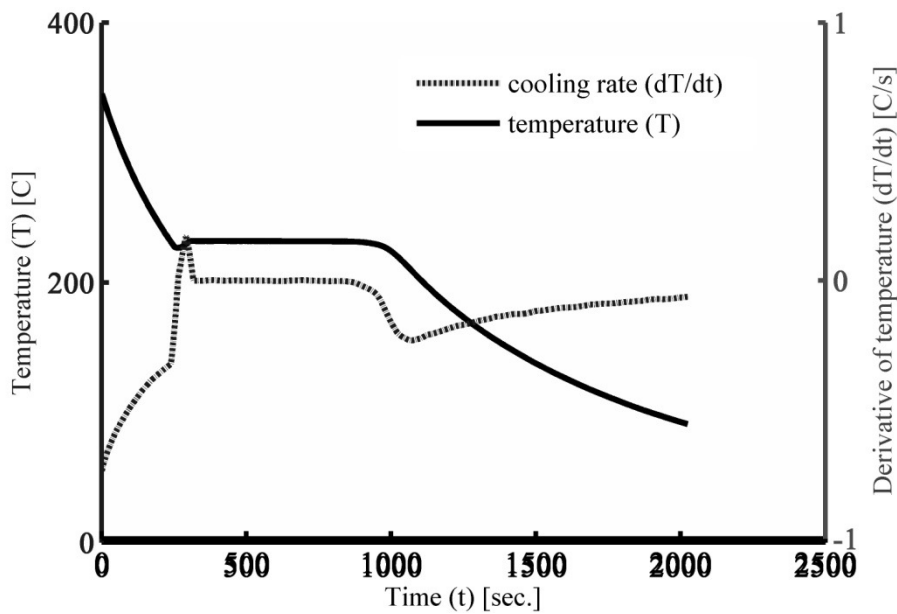
Figure 2.12: Cooling curve and its time derivative.

With the abundance of the zero curve alternatives, one may ask a question: "how is the best zero curve determined?" This question brings new ones to investigate the alternatives. These are:

1. Which type of cooling equation is better? Linear or nonlinear?
2. Which function will be chosen for curve fitting? The differential equation itself or its solutions?
3. Which curve fitting interval is better? Wide or narrow?

Several alternatives were tried on an experiment made by thermally insulated metal from the mold to answer those questions. These alternatives are the choice of cooling equation type, the function to apply curve fitting, and the interval of curve fitting.

Two types of differential equations were tried for this experiment: one is linear; the other is quadratic. For the derivation of zero curve, three types of function were applied to curve fitting: temperature rate as a function of temperature, temperature rate as a function of time, and temperature as a function of time. The cooling region temperatures (T_c), used in curve fitting are explained below.

The first type of fit function is NLC, which is linear in the non-solidification interval.

$$\dot{T}_c = p_1 T_c + p_2 \tag{2.35}$$

38

The solution of Equation 2.35 in cooling regions can be expressed with two different integration constants for solid and liquid phases (a_s and a_l). The solution is seen below, where θ is Heaviside step function.

$$T_c = \left(a_s\theta(t-t_e) + a_l\theta(t_s-t)\right)e^{p_1t} - p_2/p_1 \tag{2.36}$$

Equation 2.36 is directly applied to the T vs. t data to find the required parameters for zero curve. Zero curve is calculated by substituting of p_1 and p_2 in Equation 2.35. Alternatively, p_1 and p_2 can be directly calculated by applying Equation 2.35 to the dT/dt vs. T data for curve fitting.

NBL is obtained by applying Equation 2.37 to dT/dt vs t data for curve fitting.

$$\dot{T}_c = Ae^{-bt} \tag{2.37}$$

Another application of curve fitting is Equation 2.38 and Equation 2.39

$$\dot{T}_c = p_1 T_c^2 + p_2 T_c + p_3 \tag{2.38}$$

The solution of the quadratic differential equation with different integration constants for solid and liquid phases is shown in Equation 2.39.

$$T_c = \left(\frac{a}{c_s e^{abt} - 1} + T_\infty\right)\theta(t-t_e) + \left(\frac{a}{c_l e^{abt} - 1} + T_\infty\right)\theta(t_s - t) \tag{2.39}$$

The quadratic baselines can be calculated by curve fitting of both Equations 2.38 and 2.39.

In summary, there may be lots of zero curve calculation choices for different curve fitting intervals. The intervals of curve fittings are divided by two categories as wide and narrow. These intervals are defined below in terms of both time and temperature in units of second and centigrade.

$$I_{wide}: t \in (0, 237) \cup (1070, 2024) \quad or \quad T \in (232, 345) \cup (91, 209) \tag{2.40}$$

$$I_{narrow}: t \in (114, 237) \cup (1070, 1333) \quad or \quad T \in (232, 280) \cup (180, 209) \tag{2.41}$$

where t_s and t_e are 237 and 1070 seconds respectively. The temperatures at the start and end times of solidification are taken 232 and 209 ^{0}C respectively. The pictures of the exclusion factors for curve fitting sessions are shown in Figures 2.13-2.15.
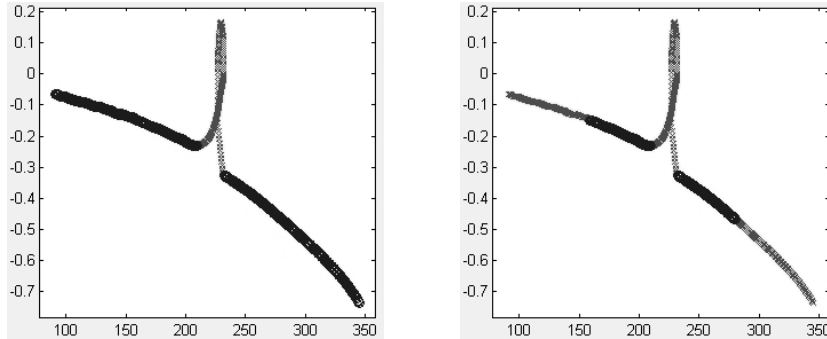
Figure 2.13: Exclusion factors of Tdot vs. T data for wide and narrow scales respectively.
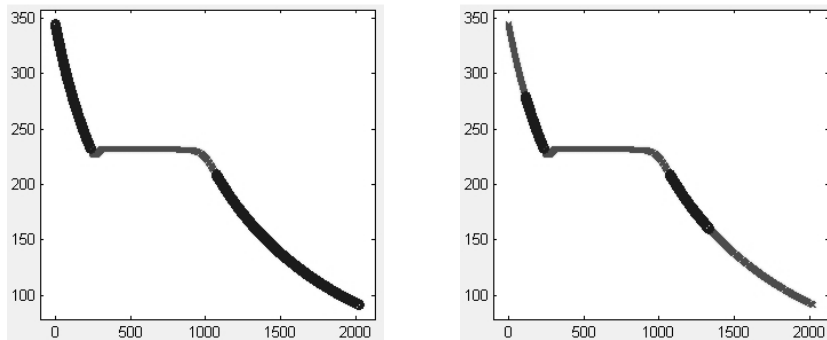
Figure 2.14: Exclusion factors of T vs. t data for wide and narrow scales respectively.
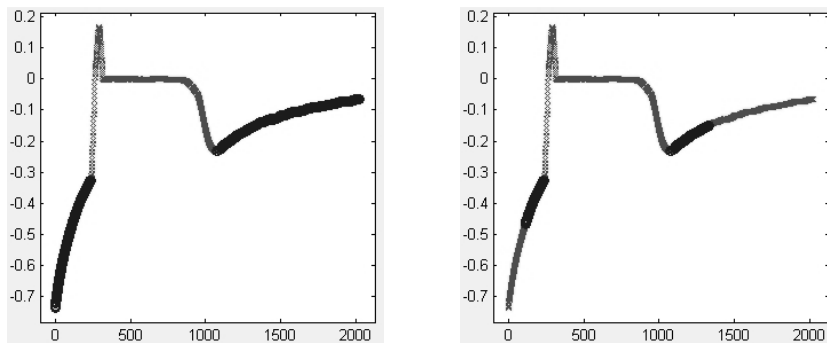
Figure 2.15: Exclusion factors of Tdot vs. t data for wide and narrow scales respectively.

The curve fitting of several methods used in this section are seen in Figures 2.16-2.18. Types of curve fittings and their results are shown in Table 2.10.
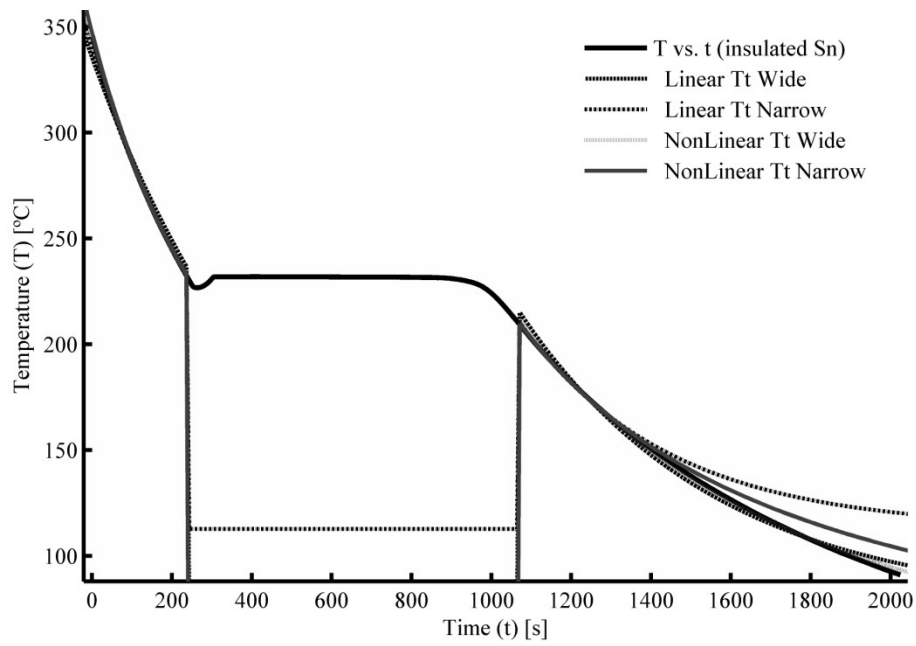
Figure 2.16: Functions of curve fitting tried on cooling curve. Equation 2.36 and 2.39 were executed on the T vs. t graph, named linear and nonlinear respectively. Each choice is repeated for the wide and narrow intervals.
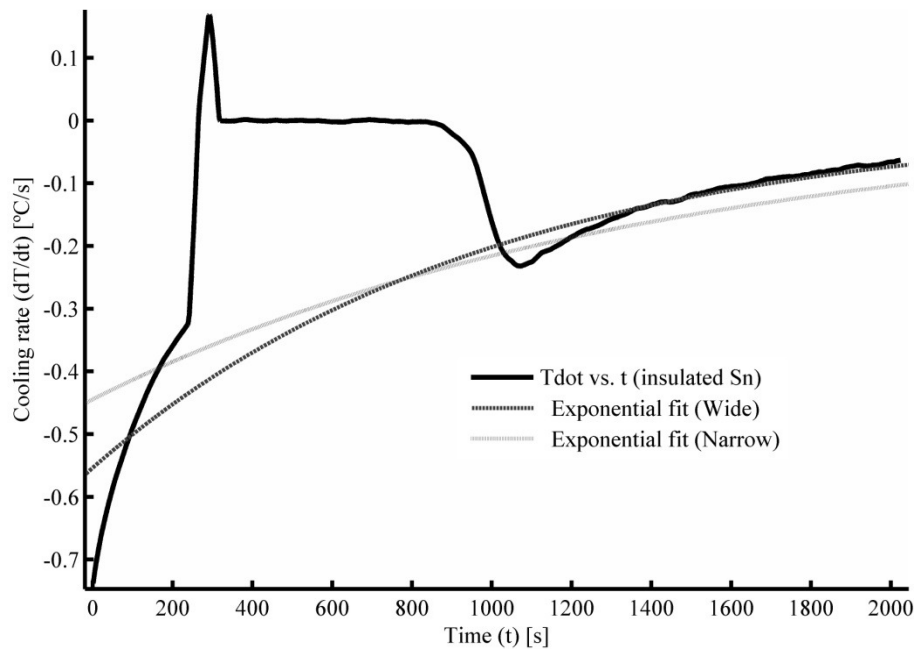
Figure 2.17: Functions of curve fitting tried on cooling curve. Equation 2.37 was executed on the Tdot vs. t graph, called exponential fit. Each choice is repeated for the wide and narrow intervals.
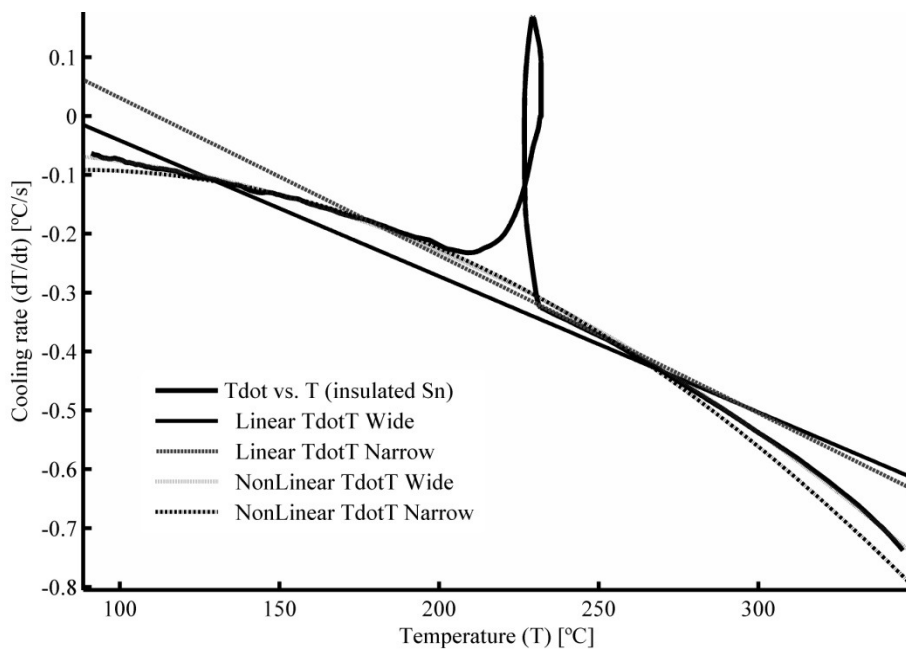
Figure 2.18: Functions of curve fitting tried on cooling curve. Equation 2.35 and 2.38 were executed on the Tdot vs. T graph, called linear and nonlinear respectively. Each choice is repeated for the wide and narrow intervals.

Table 2.7: Types of curve fitting with their results. R-square values of each fit, calculated latent heat per specific heat values (L/c), and its percentage deviations from literal value (error) are seen.

Type of Equation	Data set used in curve fitting	Fit function	Type of exclusion	R-Square	L/c [^{0}C]	Percentage error [%]
Linear	Tdot vs. T	Equation 2.35	Wide	0.9518	261.59	5.06
			Narrow	0.9852	241.40	-3.05
	Tdot vs. t	Equation 2.37	Wide	0.9410	222.95	-10.46
			Narrow	0.9552	211.55	-15.04
	T vs. t	Equation 2.36	Wide	0.9979	236.49	-5.02
			Narrow	0.9999	240.32	-3.49
Quadratic	Tdot vs. T	Equation 2.38	Wide	0.9989	231.83	-6.90
			Narrow	0.9964	230.42	-7.46
	T vs. t	Equation 2.39	Wide	0.9996	238.12	-4.37
			Narrow	1.0000	234.80	-5.70

2.4 Summary of Evaluations

The results of curve fitting from Table 2.7 show us the general profile for thermally insulated solidification experiment. The summary of the table may be written as follows:

1. Linear equations are more reliable than nonlinear equations, quadratic and cubic, for the closeness of the latent heat calculation although nonlinear functions give higher R-Squares in curve fitting.
2. Traditional Newtonian zero curve (NBL) has significantly different results from the other baselines and literal values (Equation 2.37).
3. There is no significant difference between the usage of derivative data and temperature data, unless the initial conditions is assumed the same.
4. Narrow intervals for the linear approach produce consistent results.

Considering the results of the simplified experiments, some suggestions may be made to the possible restrictions in Section 2.3. The most important problem on the variations of data analysis is the ignorance of the different initial conditions in curve fitting session. Two different integration constants for both phases should be taken into account when curve fitting is applied. Using temperature data, rather than temperature derivative, will give more reliable outputs. Moreover, the interval of temperature should be so narrow that Taylor approximation can be satisfied. By the experience of several trials, including 50 ^{0}C below and above the melting temperature may be an ideal interval. The ambient temperature should not be limited to the measured room temperature, but it should be set free to be calculated by the curve fitting.

Scanning the percentage errors in Table 2.4, it is seen that mold-insulated experiment, Sn3, is reliable for all methods. Thermal contact of the metal-mold system violates NLC proportional with the thermal mass of the mold [19]. It shows that one of the significant restrictions of NTA is the ignorance of thermal capacity of the mold.

Although variations of thermal properties in temperature and radiative contributions require high degree polynomial approximation of the cooling rate, the experimental outcomes show that the linear approximation is enough for a narrow interval. Linear Tdot vs. T and linear T vs. t in Equations 2.35 and 2.36 gave less error than the nonlinear equations.

In conclusion, a thermal analysis researcher should

- take the thermal capacity of the mold into account.
- assume linear approximation, and set free the ambient temperature.
- take a narrow interval which is in the limit of 50 ^{0}C below and above melting temperature.
- consider different initial conditions for both phases.

CHAPTER 3

SUGGESTION OF A NEW MODEL: TWO CAPACITIVE SYSTEM BASELINE (TCSBL)

The effects of mold's temperature are significant in the cooling curve of the cast; thus, its latent heat and solid fraction evolution are determined by considering these effects. The temperature of the metal at the initial stages of cooling falls more rapidly than that at the final stages because the mold's temperature is low and absorbs the heat of the metal at a high rate. At the final stages, the metal's and mold's temperatures become close to each other, and cooling rate decreases. Figure 3.1 shows the photo and figure of the experimental setup that measures the temperatures of pure tin and sand mold at the same time. Figure 3.2 shows the experimental cooling curves of both thermocouples.
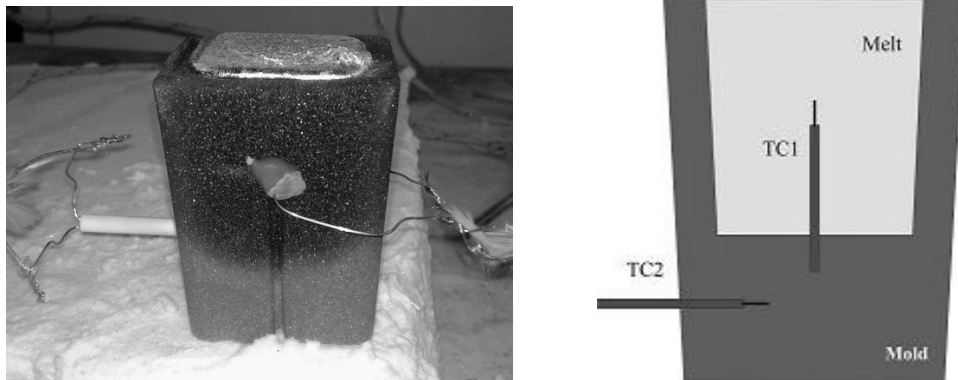
Figure 3.1: Two thermocouples placed in the metal and mold.
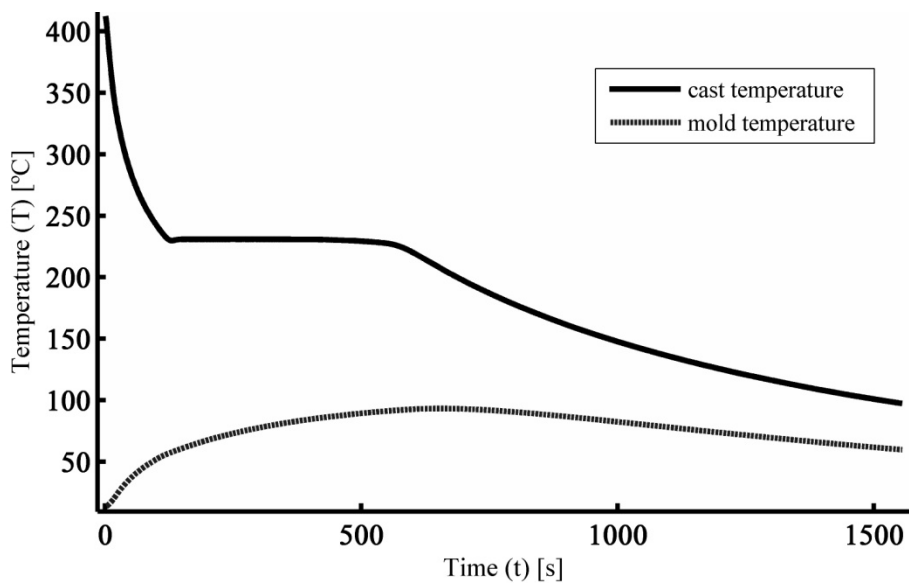
Figure 3.2: Temperature vs. time graphs of the metal and mold.

It is seen that metal's temperature falls more rapidly than it should at the beginning of the cooling. This phenomenon may be observed better by analyzing Tdot – T graph of the metal's temperature by considering the Newton's law of cooling. Figure 3.3 shows that cooling parameter is very different in the initial and final stages of cooling session.

$$\frac{dT}{dt} = -\frac{hA}{V\rho c_p}\left(T - T_\infty\right)$$ (3.1)
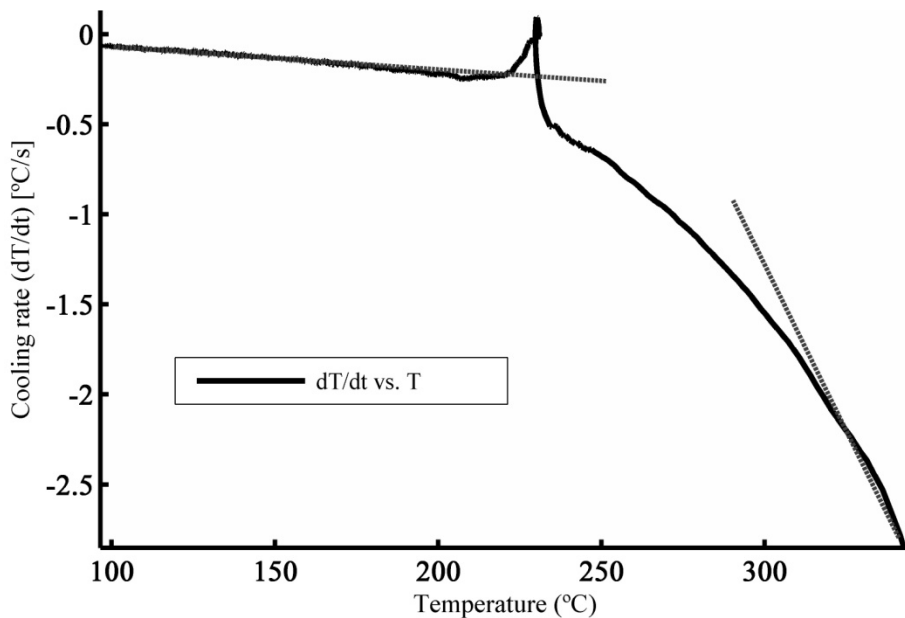
Figure 3.3: Cooling rate of the metal vs. its temperature.

Two mathematical models were proposed in this study to evaluate this effect. One is to consider mold as a heat capacitor in a similar way for electrical discharging capacitor system; the other is to make a linearization of heat flux function in terms of the temperatures of the metal and mold.

3.1 Thermal Circuit Analogy: Mold as a Heat Capacitor

3.1.1 Derivation of the equation

Convective heat transfer can be analyzed from

$$q_{conv} = hA(T - T_\infty)$$ (3.2)

where q_{conv} is the heat flux through the interface of two media, h is the heat transfer coefficient between two media, A is the surface area of the interface, T and T_∞ are the temperatures of the media. For a simple convectional process, T and T_∞ are the temperatures of the metal and surroundings.

It can be rewritten to draw an electrical analogy [6].

$$q_{cov} = \frac{(T - T_\infty)}{1/hA}$$ (3.3)

The terms: q_{conv}, T, and $1/hA$ remind of electrical current, resistance, and potential in the Ohm's law respectively. Thus, thermal resistance for convectional change of temperature is

$$R_{th} = \frac{1}{hA}$$ (3.4)

where R_{th} is thermal resistance [3].

Another thermal concept that can be transformed from the electrical circuit is heat capacity (Equation 3.5). It is obvious that heat capacity corresponds to electrical capacity, so the cooling equation (Equation 3.6) is rewritten as in Equation 3.7.

$$C_{th} = V\rho c_p$$ (3.5)

$$V\rho c_p \frac{dT}{dt} = -hA(T - T_\infty)$$ (3.6)

$$\frac{dT}{dt} = -\frac{1}{RC}(T - T_\infty)$$

<div align="right">(3.7)</div>

However, there are two capacitors in a sand mold casting process: One is the hot metal; the other is the chill mold. They are represented by full and empty capacitors respectively. Figure 3.4 shows the dimensions, thermal resistors, and capacitors on the picture of the mold-metal system.
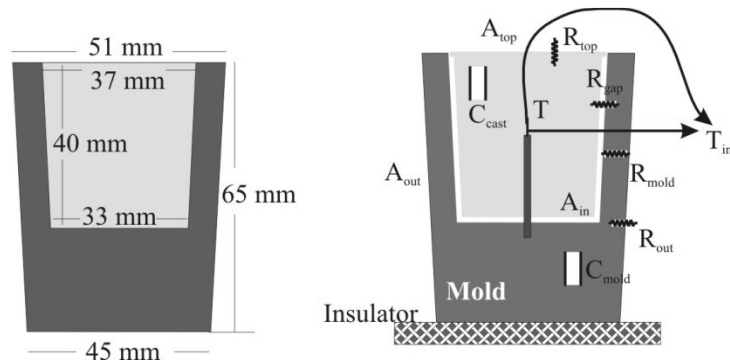
Figure 3.4: Dimensions of the quick cup and resistance-capacitance representation for heat transfer.

The abrupt changes in the temperature mean thermal resistance for the heat transfer. These changes are seen on the top surface, in the air gap between metal and mold, and within the mold itself because of the low thermal conductivity of the mold. The electrical representation of this system is shown in Figure 3.5.
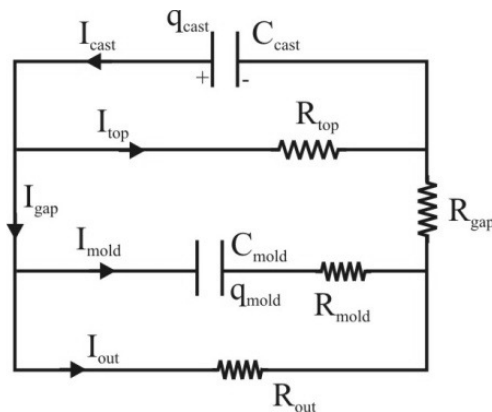
Figure 3.5: RC circuit representation of metal-mold system in terms of electrical devices.

It can be imagined that the metal is a full capacitor, while the mold is an empty capacitor. In addition, the heat flux flows through a surface is imagined as electrical current. The definitions of terms of Figure 3.5 are explained in Table 3.1 with its symbols and units [27].

Table 3.1: Comparison of electrical and thermal quantities [27].

Electrical quantities	Thermal quantities
Electrical charge (q) [coulomb]	Thermal energy (Q) [joule]
Voltage (V) [volt]	Relative temperature (u) [kelvin]
Current (I) [ampere]	Thermal power through a surface (P=-dQ/dt) [watt]
Electrical capacitance (C) [farad]	Thermal capacitance (C=Vρc$_p$) [joule/kelvin]
Electrical resistance (R) [ohm]	Thermal resistance (kelvin/watt)

In the RC circuit diagram (Figure 3.5), Kirchhoff's rules may be applied as in Equations 3.8-3.12. Matrix forms of this linear set of equations with 5 variables are shown in Equations 3.13 and 3.14 with its solution.

$$\frac{q_{cast}}{C_{cast}} = I_{top}R_{top} \tag{3.8}$$

$$\frac{q_{mold}}{C_{mold}} = I_{out}R_{out} - I_{mold}R_{mold} \tag{3.9}$$

$$\frac{q_{cast}}{C_{cast}} = I_{out}R_{out} + I_{gap}R_{gap} \tag{3.10}$$

$$I_{cast} = I_{gap} + I_{top} \tag{3.11}$$

$$I_{gap} = I_{mold} + I_{out} \tag{3.12}$$

$$\begin{pmatrix} q_{cast}/C_{cast} \\ q_{mold}/C_{mold} \\ q_{cast}/C_{cast} \\ 0 \\ 0 \end{pmatrix} = \begin{pmatrix} 0 & 0 & R_{top} & 0 & 0 \\ 0 & -R_{mold} & 0 & R_{out} & 0 \\ 0 & 0 & 0 & R_{out} & R_{gap} \\ 1 & 0 & -1 & 0 & -1 \\ 0 & 1 & 0 & 1 & -1 \end{pmatrix} \cdot \begin{pmatrix} I_{cast} \\ I_{mold} \\ I_{top} \\ I_{out} \\ I_{gap} \end{pmatrix} \tag{3.13}$$

$$\begin{pmatrix} I_{cast} \\ I_{mold} \\ I_{top} \\ I_{out} \\ I_{gap} \end{pmatrix} = \begin{pmatrix} 0 & 0 & R_{top} & 0 & 0 \\ 0 & -R_{mold} & 0 & R_{out} & 0 \\ 0 & 0 & 0 & R_{out} & R_{gap} \\ 1 & 0 & -1 & 0 & -1 \\ 0 & 1 & 0 & 1 & -1 \end{pmatrix}^{-1} \cdot \begin{pmatrix} q_{cast}/C_{cast} \\ q_{mold}/C_{mold} \\ q_{cast}/C_{cast} \\ 0 \\ 0 \end{pmatrix} \tag{3.14}$$

The solution for currents in terms of q, C, and R values of the system is given in Equation 3.14. The matrix operations were done by MATLAB Symbolic Math Tool. The results are shown in Equations 3.15-3.19.

$$I_{cast} = \frac{q_{cast}}{C_{cast}} \left(\frac{1}{R_{top}} + \frac{R_{mold} + R_{out}}{R_{gap}R_{mold} + R_{gap}R_{out} + R_{out}R_{mold}} \right)$$
$$- \frac{q_{mold}}{C_{mold}} \left(\frac{R_{out}}{R_{gap}R_{mold} + R_{gap}R_{out} + R_{out}R_{mold}} \right) \tag{3.15}$$

$$I_{mold} = \frac{q_{cast}}{C_{cast}} \left(\frac{R_{out}}{R_{gap}R_{mold} + R_{gap}R_{out} + R_{out}R_{mold}} \right)$$
$$- \frac{q_{mold}}{C_{mold}} \left(\frac{R_{gap} + R_{out}}{R_{gap}R_{mold} + R_{gap}R_{out} + R_{out}R_{mold}} \right) \tag{3.16}$$

$$I_{top} = \frac{q_{cast}}{R_{top}C_{cast}} \tag{3.17}$$

$$I_{out} = \frac{q_{cast}}{C_{cast}} \left(\frac{R_{mold}}{R_{gap}R_{mold} + R_{gap}R_{out} + R_{out}R_{mold}} \right)$$
$$+ \frac{q_{mold}}{C_{mold}} \left(\frac{R_{gap}}{R_{gap}R_{mold} + R_{gap}R_{out} + R_{out}R_{mold}} \right) \tag{3.18}$$

$$I_{gap} = \frac{q_{cast}}{C_{cast}} \left(\frac{R_{mold} + R_{out}}{R_{gap}R_{mold} + R_{gap}R_{out} + R_{out}R_{mold}} \right)$$
$$- \frac{q_{mold}}{C_{mold}} \left(\frac{R_{out}}{R_{gap}R_{mold} + R_{gap}R_{out} + R_{out}R_{mold}} \right) \tag{3.19}$$

Equations 3.15 and 3.16 are important because it involves information about the capacities and temperatures of the metal-mold system. A two dimensional system of the

differential equation can be obtained by using the definition of capacitance (Equation 3.20) and conservation of charge (Equations 3.21 and 3.22).

$$q = CV \tag{3.20}$$

$$I_{cast} = -\dot{q}_{cast} = -C_{cast}\dot{V}_{cast} \tag{3.21}$$

$$I_{mold} = \dot{q}_{mold} = C_{mold}\dot{V}_{mold} \tag{3.22}$$

If Equations 3.21 and 3.22 are written in Equations 3.15 and 3.16, differential equation set in terms of voltages are obtained as in Equations 3.23 and 3.24. The coefficients of voltages are also named in Equations 3.25-3.28.

$$\dot{V}_{cast} = -\frac{V_{cast}}{C_{cast}}\left(\frac{1}{R_{top}} + \frac{R_{mold} + R_{out}}{R_{gap}R_{mold} + R_{gap}R_{out} + R_{out}R_{mold}}\right)$$
$$+ \frac{V_{mold}}{C_{cast}}\left(\frac{R_{out}}{R_{gap}R_{mold} + R_{gap}R_{out} + R_{out}R_{mold}}\right) \tag{3.23}$$

$$\dot{V}_{mold} = \frac{V_{cast}}{C_{mold}}\left(\frac{R_{out}}{R_{gap}R_{mold} + R_{gap}R_{out} + R_{out}R_{mold}}\right)$$
$$- \frac{V_{mold}}{C_{mold}}\left(\frac{R_{gap} + R_{out}}{R_{gap}R_{mold} + R_{gap}R_{out} + R_{out}R_{mold}}\right) \tag{3.24}$$

$$p_1 = \frac{1}{C_{cast}}\left(\frac{1}{R_{top}} + \frac{R_{mold} + R_{out}}{R_{gap}R_{mold} + R_{gap}R_{out} + R_{out}R_{mold}}\right) \tag{3.25}$$

$$p_2 = \frac{1}{C_{cast}}\left(\frac{R_{out}}{R_{gap}R_{mold} + R_{gap}R_{out} + R_{out}R_{mold}}\right) \tag{3.26}$$

$$p_3 = \frac{1}{C_{mold}}\left(\frac{R_{out}}{R_{gap}R_{mold} + R_{gap}R_{out} + R_{out}R_{mold}}\right) \tag{3.27}$$

$$p_4 = \frac{1}{C_{mold}}\left(\frac{R_{gap} + R_{out}}{R_{gap}R_{mold} + R_{gap}R_{out} + R_{out}R_{mold}}\right) \tag{3.28}$$

Thermal correspondence of voltage is the temperature difference with respect to ambient temperature. Equations 3.29 and 3.30 transform electrical circuit statement of equations

to thermal statement. Equation 3.31, where p_1, p_2, p_3, and p_4 are defined above, is the final differential equation system in terms of relative temperatures of metal and mold (u_1 and u_2 respectively).

$$V_{cast} \rightarrow T_{cast} - T_\infty = u_1 \qquad (3.29)$$

$$V_{mold} \rightarrow T_{mold} - T_\infty = u_2 \qquad (3.30)$$

$$\frac{d}{dt}\begin{pmatrix} u_1 \\ u_2 \end{pmatrix} = \begin{pmatrix} -p_1 & p_2 \\ p_3 & -p_4 \end{pmatrix} \cdot \begin{pmatrix} u_1 \\ u_2 \end{pmatrix} \qquad (3.31)$$

The intended differential equation has been obtained without any phase transformation source term. One more modification should be done in order to include phase transformational source term containing solid fraction and latent heat. The phase transformational heat source occurs in metal as a thermal power term which electrically corresponds to a current source. Therefore, in the current of the cast, it appears with the same direction with the cast current. These transformations are explained in Equations 3.32-3.34 where ΔH_f is total enthalpy of solidification, C_{cast} is thermal capacity of the cast and f_s is the solid fraction.

$$I_{cast} \rightarrow I_{cast} + \Delta H_f \dot{f}_s \qquad (3.32)$$

$$-C_{cast}\dot{V}_{cast} \rightarrow -C_{cast}\dot{V}_{cast} + \Delta H_f \dot{f}_s \qquad (3.33)$$

$$\dot{V}_{cast} \rightarrow \dot{V}_{cast} + \frac{\Delta H_f}{-C_{cast}} \dot{f}_s \qquad (3.34)$$

Total enthalpy and heat capacity can be stated in terms of volume (V), density (ρ), latent heat of fusion (L_f), and specific heat (c_p) as in Equation 3.35, so the transformation in Equation 3.34 becomes Equation 3.36.

$$\frac{\Delta H_f}{C_{cast}} = \frac{V\rho L_f}{V\rho c_p} = \frac{L_f}{c_p} \qquad (3.35)$$

$$\dot{u}_1 \rightarrow \dot{u}_1 - \frac{L_f}{c_p} \dot{f}_s \qquad (3.36)$$

When the transformed temperature derivative in Equation 3.36 is replaced into Equation 3.31, the general heat equation system with phase transformation is obtained as in Equations (3.37-39). The term θ_{PT} defines the interval of solidification in which solid

fraction occurs. Its definitions are seen in Equation 3.39 where t_s and t_e are start and end times of solidification, and θ is Heaviside step function. In this derivation, it is assumed that there is no heat sources or sinks in the mold. A burning reaction, maybe, in sand molds may be formed. However, it is assumed that its rate of heat is negligible.

$$\dot{u}_1 = -p_1 u_1 + p_2 u_2 + \frac{L_f}{c_p} \dot{f}_s \, \theta_{PT} \tag{3.37}$$

$$\dot{u}_2 = p_3 u_1 - p_4 u_2 \tag{3.38}$$

$$\theta_{PT} = \theta(t - t_s) - \theta(t - t_e) = \begin{cases} 1 & \text{if } t_s \leq t \leq t_e \\ 0 & \text{otherwise} \end{cases} \tag{3.39}$$

3.1.2 Calculating Solid Fraction

In the previous section, we have developed a differential equation system in terms of metal's and mold's relative temperatures: u_1 and u_2 respectively. Actually, these temperatures correspond to the average temperatures of the materials through its volume. Therefore, it is hard to measure the temperature of the mold, while the metal's average temperature can be measured because of its high conductivity. In a typical Newtonian thermal experiment, a thermocouple is placed at the center of the cup, and it records the instantaneous temperature at every second. Therefore, in the heat equation generated, u_1 is a known data, while u_2 is an unknown data. For u_2, all we know is its initial condition at t=0. At the pouring time, the temperature of the mold is at the ambient temperature, so its relative temperature to the ambient, must be zero. Other known parameters about the system are: start and end time of solidification (t_s and t_e) and solid fraction boundary conditions. All the information is seen in Equations 3.40-3.42.

$$\dot{u}_1(t) = -p_1 u_1(t) + p_2 u_2(t) + \frac{L_f}{c_p} \dot{f}_s(t) \tag{3.40}$$

$$\dot{u}_2(t) = p_3 u_1(t) - p_4 u_2(t) \tag{3.41}$$

$$f_s(t_s) = 0, \quad f_s(t_e) = 1, \quad u_2(0) = 0 \tag{3.42}$$

$$f_s(t) = \begin{cases} 0 & t \leq t_s \\ f(t) & t_s < t < t_e \\ 1 & t_e \leq t \end{cases} \qquad \dot{f}_s(t) = \begin{cases} 0 & t < t_s \\ \dot{f}(t) & t_s \leq t \leq t_e \\ 0 & t_e < t \end{cases} \qquad (3.43)$$

Finding the solidification parameter (L_f/c_p) and solid fraction f_s, which are the main aims of this study, depends on calculating the parameters of the differential equation correctly. Unknown parameters of the suggested equations (Equation 3.40-3.42) are p_1, p_2, p_3, p_4, L_f/c_p, t_s, and t_e. An equation giving solid fraction should be written first in order to understand what parameters to find primarily. Mold's temperature (u_2) may be written in terms of metal's temperature (u_1) because u_2 corresponds the average temperature of the mold, which is hard to measure owing to its low thermal conductivity. Equation 3.41 is a first order linear differential equation, so it can be solved by the help of integrating factor [18]. When Equation 3.44 is multiplied by the integrating factor of $\exp(p_4 t)$, it yields a derivative of a multiplication.

$$\dot{u}_2 + p_4 u_2 = p_3 u_1 \qquad (3.44)$$

$$\dot{u}_2 e^{p_4 t} + p_4 u_2 e^{p_4 t} = p_3 u_1 e^{p_4 t} \qquad (3.45)$$

$$\frac{d}{dt}\left(u_2 e^{p_4 t}\right) = p_3 u_1 e^{p_4 t} \qquad (3.46)$$

$$\left[u_2 e^{p_4 t}\right]_0^t = p_3 \int_0^t u_1 e^{p_4 t}\, dt \qquad (3.47)$$

With the help of Equations 3.47 and 3.48, Equation 3.49, giving the average temperature of the mold, is obtained.

$$u_2(0) = 0 \qquad (3.48)$$

$$u_2 = p_3 e^{-p_4 t} \int_0^t u_1 e^{p_4 t}\, dt \qquad (3.49)$$

If Equation 3.49 is replaced in Equation 3.40, it gives

$$\dot{u}_1 = -p_1 u_1 + p_2 p_3 e^{-p_4 t} \int_0^t u_1 e^{p_4 t}\, dt + \frac{L_f}{c_p}\dot{f}_s \qquad (3.50)$$

If Equation 3.50 is integrated between t_s and t_e, latent heat formulation is obtained by the help of the initial conditions in Equation 3.42,

54

$$\int_{t_s}^{t_e} \dot{u}_1 dt = \int_{t_s}^{t_e} \left[-p_1 u_1 + p_2 p_3 e^{-p_4 t} \int_0^{t'} u_1(t') e^{p_4 t'} dt' + \frac{L_f}{c_p} \dot{f}_s \right] dt \tag{3.51}$$

$$u_1(t_e) - u_1(t_s) = \int_{t_s}^{t_e} \left[-p_1 u_1 + p_2 p_3 e^{-p_4 t} \int_0^{t'} u_1(t') e^{p_4 t'} dt' \right] dt$$
$$+ \frac{L_f}{c_p} \left(f_s(t_e) - f_s(t_s) \right) \tag{3.52}$$

$$\frac{L_f}{c_p} = u_1(t_e) - u_1(t_s) + \int_{t_s}^{t_e} \left[p_1 u_1 - p_2 p_3 e^{-p_4 t} \int_0^t u_1(t') e^{p_4 t'} dt' \right] dt \tag{3.53}$$

Taking integral of Equation 3.51 between t and t_s values, solid fraction evolution is found.

$$f_s(t) = \frac{u_1(t) - u_1(t_s) + \int_{t_s}^t \left[p_1 u_1 - p_2 p_3 e^{-p_4 t} \int_0^t u_1(t') e^{p_4 t'} dt' \right] dt}{L_f / c_p} \tag{3.54}$$

As seen in the formulations of the latent heat and solid fraction, the parameters that will be searched are p_1, p_4, and $p_2.p_3$ values. t_s and t_e values are determined from the cooling or cooling rate curve mentioned in Chapter 1.

3.1.3 Finding the Parameters

Before calculating solid fraction and the solidification parameter (L_f/c_p), one should calculate the parameters p_1, p_4, and $p_2.p_3$. They can be calculated by two ways: theoretical and experimental. Theoretical calculations require information about heat transfer coefficients, dimensions and heat capacities by the help of Equations 3.25-3.28. However, experimental calculations gather information from the cooling curve analysis.

3.1.3.1 Theoretical Calculations of the Parameters

Thermal resistance and capacitance formulas for convective and conductive heat transfer are shown in Equations 3.55 and 3.56 [3]. The definitions of the symbols are given in Table 3.2.

$$R_{top} = \frac{1}{h A_{top}} \qquad R_{out} = \frac{1}{h A_{out}}$$
$$R_{gap} = \frac{1}{h_{gap} A_{in}} \qquad R_{mold} = \frac{2d}{k_{mold}(A_{in} + A_{out})} \tag{3.55}$$

$$C_{cast} = V_{cast} \rho_{cast} c_{p,cast} \qquad C_{mold} = V_{mold} \rho_{mold} c_{p,mold} \tag{3.56}$$

Table 3.2: Definitions of the symbols used for the calculation of thermal parameters.

Symbol	Definition
h_{air}	convectional heat transfer coefficient due to free convection with the medium
h_{gap}	gap heat transfer coefficient
d	Thickness of the mold
A_{in}	Area of the inside surface of the mold
A_{out}	Area of the outside surface of the mold
A_{top}	Area of the top surface of the metal
V_{cast}	Volume of the casting metal
V_{mold}	Volume of the mold
k_{mold}	Thermal conductivity of the mold
ρ_{cast}	Density of the casting metal
ρ_{mold}	Density of the mold
c_{cast}	Specific heat of the casting metal
c_{mold}	Specific heat of the mold
R_{top}	Thermal resistance of the top surface due to air convection
R_{out}	Thermal resistance of the outside surface of the mold due to air convection
R_{mold}	Thermal resistance of the mold due to conduction
R_{gap}	Thermal resistance of the side surface of the metal due to gap heat transfer

The convectional heat transfer coefficient was calculated by

$$h = Nu \frac{k}{L} \tag{3.57}$$

where Nu is the Nusselt number, k is the thermal conductivity of air and L is the characteristic length (L=0.065 m in this experiment). The Nusselt number is calculated by

$$Nu = C \cdot (Pr \cdot Gr)^m \tag{3.58}$$

where Pr and Gr are Prandtl and Grashof numbers. C and m are the parameters which will be found from Table 7 at page 22 of [ref. 19]. Grashof number is given by

$$Gr = \frac{g \beta \rho^2}{\mu^2} (T_0 - T_\infty) \tag{3.59}$$

where g is the gravitational acceleration , β is $1/T_f$, (where $T_f=(T_0+T_\infty)/2$), ρ is the density, and μ is the viscosity of air for T_f value (from Table 4 at page 19 of [ref. 19]). For the cooling experiment of Pure tin, T_0 and T_∞ were taken 500 K and 289 K. T_f is (500+289)/2=394.5. The parameters for 394.5 K are listed in the table below. According

to the calculations above, the values of the parameters for the thermal circuit are listed in Table 3.4.

Table 3.3: Parameters and properties of air at 394.5 K in SI units.

g [m.s^{-2}]	9.80
β [K^{-1}] x10^{-3}	2.54
ρ [kg.m^{-3}]	0.90
μ [kg.m^{-1}.s^{-1}] x10^{-5}	2.265
k [Wm^{-1}K^{-1}] x10^{-2}	3.32
Pr	0.69
C	0.59
m	0.25

Table 3.4: Results of the calculations for the thermal circuit in SI units.

h [Wm^{-2}K^{-1}]	10.70	R_{top} [KW^{-1}]	68.20
h_{gap} [Wm^{-2}K^{-1}]	400.00	R_{out} [KW^{-1}]	7.50
d [m]	0.01	R_{mold} [KW^{-1}]	2.02
k_{mold} [Wm^{-1}K^{-1}]	0.52	R_{gap} [KW^{-1}]	0.38
A_{out} [m^2] x10^{-3}	1.25e-02	C_{cast} [JK^{-1}]	74.85
A_{in} [m^2] x10^{-3}	6.50e-03	C_{mold} [JK^{-1}]	130.00
A_{top} [m^2] x10^{-3}	1.40e-03		

The matrix and its eigenvectors of Equation 3.31 are finally obtained in Equations 3.60 and 3.61 with eigenvalues λ_1 and λ_2 which are -0.0095 and -0.0006 respectively.

$$M = \begin{bmatrix} -p_1 & p_2 \\ p_3 & -p_4 \end{bmatrix} = \begin{bmatrix} -0.0069 & 0.0053 \\ 0.0031 & -0.0032 \end{bmatrix} \tag{3.60}$$

$$v_1 = \begin{pmatrix} -0.90 \\ 0.44 \end{pmatrix} \qquad v_2 = \begin{pmatrix} -0.64 \\ -0.76 \end{pmatrix} \tag{3.61}$$

3.1.3.2 Experimental Calculations of the Parameters

Cooling curve analysis is required to find the parameters experimentally. Since metals temperature is known, they can be calculated from curve fitting of the solution of the differential equation. The solution for u_1 of no phase transformation case of Equation 3.31 is a typical eigenvalue problem in two dimensions. Its general solution is shown in Equation 3.62 in vector format, where λ_1 and λ_2 are the eigenvalues, v_1 and v_2 are the corresponding eigenvectors of the eigenvalues, A_1 and A_2 are integration constants coming from the initial conditions. However, we know that the eigenvalues must be negative numbers because the metal-mold system is a decay system, so the eigenvalues can be notated by negative real numbers, for example, $-b$ and $-d$. Together with the initial condition of the mold's temperature in Equation 3.48, the relative average temperatures of metal and mold, u_1 and u_2, are written in Equations 3.62 and 3.63, where a, c and A are the integration constants, representing the initial conditions.

$$\vec{u} = A_1 \vec{v}_1 e^{\lambda_1 t} + A_2 \vec{v}_2 e^{\lambda_2 t} \tag{3.62}$$

$$u_1 = ae^{-bt} + ce^{-dt} \tag{3.63}$$

$$u_2 = Ae^{-bt} - Ae^{-dt} \tag{3.64}$$

However, the integration constants should be different for the solid and liquid phases. The phase transformational term between two phases changes the initial conditions, and the system goes on with the same thermal parameters but with different start points. Therefore, the temperature evolutions must be written by the same eigenvalues ($-b$ and $-d$) but different constants (a and c) for two phases. Equation 3.65 is the right statement for the temperature of metal, where θ is Heaviside step function.

$$u_1 = \left(a_l e^{-bt} + c_l e^{-dt} \right) \theta(t_s - t) + \left(a_s e^{-bt} + c_s e^{-dt} \right) \theta(t - t_e) \tag{3.65}$$

In the expression of u_1, a_l and c_l are the integration constants for liquid case, while a_s and c_s are for the solid phase. t_s and t_e represent start and end of solidification defining the interval of validity for the parameters with the help of Heaviside step function. The parameters a_l, c_l, a_s, c_s, b and d was calculated by using curve fitting tool of MATLAB R2010a. Actually the main interest is to find p_1, p_4 and $p_2.p_3$ of the matrix and these parameters are used in the eigenvalue problem shown in Equation 3.66 [28]. The solution of the problem is explained in Equations 3.67-3.71.

$$\begin{pmatrix} -p_1 & p_2 \\ p_3 & -p_4 \end{pmatrix} \cdot \begin{pmatrix} u_1 \\ u_2 \end{pmatrix} = \lambda \begin{pmatrix} u_1 \\ u_2 \end{pmatrix} \tag{3.66}$$

$$\begin{vmatrix} -p_1 - \lambda & p_2 \\ p_3 & -p_4 - \lambda \end{vmatrix} = 0 \tag{3.67}$$

$$\lambda^2 + (p_1 + p_4)\lambda + p_1 p_4 - p_2 p_3 = 0 \tag{3.68}$$

$$\lambda_{1,2} = \frac{-(p_1 + p_4) \pm \sqrt{(p_1 + p_4)^2 - 4(p_1 p_4 - p_2 p_3)}}{2} \tag{3.69}$$

$$b = \frac{(p_1 + p_4) - \sqrt{(p_1 + p_4)^2 - 4(p_1 p_4 - p_2 p_3)}}{2} \tag{3.70}$$

$$d = \frac{(p_1 + p_4) + \sqrt{(p_1 + p_4)^2 - 4(p_1 p_4 - p_2 p_3)}}{2} \tag{3.71}$$

From the above equations, it is deduced that:

$$b + d = p_1 + p_4 \tag{3.72}$$

$$bd = p_1 p_4 - p_2 p_3 \tag{3.73}$$

Initial condition for u_2 can be used to separate p_1 and p_4 in Equation 3.72 and 3.73. For the no- phase transformation case of Equation 3.37, the equation at t=0 is Equation 3.74.

$$\dot{u}_1(0) = -p_1 u_1(0) + p_2 u_2(0) \tag{3.74}$$

In this equation, $u_2(0)$ is zero, and initial temperatures and derivatives can be calculated by Equation 3.65. u_1 and its derivatives with its initial values in terms of curve fit parameters are shown in Equations 3.75-3.78.

$$u_1 = \left(a_l e^{-bt} + c_l e^{-dt}\right)\theta(t_s - t) + \left(a_s e^{-bt} + c_s e^{-dt}\right)\theta(t - t_e) \tag{3.75}$$

$$\dot{u}_1 = \left(-ba_l e^{-bt} - dc_l e^{-dt}\right)\theta(t_s - t) + \left(-ba_s e^{-bt} - dc_s e^{-dt}\right)\theta(t - t_e) \tag{3.76}$$

$$u_1(0) = a_l + c_l \tag{3.77}$$

$$\dot{u}_1(0) = -ba_l - dc_l \tag{3.78}$$

Writing Equations 3.77 and 3.78 into 3.74, it yields

$$-ba_l - dc_l = -p_1(a_l + c_l)$$ (3.79)

$$p_1 = \frac{ba_l + dc_l}{(a_l + c_l)}$$ (3.80)

Once p_1 is found, other parameters can be calculated by Equations 3.72 and 3.73 as follows.

$$p_4 = b + d - \frac{ba_l + dc_l}{(a_l + c_l)} = \frac{da_l + bc_l}{(a_l + c_l)}$$ (3.81)

$$p_2 p_3 = \frac{(da_l + bc_l)}{(a_l + c_l)} \frac{(ba_l + dc_l)}{(a_l + c_l)} - bd = \frac{a_l c_l (d - b)^2}{(a_l + c_l)^2}$$ (3.82)

The parameters required for latent heat and solid fraction calculation have been found (Equations 3.80-82). The formulation of Equations 3.53 and 3.54 can be interpreted by the curve fit parameters now. One-step further, we can calculate p_2 and p_3 approximately. From Equations 3.27 and 3.28, p_3 and p_4 are approximately equal because of the low resistance of the gap.

$$R_{gap} \approx 0 \Rightarrow p_3 \approx p_4$$ (3.83)

$$p_2 \approx \frac{a_l c_l (d - b)^2}{(a_l + c_l)(da_l + bc_l)}$$ (3.84)

From Equation 3.25-28, it is obvious that

$$\frac{p_2}{p_3} = \frac{C_{mold}}{C_{cast}}$$ (3.85)

$$C_{cast} \approx \frac{(da_l + bc_l)^2}{a_l c_l (d - b)^2} C_{mold}$$ (3.86)

The equation that provides the thermal capacity of cast was derived from the assumption of zero gap resistance. Therefore, it is not a reliable specific heat formulation. It only gives an idea for the range of specific heat of the metal in terms of heat capacity of the mold.

3.2 A More General Approach to the Metal-Mold System

In the previous section, we made some assumptions, so restrictions, to propose a linear differential model. These restrictions include:

1. Radiation was neglected.
2. Temperature dependence of the specific heat was not calculated.
3. Variable heat transfer coefficient due to the contraction or temperature change was omitted.
4. Heat transfer coefficients or specific heats of metals were assumed the same for all phases.

To include all these effect is very hard for such a simple thermal analysis. Rather we should try to linearize for the sake of simplification.

3.2.1 Cooling Rates as a Function of Temperatures

The average temperature derivatives of the metal-mold system may be thought as very complicated functions of the temperatures because the average temperatures are proportional to the heat fluxes of the elements of the system. These function may be

$$
\begin{aligned}
\dot{T}_1 &= F_1(T_1, T_2) \\
\dot{T}_2 &= F_2(T_1, T_2)
\end{aligned}
\tag{3.87}
$$

Taylor series expansions of a function with two variables around the point (x_0, y_0) is [29]

$$
F(x, y) = \sum_{n=0}^{\infty} \frac{1}{n!} \left((x - x_0) \frac{\partial}{\partial x} + (y - y_0) \frac{\partial}{\partial y} \right)^n F\big|_{x_0, y_0}
\tag{3.88}
$$

According to this general formula, Taylor's expansion of Equation 3.87 with the first degree approximation around melting and the average temperature of the mold during solidification (T_m, T_s) is given by

$$
\dot{T}_1 = F_1(T_m, T_s) + (T_1 - T_m) \frac{\partial F_1}{\partial T_1}\bigg|_{T_m, T_s} + (T_2 - T_s) \frac{\partial F_1}{\partial T_2}\bigg|_{T_m, T_s}
\tag{3.89}
$$

$$
\dot{T}_2 = F_2(T_m, T_s) + (T_1 - T_m) \frac{\partial F_2}{\partial T_1}\bigg|_{T_m, T_s} + (T_2 - T_s) \frac{\partial F_2}{\partial T_2}\bigg|_{T_m, T_s}
\tag{3.90}
$$

61

where T_m is the melting point of metal, and T_s is the average temperature of the mold during solidification. The point (T_m, T_s) was chosen for the center of expansion because the solid fraction, which we intend to find, occurs around this point. Equations 3.89 and 3.90 can be stated more simply as:

$$\dot{T}_1 = a_{10} + a_{11}T_1 + a_{12}T_2 \tag{3.91}$$

$$\dot{T}_2 = a_{20} + a_{21}T_1 + a_{22}T_2 \tag{3.92}$$

where the parameters a_{10}, ... a_{22} are constants coming from the Taylor expansion coefficients. It is very hard to calculate these parameters theoretically because they contain many parameters coming from radiative cooling, temperature dependence of specific heat, or heat transfer coefficients etc. One can say; however, these parameters do not represent directly the real heat transfer coefficients or thermal resistances anymore. One can say that Equations 3.91 and 3.92 are the same with the equation that developed in Section 3.1, which is Equation 3.31. They are close to each other in format and calculation structure, but the method of parameter determination differs. Since we thought the expansion around the melting point, we must consider a narrow temperature interval around the melting point for the curve fitting. Maybe, the most important difference is the stable points of the matrix system, which are different for two models.

The linear system in Equations 3.91 and 3.92 can be written in matrix notation as follows:

$$\begin{pmatrix} \dot{T}_1 \\ \dot{T}_2 \end{pmatrix} = \begin{pmatrix} a_{11} & a_{12} \\ a_{21} & a_{22} \end{pmatrix} \begin{pmatrix} T_1 \\ T_2 \end{pmatrix} + \begin{pmatrix} a_{10} \\ a_{20} \end{pmatrix} \tag{3.93}$$

$$\dot{\vec{T}} = \hat{M}\vec{T} + \vec{A}_0 \tag{3.94}$$

where M is the 2x2 coefficient matrix, and A_0 is the vector of non-homogeneous term. It can be made homogeneous by the operations through Equations 3.95-3.99.

$$\dot{\vec{T}} = \hat{M}\left(\vec{T} + \hat{M}^{-1}\vec{A}_0\right) \tag{3.95}$$

$$\dot{\vec{T}} = \hat{M}\left(\vec{T} - \vec{T}_\infty\right) \tag{3.96}$$

$$\vec{T}_\infty = \begin{pmatrix} T_{\infty,1} \\ T_{\infty,2} \end{pmatrix} = -\hat{M}^{-1}\begin{pmatrix} a_{10} \\ a_{20} \end{pmatrix} \tag{3.97}$$

$$\vec{T} - \vec{T}_\infty = \vec{u} \tag{3.98}$$

$$\dot{\vec{u}} = \hat{M}\vec{u} \tag{3.99}$$

where u vector is the relative temperatures of metal and mold with respect to their fixed points, which have not to be the real ambient temperature anymore. $T_{\infty,1}$ and $T_{\infty,2}$ represent the virtual asymptotic temperatures of metal and mold.

3.2.2 Finding the Parameters and Solid Fraction Evolution

The linear system constructed in section 3.2.1 has the same structure and solution for except for the ambient temperature interpretation. Two additional unknowns, the virtual ambient temperatures, must be calculated now. Since the mold has narrow temperature interval around the actual ambient temperature, it can be set by

$$T_{\infty,2} = T_{\infty} \tag{3.100}$$

where T_{∞} is the actual ambient temperature so it can be measured as room temperature in the time of the experiment. However, metal has higher temperatures than that of mold around solidification region (Figure 3.6). Therefore, its virtual ambient temperature should be higher than the real ambient temperature. The virtual ambient temperature of metal is calculated by fitting of Equation 3.101 with the measured temperature data of metal.

$$T_l = \left(a_l e^{-bt} + c_l e^{-dt}\right)\theta(\, t_s - t\,) + \left(a_s e^{-bt} + c_s e^{-dt}\right)\theta(\, t - t_e\,) + T_{\infty,1} \tag{3.101}$$

The rest of the procedure is the same with the method discussed in the previous section. The point is the fitted function and the part of temperature data for the curve fitting, which must be narrowed around the melting point. The method will be discussed in the next chapter in detail.
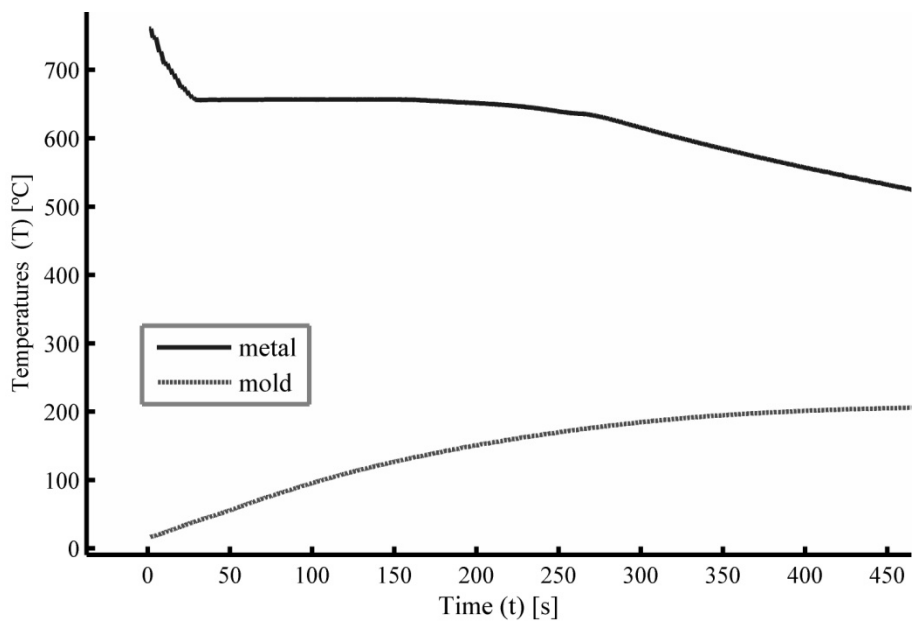
Figure 3.6: Temperatures of metal and mold in the solidification experiment of pure Aluminum.

CHAPTER 4

EXPERIMENTAL AND CALCULATIONAL DETAILS

The aim of Newtonian thermal analysis is to explain solidification process in terms of solid fraction evolution as a function of time and finding thermal characteristics, such as latent heat per specific heat of the metal. To this end, an appropriate cooling experiment setup is prepared for casting process first, and thermal measurements are recorded in a way that can be analyzed by a computer. Therefore, a typical thermal analysis experiments may be categorized as two main stages: pre-experimental and post-experimental. The choice of appropriate thermal measurement tools and adjusting the setup for the properties of casting metal are typical procedures before the cooling process. The analytical procedures, such as smoothing, differentiating, and fitting data start with the end of measurements.

4.1 Taking Thermal Data

Before starting thermal analysis, having ideas about the metal that will be studied is very important for the quality of the experiment because there are several types of thermocouples and measuring devices that can be used for the different type of metals and temperature scales. The main point of pre-experimental process can be listed as follows:

1. Choosing the type of thermocouple
2. Determining the most appropriate type and dimension of the mold
3. Adjusting the thermal scanner for the most accurate thermal measurements
4. Determining the pouring temperature of the casting metal

Thermocouples are widely used elements of temperature measurements in industry. They are produced by welding the terminals of two different alloy wires, but rest of them is isolated from each other. Their working principle is voltage production in the millivolt range between hot and cold terminals. The welded terminal is the hot point, and other two open terminals are cold points. However, the linear relationship between the temperature difference and the voltage produced can not always be fulfilled. Therefore, different types of thermocouples are produced for different temperature range

and media. It is very important that one should determine the types of thermocouple according to the temperature range of the experiment before casting. DIN 43710 standards are widely used guide for researchers for this purpose. Thermocouple types and their temperature limits are seen in Table 4.1. [30]

Table4.1: Types of thermocouples and their corresponding temperature limits [30].

COMPOSITION	DIN 43710	TEMPERATURE LIMITS
Cu-Const	T	-200 – +300 $^{\circ}$C
Fe-Const	J	-200 – +800 $^{\circ}$C
Cr-Al	K	-200 – +1200 $^{\circ}$C
NiCr-Ni	K	-200 – +1200 $^{\circ}$C
Cr-Const	E	-200 – +1200 $^{\circ}$C
Nicrosil-Nisil	N	0 – +1200 $^{\circ}$C
Pt%10Rh-Pt	S	0 – +1500 $^{\circ}$C
Pt%13Rh-Pt	R	0 – +1600 $^{\circ}$C
Pt%18Rh-Pt	B	0 – +1800 $^{\circ}$C
Tn-Tn%26Re	W	0 – +2000 $^{\circ}$C

Since this study was carried on low melting point metals (Tin, Zinc, Aluminum), the maximum temperature reached is almost 800 $^{\circ}$C, which can be seen as a maximum pouring temperature for pure Al, which melts at 660 $^{\circ}$C. For this reason, K type NiCr-Ni thermocouples were chosen for the experiments.

Another case to consider before experiment is choice of casting cup. As one can prepare his own cup, it is found from any purveyor producing molds especially for the thermal analysis purpose. In this study, shell molded sand cups with K type thermocouples were used. Their photos are seen in Figure 4.1.
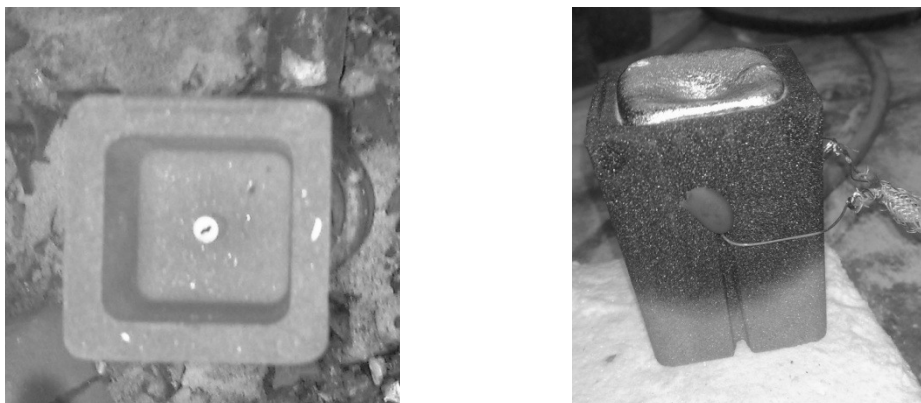
Figure 4.1: QuiK cups used in this study.

The most effective factors that influence the quality of thermal analysis related with the mold are its dimensions and thermal properties: specific heat, conductivity etc. Thickness of the mold is responsible for high heat capacity, causing rapid cooling and insensitive measurement; however, the dimensions determine validity of Newtonian thermal analysis. The key concept for validity of Newtonian thermal analysis is Biot number, which depends on heat transfer coefficient, thermal conductivity of material, and characteristic length of the cooling body. Its mathematical definition is

$$Bi = \frac{hL}{k} \tag{4.1}$$

where h is the heat transfer coefficient, L is the characteristic length (volume per surface area), and k is thermal conductivity of metal.

If the value of Biot number is high, the temperature distribution within the metal can not be assumed uniform, and conduction heat transfer methods are required. For instance, less than 5% error will be arisen when lumped capacitance model is assumed with a Biot number smaller than 0.1 [1]. The Biot numbers and thermal properties of some pure metals surveyed in this study are listed in Table 4.2.

Table4.2: Thermal properties of the materials at their melting temperature.

metals	h (W/m^2.K)	L (m)	k (W/m.K)	Bi
Aluminum (Al)	12.30		220	0.0036
Lead (Pb)	11.40	0.065	31	0.0239
Tin (Sn)	11.19		60	0.0121
Zinc (Zn)	11.78		110	0.0070

In general, there are two types of mold materials: insulators and conductors. Insulators are plaster full molds, ceramic shell molds, and silica sand molds. The effect of temperature on the thermal conductivity of insulating molds depends on AFS sand number [3]. Therefore, researchers should consider the variable thermal conductivity of insulating molds.

Another factor that influences the quality of thermal analysis is adjustment of thermal scanner and computer. For instant and accurate measurement, adjustments for the type of thermocouple, temperature range and number of temperature reading digits should be introduced to the thermal scanner and computer. One-decimal-digit sensitivity is appropriate for the temperature reading at every second. If the temperature is recorded with integer numbers, then the cooling graph will seem horizontal steps as in Figure 4.2.
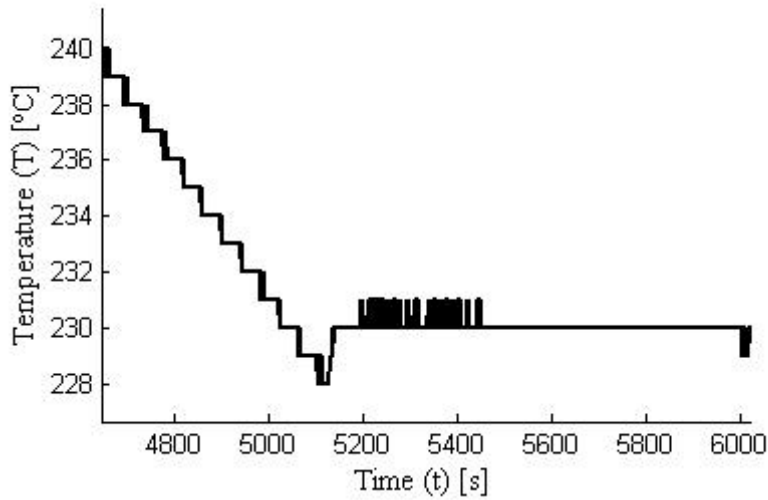
Figure 4.2: Cooling curve of pure Sn zoomed to its undercooling point.

The repetitive points are caused by the adjustment of the scanner which measures temperature with integers. These horizontal dots make differentiation impossible, but it can be corrected by data smoothing. Although data smoothing is a helpful tool to modify data for differentiation, it deforms the data, and produces deviated data from the actual temperature. Therefore, the most accurate measurement mode must be adjusted on the thermal scanner in order to be appropriate for the Computer Aided Cooling Curve Analysis (CA-CCA).

4.2. Data Analysis

The post-experimental part of thermal analysis involves processing thermal data to produce information about the sample. Data smoothing, data exclusion, making curve fitting, differentiation, integration and solving differential equations are widely used computational tools by researchers. In this study, MATLAB 7.10.0 (R2010a) is used for this purpose with its curve fitting tool.

The first task is to import the thermal data into the software. A typical Newtonian thermal analysis involves time and temperature measurements, so there should be at least two data sets as independent and dependent variables. These variables should be recorded as column vectors to the computer software. As a sample, the output of the thermal scanner used in this study is shown in Table 4.3.

Table 4.3: Output of the thermal scanner.

t(s)	T(^{0}C)	t(s)	T(^{0}C)	t(s)	T(^{0}C)	t(s)	T(^{0}C)	t(s)	T(^{0}C)	t(s)	T(^{0}C)
1	316	14	268.7	27	244.2	40	231	53	231.2	66	231,2
2	309,2	15	264,3	28	241,6	41	231,1	54	231,2	67	231,2
3	309.2	16	264.3	29	241.6	42	231.1	55	231.3	68	231.2
4	299.2	17	264.3	30	238.8	43	231.1	56	231.3	69	231.5
5	299.2	18	259.6	31	235.6	44	231	57	231.2	70	231.5
6	292.2	19	259.6	32	235.6	45	231.2	58	231.2	71	231.3
7	292.2	20	256.2	33	235.6	46	231.2	59	231.2	72	231.3
8	286.4	21	256.2	34	233.4	47	231.1	60	231.2	73	231.4
9	286.4	22	252.3	35	231.5	48	231.1	61	231.2	74	231.4
10	280.7	23	248.3	36	231.5	49	231.3	62	231.2	75	231.4
11	280.7	24	248.3	37	230.8	50	231.3	63	231.2	76	231.4
12	273.5	25	248.3	38	230.8	51	231.3	64	231.2	77	231.3
13	273.5	26	244.2	39	231	52	231.2	65	231.2	78	231.3

The graph of data in Table 4.3 is represented by Figure 4.3. It is noteworthy that the raw data have repetitive points, so the graph contains horizontal steps, which complicates differentiation and curve fitting. The data should be revised for mathematical analyses especially for differentiation.
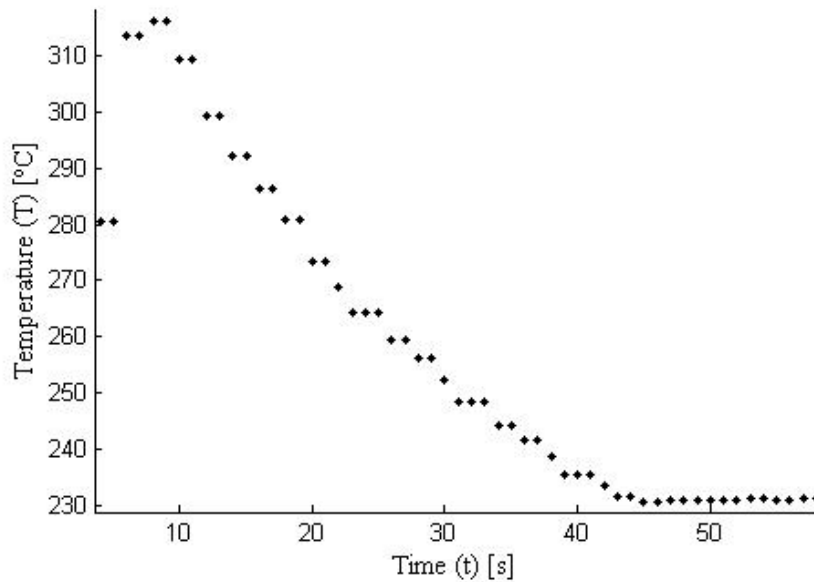
Figure 4.3: Temperature vs. time graph (unrevised).

The result of differentiation looks like Figure 4.4 unless the raw data is not revised. The repetitive dots give noisy results for the derivative of temperature with respect to time.
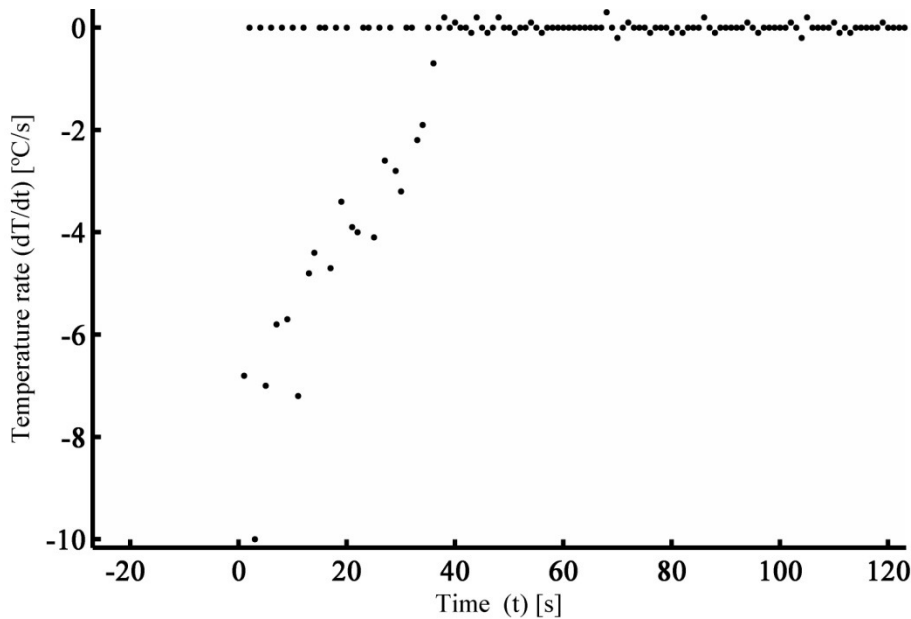
Figure 4.4: Time derivative of the raw temperature data.

As seen from Figures 4.3 and 4.4, the directly measured temperature record is not appropriate for differentiation, so it needs to be corrected for the sake of smoothness. Data smoothing is a kind of modification that attempts to approximate the data set to a function in order to modify noisy points. It should not be confused by curve fitting in some ways. In contrast to curve fitting, smoothing does not use any functional forms, and gives little attention to close matching of data. There are, in general, two types of smoothing: filtering and local regression. While filtering methods depend on averaging data within a specified number of neighboring points, called as span, but local regression methods fit a defined number of points to a function which may be linear or quadratic [31]. Among the filtering methods for data smoothing, moving average and Savitzky-Golay filtering methods are widely preferred in this study because they work most properly for cooling data. Moving average filters work by averaging the neighboring points defined in the span. Savitzkty-Golay filtering uses unweighted linear least-squares fit using a polynomial of a given degree. Therefore, span must be an odd number because of the neighboring average principle [32].

Lowess, loess, robust lowess and robust loess smoothing methods are included to local regression data smoothing. All these methods have some special parameters such as span and degree. Non-smoothed cooling curve and its corresponding smoothed data whose methods are given can be seen in Figures 4.5 – 4.7. In these figures, undercooling region of pure Sn is zoomed in order to show the deformation from smoothing.

70
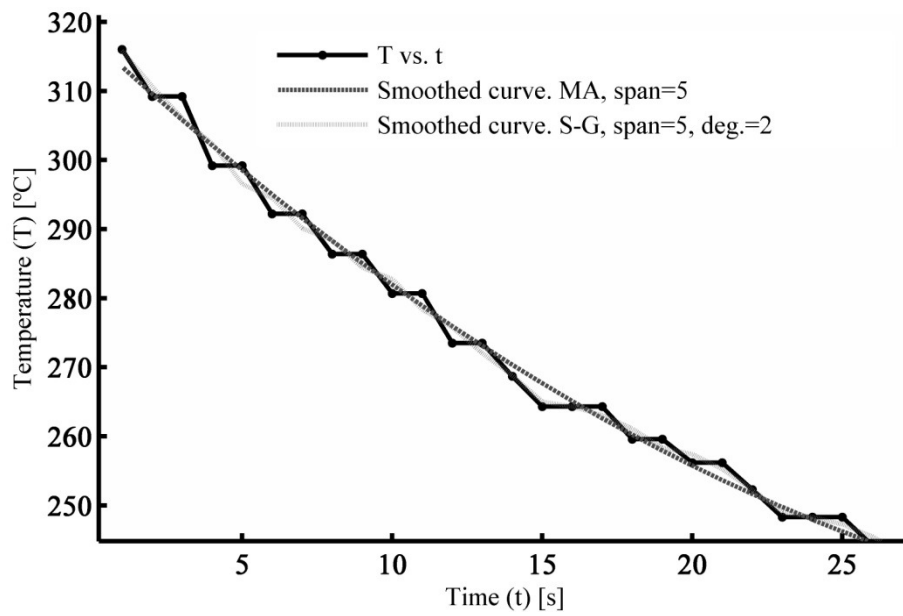
Figure 4.5: Cooling curve and its smoothed curves (filtering methods, MA: Moving average, S-G: Savitzky-Golay).
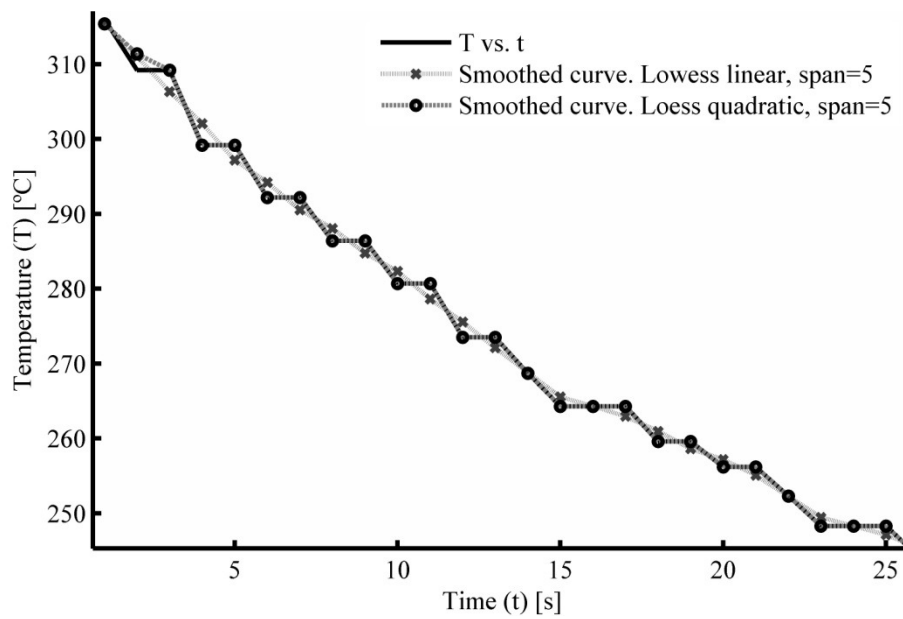
Figure 4.6: Cooling curve and its smoothed curves (local regression methods).
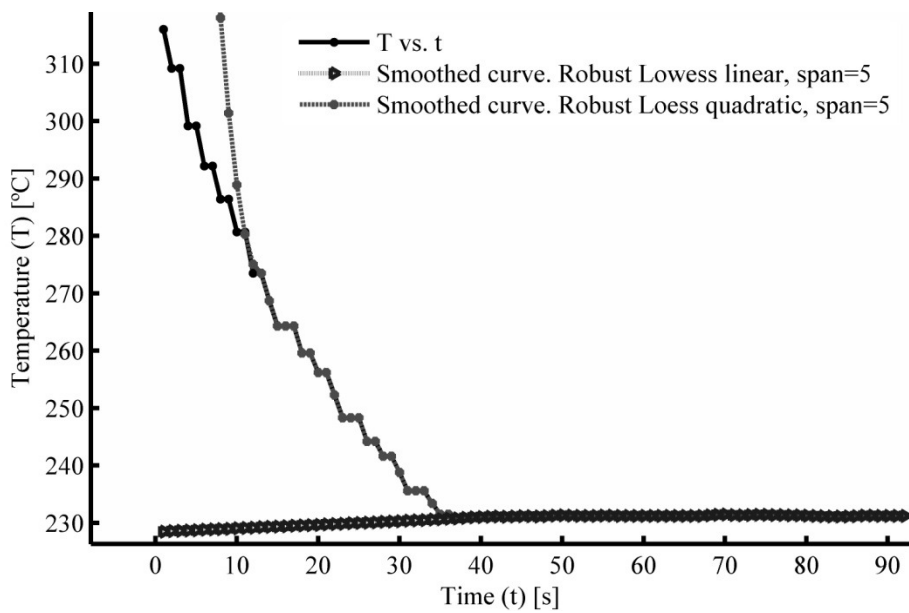
Figure 4.7: Cooling curve and its smoothed curves (robust local regression methods).

Differentiation is a valuable mathematical tool to determine the instants of the boundaries of the solidification. However, smoothing may deform data and can cause wrong but smooth results. Span parameters of data smoothing should be determined so as to balance these effects. Higher span factor means smoother but less representative curve because span factor determines the validity of the derivative. In Figure 4.8, smoothed curves with different span factors are shown.
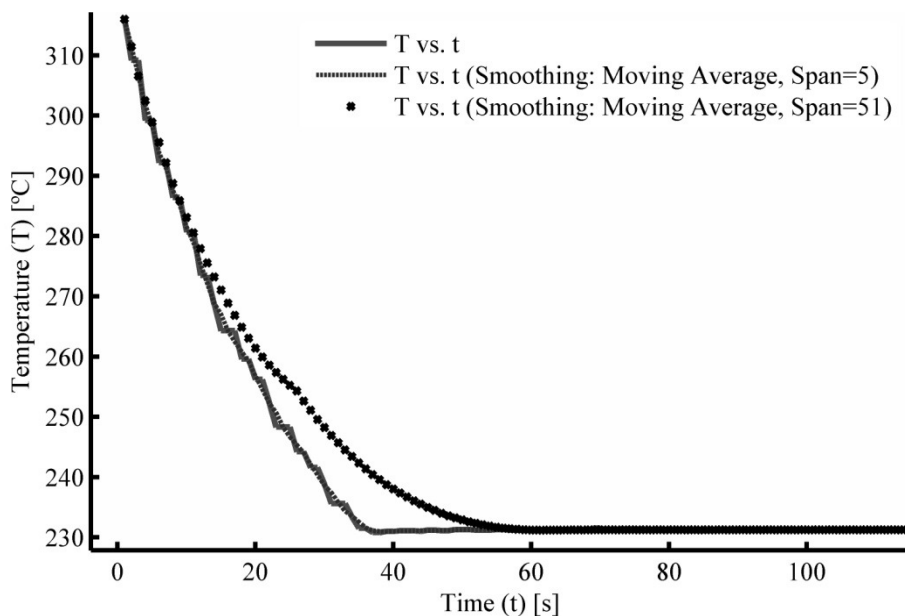
Figure 4.8: Non-smoothed and smoothed curves with different spans for moving average filtering.

The smoothed curve with span 51 is smoother than the other with span 5, but higher spanned curves deviate much more from the original curve. The results of differentiation with different smoothed curves are shown in Figure 4.9.
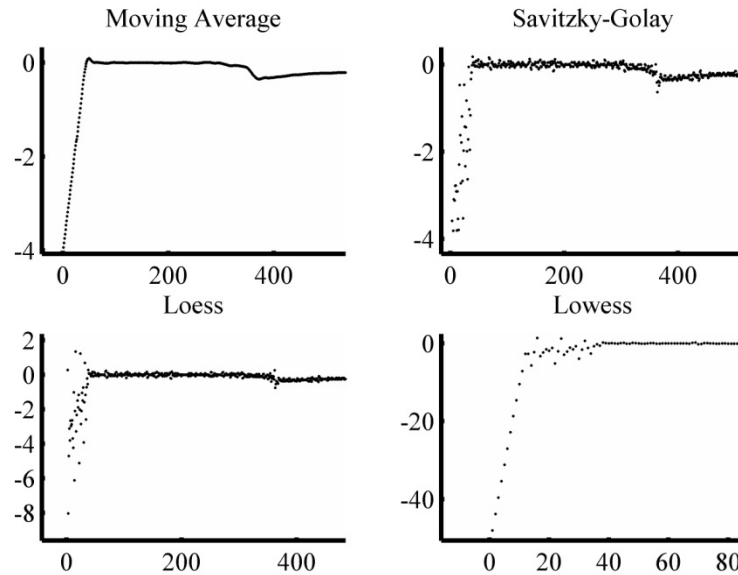
Figure 4.9: Cooling rate vs. t graphs from different smoothing methods with span 5.

Taking derivative of a data set with respect to the independent variable may be done by discrete or fitting methods. Discrete differentiation finds the difference between adjacent elements of dependent and independent data, and then divides them. Simple command for the derivative of temperature (T) with respect to time (t) in MATLAB is

$$Tdot = diff(T) ./ diff(t); \tag{4.2}$$

In this command, temperature and time measurements must be named as T and t respectively in the Matlab workspace. It is possible to take derivative of temperature by using curve fitting tool. When cooling curve is fitted by interpolation methods, curve fitting tool takes the derivative of the fit by using the analysis tab. Figures 4.10 and 4.11 shows the cooling curve of pure aluminum and its smoothed curves. Moving average smoothing methods with spans 5, 11, 21 and 51 are used, and corresponding smoothed data are depicted. It can be seen that higher span values make the curve smoother, but less similar to the original curve. Time derivatives of these curves are shown in Figure 4.12. Before taking derivative, temperature data were fitted to interpolant in the curve fitting tool then cubic spline method was chosen. Derivatives were made by analysis tab on the curve fitting tool of Matlab.

73
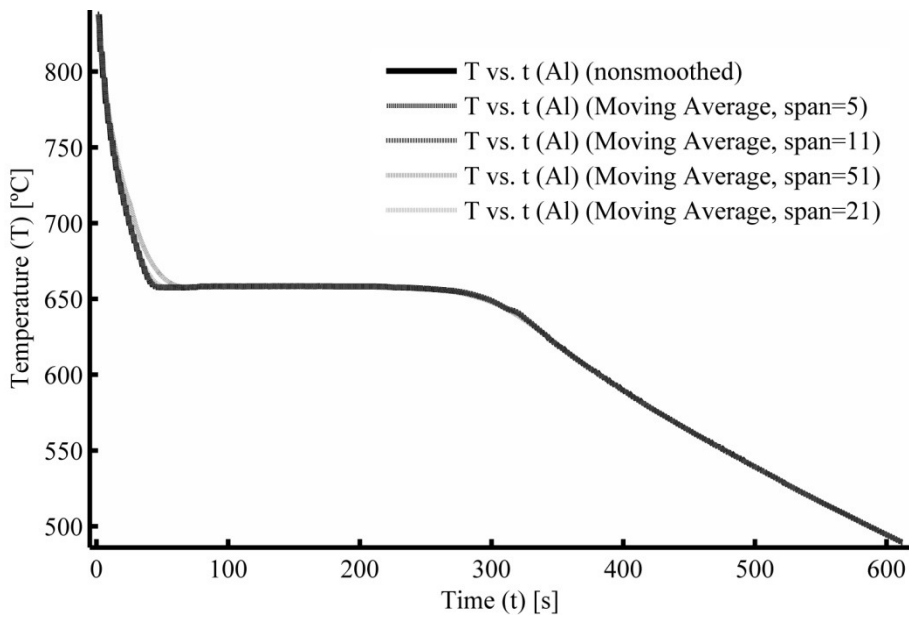
Figure 4.10: Temperature vs. time graph and its smoothed curves made by moving average methods with different spans.
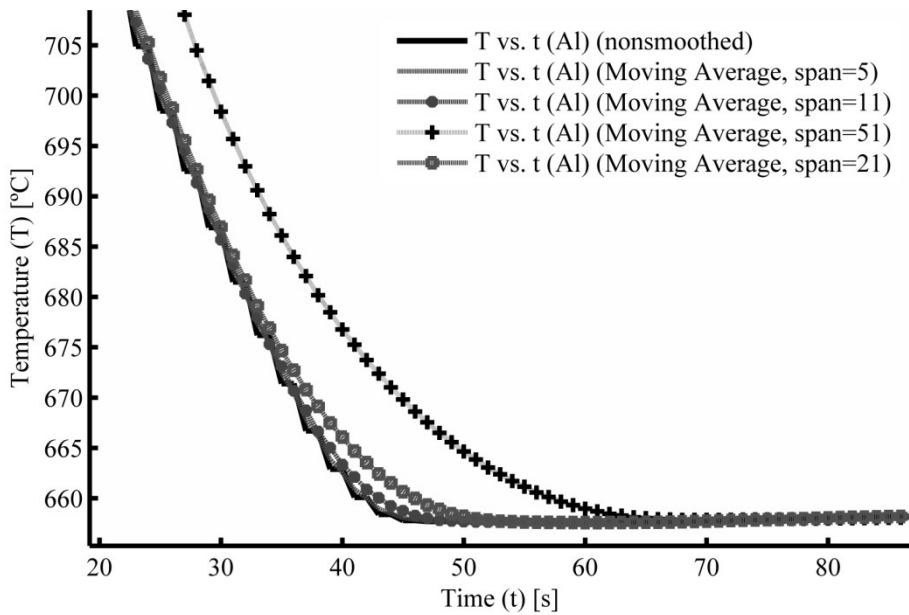
Figure 4.11: Temperature vs. time graph and its smoothed curves made by moving average methods with different spans (focused to undercooling region).

74
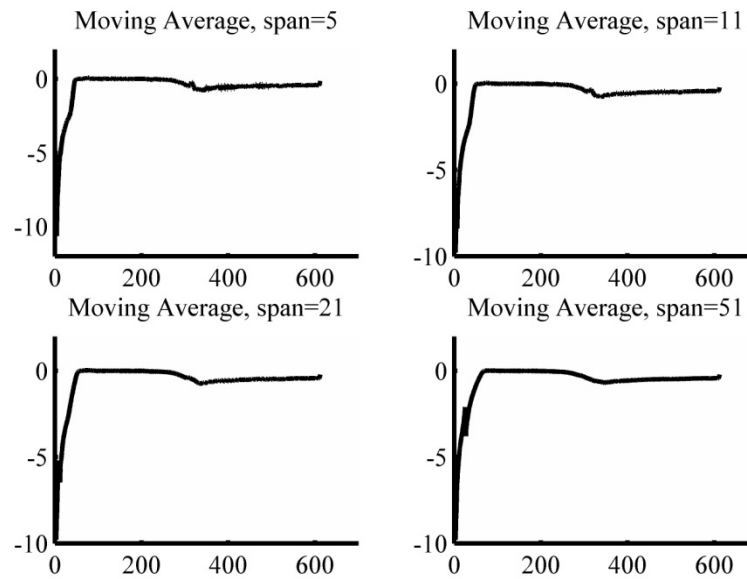
Figure 4.12: Derivatives of temperatures obtained by different smoothed curves.

The most proper derived temperature may be chosen from the results in Figure 4.12 by comparing them with its own temperature curve. It is obvious that undercooling local minimum of the temperature curve has zero derivative at that instant. Moreover, the turning point of curvature at the end of solidification means that the second derivative is zero, so the first derivative must be a minimum at the saddle point of cooling the graph. The critical points are shown in Figures 4.13 and 14. Original temperature vs. time graph can be compared with its derivative, which is derived from the smoothed temperature data with different spans. Two span numbers are used for comparison: the derivative by span 5 and 31 smoothing. It can be seen that undercooling local minimum has more deviation when span factor is increased. Local minimum is at t=128 seconds on the cooling graph itself, but it corresponds to the point that the derivative is zero which corresponds to 129th and 137th seconds for Figures 4.13 and 14 respectively.
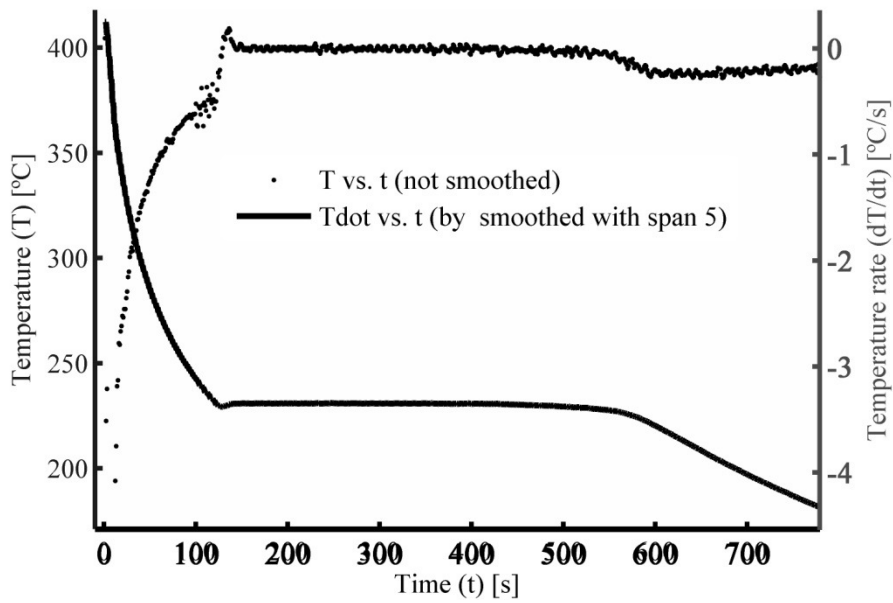
Figure 4.13: Temperature and its derivative (data is smoothed by moving average method with span 5).
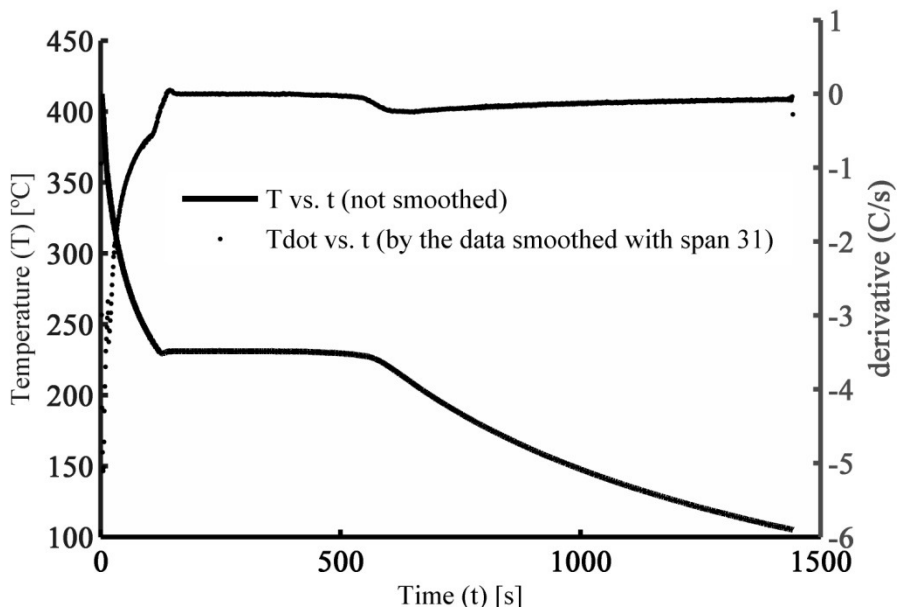
Figure 4.14: Temperature and its derivative (data is smoothed by moving average method with span 31).

The difference between local minimum instants from the temperature and derivative curves increases with the span number of smoothing, which must be done to be able to differentiate the cooling curve. If Figures 4.13 and 14 are compared, it can be seen that undercooling point deviates 1 and 9 seconds from the temperature curves when it is

76

found by derivative curves. Therefore, researchers should consider this deviation and deformation when they work on derived curves.

4.3. Curve Fitting for Thermal Analysis

It is imperative that thermal data be modeled by an expected function in order to find the parameters of thermal system or initial conditions. Curve fitting process is a useful mathematical tool that may describe a data set in terms of known functions. It involves interpolation or smoothing [33]. A simple cooling data is depicted in Figure 4.15 as an example of curve fitting process. The graph is obtained by recording the temperature of solid tin without mold, so it is expected that an exponential decay explain this data. The type of function, which models temperature in terms of time, may be written as:

$$T = ae^{-bt} + T_\infty \tag{4.3}$$

or in terms of Matlab default notation:

$$y = a*exp(-b*x) + T\,inf \tag{4.4}$$

where x and y are independent and dependent variables. a, b and *Tinf* are the parameters that will be calculated by curve fitting tool. When exponential type of fit is chosen for the data set imported to curve fitting toolbox, it yields a graph of the fitted function and output which contains information about the fit such as; values of the parameters, R-square and adjusted R-square etc. The results of this exponential fit are seen in Figure 4.16 and Table 4.4.

Table 4.4: Output of curve fitting.

General model:	Goodness of fit:
f(x) = a*exp(-b*x)+Tinf	SSE: 2808
Coefficients (with 95% confidence bounds):	R-square: 0.9994
Tinf = 27.9 (27.85, 27.95)	Adjusted R-square: 0.9994
a = 126 (125.9, 126.1)	RMSE: 0.7496
b = 0.0008296 (0.0008283, 0.000831)	
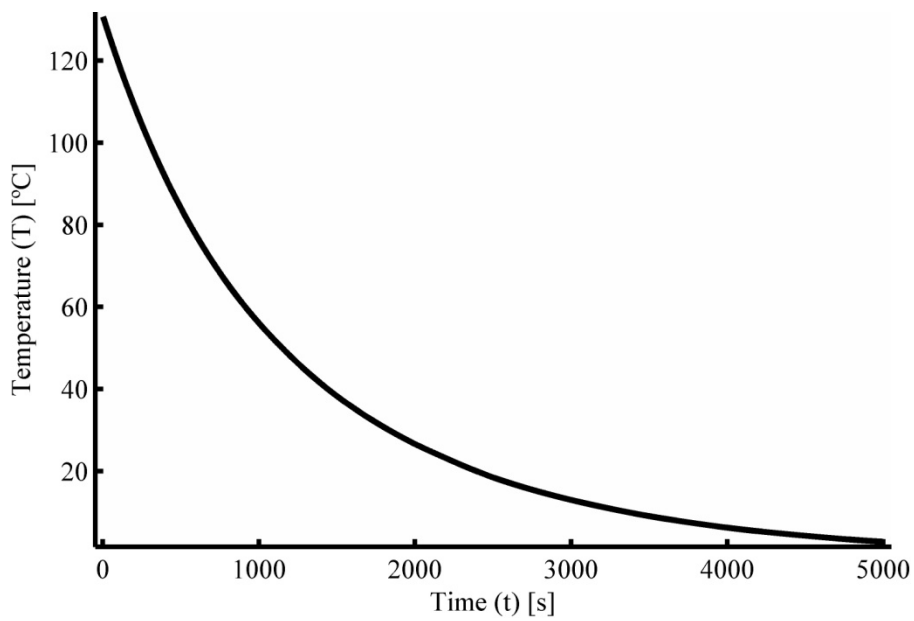
Figure 4.15: Temperature vs. time graph of the recorded data.
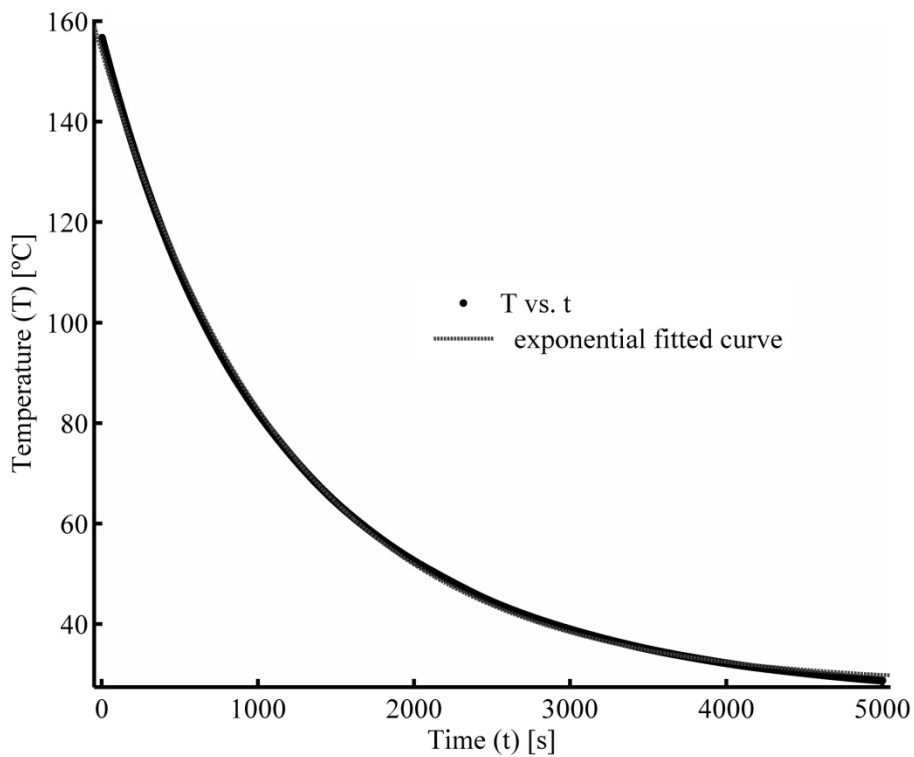
Figure 4.16: Temperature and its fitted function.

As seen in Table 4.4, the coefficients *a* and *b* and goodness of fit indicators are given by the curve fitting toolbox. In statistics, goodness of fit refers to the discrepancy between

78

observed values and expected values from a model. These indicators, respectively, include the sum of squares due to the error (SSE), R-square, adjusted R-square, and root mean squared error (RMSE) [34].

"SSE measures the total deviation of the response values from the fit to the response values. A value closer to 0 indicates that the model has a smaller random error component and that the fit will be more useful for prediction." The statistic R-square measures the success of fit in explaining the variation data. It takes any value between 0 and 1. Its value refers to how many percent of the total variation are explained by the fit. It is obvious that increasing the number of fit coefficients in a model increase its R-square value, but more coefficients may not improve the quality of fit. In this case degrees of freedom R-square is the most appropriate parameter to evaluate the success of fit [35].

One of the important points of the curve fitting that researchers can control is determining start points and intervals of the coefficients in the fit function. As an example, a fit function in Chapter 3, which has 6 coefficients, can be analyzed in detail. This fit function is given by:

$$T = \left(a_L \theta(t_s - t) + a_S \theta(t - t_e) \right) e^{-bt} + \left(c_L \theta(t_s - t) + c_S \theta(t - t_e) \right) e^{-dt} + T_\infty \qquad (4.5)$$

where T is the temperature, θ is Heaviside step function, and t is time. In Matlab notation, this must be written in custom equation from the choice of type of fit as below:

```
(aL*heaviside(112-x)+aS*heaviside(x-526))*exp(-b*x)
+(cL*heaviside(112-x)+cS*heaviside(x-526))*exp(-d*x)+Tinf
```

This script belongs to temperature of pure Zn whose start and end times of solidification are 112 and 526 seconds respectively. The data set was obtained by the difference between the temperature of the metal and the ambient temperature. Before applying curve fit, the phase transformation region must be excluded by exclusion tool of curve fitting toolbox. It is possible to see null results when the fit function is tried to fit with the data set because the start points and bounds of the coefficients may not be appropriate for a good fit. When a default setting of the coefficients in Figure 4.17 was given, the fitting application was resulted in error. Error message says,"Inf computed by model function".

Unknowns	StartPoint	Lower	Upper
Tinf	0.438	-Inf	Inf
al	0.923	-Inf	Inf
as	0.195	-Inf	Inf
b	0.817	-Inf	Inf
cl	0.992	-Inf	Inf
cs	0.150	-Inf	Inf
d	0.980	-Inf	Inf

Figure 4.17: Default start points, lower and upper bounds for the curve fitting.

Since the intervals that are limited by lower and upper bounds are between minus and plus infinity, curve fitting session fails to find the most proper fit. These coefficients' intervals should be narrowed to some extent. In order to estimate the bounds of coefficients, some information about these parameters may be useful. First of all, the coefficients b and d come from the heat transfer coefficients and thermal capacitances of the metals and mold. They may be calculated approximately by heat transfer coefficient tables or other thermo physical indices as in Section 3.1.3. The ranges of b and d are in the range of 0.0005 and 0.01. Therefore, their bounds can be narrowed to 0 and 1 and start points be set around these points. Other coefficients represent initial conditions, so their ranges may be calculated by initial conditions for the related differential equation. The ranges of parameters chosen for proper curve fitting with different types of metal are shown in Figures 4.18-4.20.

Unknowns	StartPoint	Lower	Upper
Tinf	500.000	0	1.00e+03
al	300.000	0	1.00e+03
as	400.000	0	1.00e+03
b	1.00e-04	0	1.000
cl	600.000	0	1.00e+03
cs	900.000	0	1.00e+09
d	1.00e-02	0	1.000

Figure 4.18: Start points, lower and upper bounds for the curve fitting of aluminum experiments.

Unknowns	StartPoint	Lower	Upper
Tinf	150.000	0	300.000
al	300.000	0	1.00e+03
as	400.000	0	1.00e+03
b	1.00e-04	0	1.000
cl	600.000	0	1.00e+03
cs	5.00e+03	0	1.00e+12
d	1.00e-02	0	1.000

Figure 4.19: Start points, lower and upper bounds for the curve fitting of lead experiments.

Unknowns	StartPoint	Lower	Upper
Tinf	150.000	0	200.000
al	300.000	0	1.00e+03
as	400.000	0	1.00e+03
b	1.00e-04	0	1.000
cl	600.000	0	1.00e+03
cs	900.000	0	1.00e+09
d	1.00e-02	0	1.000

Figure 4.20: Start points, lower and upper bounds for the curve fitting of tin experiments.

Unknowns	StartPoint	Lower	Upper
Tinf	150.000	0	200.000
al	300.000	0	1.00e+03
as	400.000	0	1.00e+03
b	1.00e-04	0	1.000
cl	600.000	0	1.00e+03
cs	900.000	0	1.00e+09
d	1.00e-02	0	1.000

Figure 4.21: Start points, lower and upper bounds for the curve fitting of zinc experiments.

Exclusion factor should be set so wide that the interval can let a proper fitting result, but so narrow that it cannot break the Taylor series approximation for the first degree. In this study, the most appropriate exclusion interval for this criterion is chosen 50 ^{0}C below and above the solidus and liquidus temperatures in the non-solidification region. A sample exclusion rule is depicted in Figure 4.22.
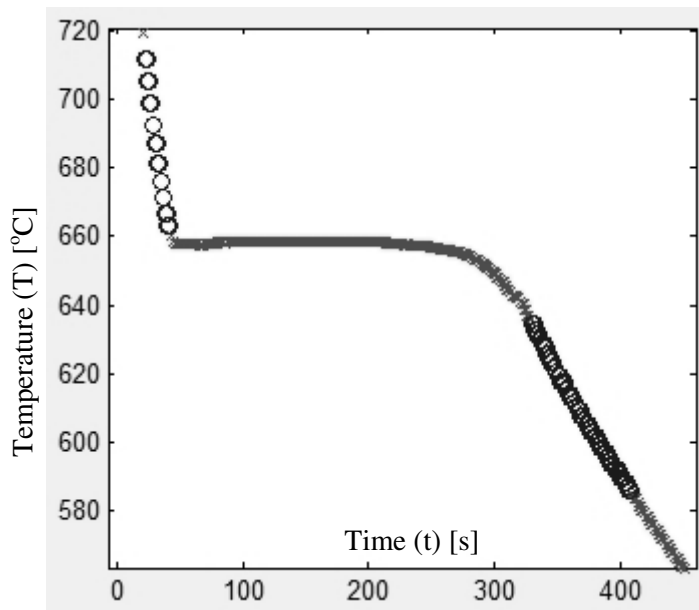
Figure 4.22: Exclusion rules for the curve fitting of all experiments. 50 ^{0}C above and below the melting point is included. Circles, or darker points, are included; crosses, or lighter points, are excluded from the curve fitting.

By the rules of start points and exclusion from Figures 4.18 and 4.22 respectively, a curve fitting result of pure aluminium is seen in Figures 4.23 and table 4.5.
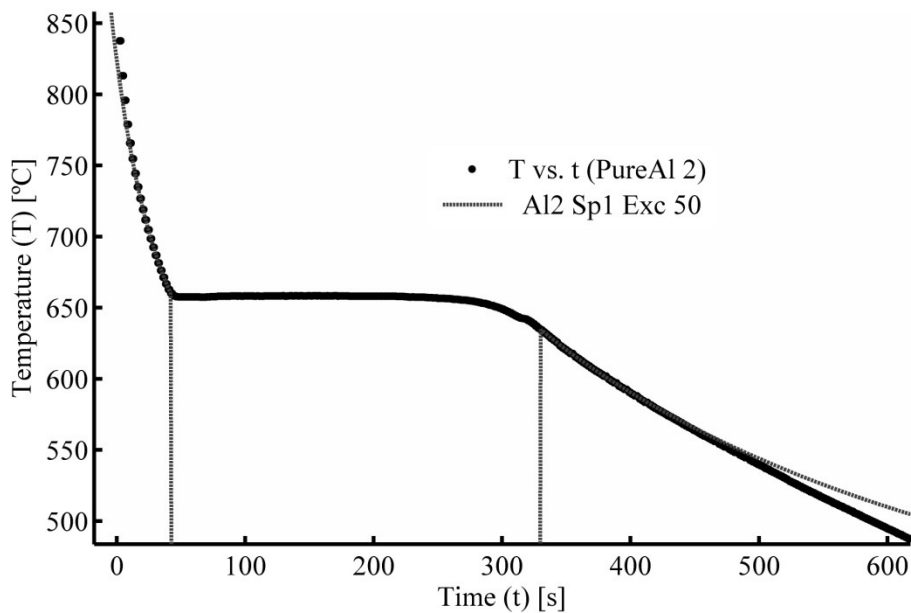
Figure 4.23: Sample curve fitting according to the start points in Figure 4.18 and exclusion in Figure 4.21.

Table 4.5: Curve fitting output.

General model:	Goodness of fit:
f(x) = (al*exp(-b*x)+cl*exp(-d*x)+Tinf)*heaviside(42-x)+(as*exp(-b*x)+cs*exp(-d*x)+Tinf)*heaviside(x-329) Coefficients (with 95% confidence bounds): Tinf = 413.2 (62.86, 763.6) al = 235.2 (-93.31, 563.7) as = 592.1 (347.4, 836.8) b = 0.003021 (-0.002943, 0.008985) cl = 174.7 (153.7, 195.8) cs = 3.804e+005 (-1.257e+006, 2.018e+006) d = 0.03553 (0.02305, 0.04801)	SSE: 50.38 R-square: 0.9996 Adjusted R-square: 0.9995 RMSE: 0.74

4.4. Calculating the Latent Heat and Solid Fraction

Once the parameters of the differential equation have been calculated from curve fitting, latent heat and solid fraction can be evaluated for the solution of the differential equation for the solid fraction. The two-capacitive system baseline (TCSBL) or zero curve can be written by the non-solidification form of Equation 3.50

$$\dot{T}_{zc} = -p_1(T - T_\infty) + p_2 p_3 e^{-p_4 t} \int_0^t (T - T_\infty) e^{p_4 t} dt \qquad (4.6)$$

where p_1, p_4 and $p_2.p_3$ are Equation 3.80-3.82. T_∞ is the parameter coming from curve fitting. In the case of phase transformation, it gives:

$$\frac{L_f}{c_p} \dot{f}_s(t) = \dot{T}_{exp} - \dot{T}_{zc} \qquad (4.7)$$

where exp and zc subscripts denote experimental and zero curve. The initial conditions of solid fraction are:

$$f_s(t_s) = 0, \quad f_s(t_e) = 1 \qquad (4.8)$$

Integration of Equation 4.7 between t_s and t_e produces the latent heat as:

$$\frac{L_f}{c_p} = \int_{t_s}^{t_e} (\dot{T}_{exp} - \dot{T}_{zc}) dt \qquad (4.9)$$

A sample Matlab script for this calculation is given below:

% Command script for TWO-CAPACITIVE SYSTEM BASELINE METHOD

% Type the start and end times of solidification
         ts=42   ; te=329   ;

% Type the parameters from the curve fitting
         Tinf = 415.5;   al= 232.6;   b = 0.00306;   cl =173.7;   d = 0.03519 ;

% The matrix elements (Do not type anything below)
         p1=(al*b+cl*d)/(al+cl);   p4=b+d-p1;

% Zero curve calculation (Do not type anything below)
         Tdotzc=-p1*(T-Tinf)+(p1*p4-b*d)*exp(-p4*t).*cumtrapz(t,(T-
         Tinf).*exp(p4*t));

% Integration and outputs (Do not type anything below)
         fsLpc=T-cumtrapz(t,Tdotzc);
         Lpc=fsLpc(te)-fsLpc(ts)
         fs=(fsLpc-fsLpc(ts))/Lpc;
         plot(t,fs,'DisplayName','t vs. fs','XDataSource','t','YDataSource','fs');figure(gcf)

4.5 Sample Thermal analysis

In order to understand TCSBL, the procedure is expressed step by step as follows.

Prepare experimental setup.
   - Chose a thermocouple appropriate for the casting.
   - Supply a mold appropriate for the metal.
   - Place the thermocouple into the mold, and connect it to the measurement device.
   - Adjust the device for the type of thermocouple and temperature scale.
   - Check the connections and adjustment, and be ready to record.

Start the measurement
   - Melt the sample up to 200 ^{0}C above its melting point.
   - Press the record button on the measurement device.
   - Pour the melt into the mold.
   - Wait until it cools at least 200 ^{0}C below its melting temperature.
   - Finish recording, and take the recorded data from the computer.

Prepare data to analyze.
- Save the time and temperature data to MATLAB or any software as a column vectors, and name them t and T.
- Transfer t and T data to curve fitting tool.
- Smooth the data set (T vs. t) by using smooth tab in the data window of curve fitting tool.
- Continue smoothing until a best no deformed and smoothed data is obtained.

Modify the cooling curve and find time derivative
- Fit the best-smoothed data to *interpolant/cubic spline* type of fit.
- Analyze this fit by pressing analysis button. Check the box first derivative and plot the results.
- Press the apply button and Save to Workspace button.
- It saves the data sets to the workspace. Chose the dydx vector, and record it as Tdot.
- Determine the end time of temperature from the first derivative data.
- Determine the start time of temperature from the temperature data.

Exclude some of data for a proper curve fitting
- Exclude the points of the solidification region on T vs t data set by using Exclude button.
- Exclude ts and te points and those between them.
- Exclude the points 50 ^{0}C higher than the liquidus temperature.
- Exclude the points 50 ^{0}C lower than the solidus temperature .
- Record this exclusion as *cooling.*

Fit excluded curve to find thermal parameters.
- On the *fitting* window, check data set as "T vs. t" , type of fit as "custom equations" and exclusion rule as "cooling".
- Select "new", and type the equation to be fitted: "*(aL*heaviside(112-x)+aS*heaviside(x-526))*exp(-b*x)   +(cL*heaviside(112-x)+cS*heaviside(x-526))*exp(-d*x)+Tinf*" (write your ts and te values in place of 112 and 526 seconds).
- Adjust the start point, lower and upper bounds.
- If the fit is not good, change the start points or bounds.
- Apply the fitting, and see the results.

Calculate latent heat and solid fraction.
- Type the parameters from curve fitting output to the command script.
- Run the command script.

CHAPTER 5

RESULTS AND DISCUSSION

5.1 Experiments and Methods Used in this Study

Twelve experiments were conducted with 4 different types of pure metals in order to evaluate the reliability of the thermal analysis methods, which are gathered from literature or proposed in this study. The types of metal used are aluminum, lead, tin and zinc. Some of the experiments were manipulated into different insulation conditions. Table 5.1 shows the list of the experiments with their explanations.

Table 5.1: List of experiments and their explanations.

Experiment	Metal	Explanation
Al 1	Aluminum	Resin-coated sand cup without insulation
Al 2		Resin-coated sand cup insulated lower base
Al 3		
Pb 1	Lead	Resin-coated sand cup insulated lower base
Sn 1	Tin	
Sn 2		
Sn 3		Resin-coated sand cup insulated from mold
Sn 4		Clay bonded graphite crucible insulated outer surface
Sn 5		Resin-coated sand cup insulated outer surface
Zn 1	Zinc	Resin-coated sand cup insulated lower base
Zn 2		
Zn 3		

All metals were poured into the sand molds (QuiK Cup [36]) except for Sn 4, in which a clay bonded graphite crucible was used. The first experiment (Al 1) was made without any insulation while the others were insulated between floor and mold. The only insulated metal from the mold is Sn 3. Sn 4 and 5 are insulated on the outer surface of the mold. To illustrate, Figures 5.1 and 5.2 show the photos of different types of insulation in this study.
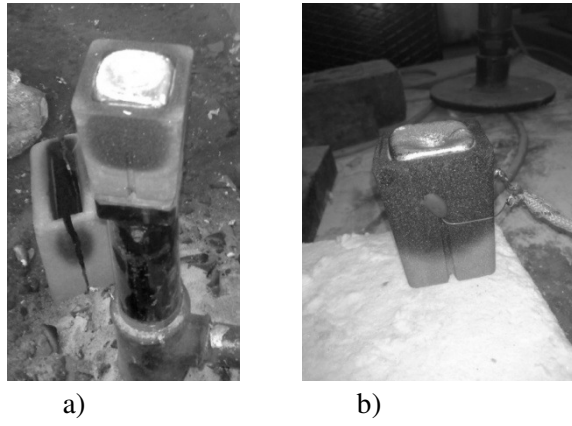
**Figure 5.1:** Experiments a) without insulation, b) insulated from the base.
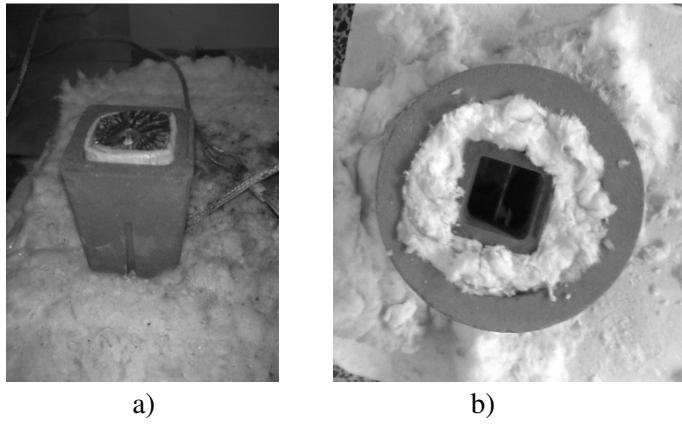
Figure 5.2: Experiments a) insulated from mold, b) insulated outer surface, c) clay bonded graphite crucible insulated from the outside surface.

The thermal conditions and properties of the metals in the experiments are shown in Table 5.2. In the Table, T_m, T_L, T_S, T_i and, T_a are the melting point, liquidus temperature, solidus temperature, initial (pouring) temperature, and the ambient temperature respectively.

Table 5.2: List of experiments and their thermal conditions.

Experiment	T_m (^{0}C)	T_L (^{0}C)	T_S (^{0}C)	T_i (^{0}C)	T_a (^{0}C)
Al 1		660	636	838	10
Al 2	660.0	657	630	773	24
Al 3		658	630	758	18
Pb 1	327.4	332	294	405	31
Sn 1		232	224	316	22
Sn 2		232	214	412	23
Sn 3	231.8	232	218	392	23
Sn 4		233	216	339	17
Sn 5		231	217	468	26
Zn 1		418	399	594	22
Zn 2	419.5	418	401	551	23
Zn 3		409	366	602	25

These 12 experiments were applied for three different thermal analysis methods, discussed earlier. Each method has its own zero curve (baseline) expression and curve fitting function. These methods are summarized in Table 5.3 in terms of their zero curve, which serves a baseline for the solidification process. Newtonian baseline (NTA) and Dynamic baseline (DBL) methods were explained in Chapter 1, while two-capacitive system baseline (TCSBL) was discovered in Chapter 3, which is a suggestion for thermal analysis of the experiments in which high-thermal-capacity molds are used.

89

Table 5.3: List of the methods used in this study. Zero curves and the function for curve fitting.

	Curve fitting function (parameters of zero curve is calculated from fitting this function to the experimental data set)	Definition of zero curve (The equations that zero curves are calculated by using the data and thermal parameters)
Newtonian baseline (NBL)	$\dot{T} = ae^{-bt}$	$\dot{T}_{zc} = ae^{-bt}$
Dynamic baseline (DBL)	$\dot{T} = p_1 T^3 + p_2 T^2 + p_3 T + p_4$	$\dot{T}_{zc} = p_1 T^3 + p_2 T^2 + p_3 T + p_4$
Two-Capacitive system baseline (TCSBL)	$T = \left(a_s \theta(t - t_e) + a_l \theta(t_s - t) \right)e^{-bt} + \left(c_s \theta(t - t_e) + c_l \theta(t_s - t) \right)e^{-dt} + T_\infty$	$\dot{T}_{zc} = -p_1(T - T_\infty) + p_2 p_3 e^{-p_4 t} \int_0^t (T - T_\infty)e^{p_4 t}\,dt$

5.2 Results of Latent Heat

From the three methods in Table 5.3, latent heat per specific heat values of each pure metal were calculated for the 12 experiments in Table 5.1. The results are summarized in Table 5.7, and the curve fitting results are shown in Tables 5.4-5.6.

Table 5.4: Curve fitting parameters of NBL.

	b (x10^{-3})	a	R^2
Al1	-4.38	-4.38	0.846
Al2	-2.68	-1.92	0.699
Al3	-4.48	-2.84	0.856
Pb1	-5.91	-2.23	0.885
Sn1	-4.10	-1.85	0.922
Sn2	-2.33	-1.06	0.920
Sn3	-0.915	-0.534	0.946
Sn4	-4.32	-2.22	0.815
Sn5	-25.6	-5.83	0.974
Zn1	-2.14	-1.33	0.914
Zn2	-2.35	-1.67	0.887
Zn3	-2.22	-1.55	0.889

Table 5.5: Curve fitting parameters of DBL.

	p_1 (10^{-7})	p_2 (10^{-4})	p_3	p_4	R^2
Al1	-3.30	4.91	-0.242	39.16	0.985
Al2	-6.43	10.1	-0.530	91.83	0.984
Al3	-2.34	3.22	-0.146	21.54	0.792
Pb1	-22.9	16.5	-0.398	31.67	0.993
Sn1	-153	90.5	-1.785	117.20	0.953
Sn2	-2.45	0.873	-0.010	0.28	0.997
Sn3	0.255	-0.254	0.005	-0.35	0.999
Sn4	-94.4	54.2	-1.034	65.40	0.963
Sn5	-4.63	1.78	-0.023	0.89	0.983
Zn1	-2.01	1.86	-0.058	5.94	0.999
Zn2	-2.47	2.20	-0.066	6.29	0.993
Zn3	-0.608	0.362	-0.007	0.26	0.983

Table 5.6: Curve fitting parameters of TCSBL.

	b x(10^{-3})	d (x10^{-2})	a_l	a_s	c_l	c_s (x10^2)	T_∞	R^2
Al1	3.02	3.55	235	592	175	3800	413	1.000
Al2	2.51	3.85	287	573	208	1.81	354	1.000
Al3	2.81	7.64	287	536	228	954	368	0.999
Pb1	5.94	12.0	196	321	172	21800	145	0.999
Sn1	2.57	4.09	118	315	136	82600	103	1.000
Sn2	2.17	2.73	170	458	177	2.35	98	1.000
Sn3	2.61	0.17	164	162	125	8.27	76	1.000
Sn4	0.47	8.75	184	294	221	7.00	47	1.000
Sn5	2.44	1.90	81	244	210	454	142	1.000
Zn1	1.75	2.82	301	578	153	29700	168	1.000
Zn2	1.44	2.70	298	553	108	17200	143	1.000
Zn3	1.33	2.66	363	566	222	0.209	94	1.000

Table 5.7: Latent heat per specific heat (L/c) results of the experiments in ^{0}C by thermal analysis methods.

Exp	NBL	DBL	TCSBL	Literal average
Al1	568.32	482.48	354.60	
Al2	297.85	435.51	340.50	349
Al3	327.85	391.11	316.50	
Pb1	103.53	113.84	167.72	179
Sn1	278.86	266.44	245.18	
Sn2	232.73	198.74	240.29	
Sn3	216.18	214.00	248.89	249
Sn4	394.68	361.33	196.57	
Sn5	251.45	191.14	217.23	
Zn1	260.44	247.27	234.37	
Zn2	359.23	291.36	224.02	214
Zn3	289.22	210.66	202.44	

According to the literally averaged L/c values of metals, percentage errors of each experiment and methods are listed in Table 5.8.

Table 5.8: Percentage errors of the latent heat per specific heat (L/c) results by thermal analysis methods. Experiments with asterisk were insulated by the outer surface of the mold.

| Exp	NBL	DBL	TCSBL
Al1	62.84	38.25	1.60
Al2	-14.66	24.79	-2.44
Al3	-6.06	12.07	-9.31
Pb1	-42.16	-36.40	-6.30
Sn1	11.99	7.00	-1.53
Sn2	-6.53	-20.18	-3.50
Sn3	-13.18	-14.06	0.04
Sn4[*]	58.51	45.11	-21.06
Sn5[*]	0.98	-23.24	-12.76
Zn1	21.70	15.55	9.52
Zn2	67.86	36.15	4.68
Zn3	35.15	-1.56	-5.40
Absolute average	*28.47*	*22.86*	*6.51*

In table 5.8, the last row shows the average of the absolute values of the errors for each type of methods. In the average, TCSBL seems the most reliable with its average percentage error 6.51 %. Sn4[*] and Sn5[*] were insulated from the outside of the mold.

## 5.3 Solid Fraction Evolutions

Once the latent heat is calculated by iterating the area between zero curve and cooling rate, solid fraction evolution can be obtained by cumulative iteration of the area. The solid fraction evolutions for 12 experiments by two-capacitive-system baseline (TCSBL) were plotted with their cooling curve, time derivative (dT/dt), and baseline. The results are shown in Figures 5.3-5.14.
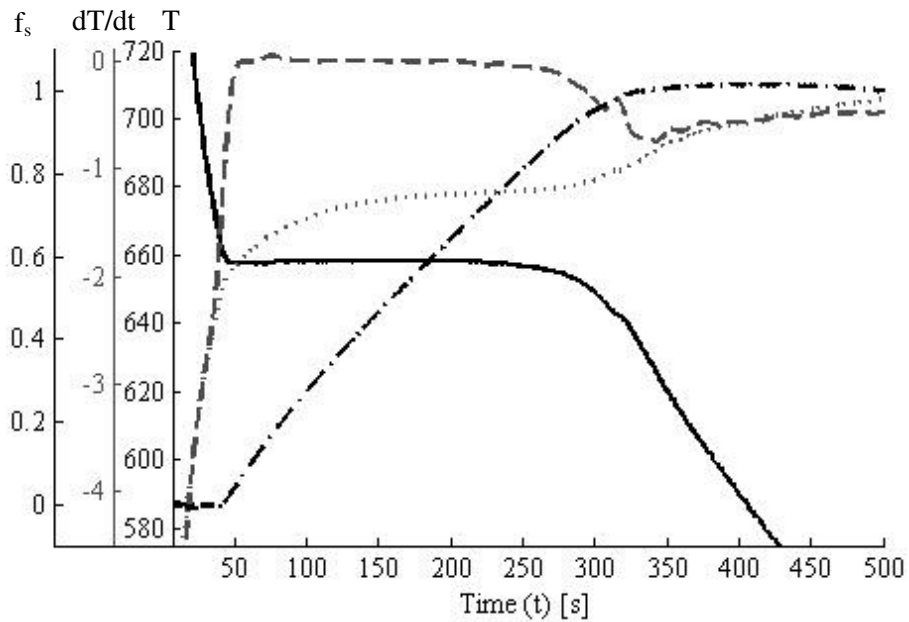

Figure 5.3: Graphs of Al 1. ___ Temperature (T), [^{0}C], --- Cooling rate (dT/dt), [^{0}C/s], … baseline (dT/dt)$_{zc}$, [^{0}C/s], _._ solid fraction (f$_s$).
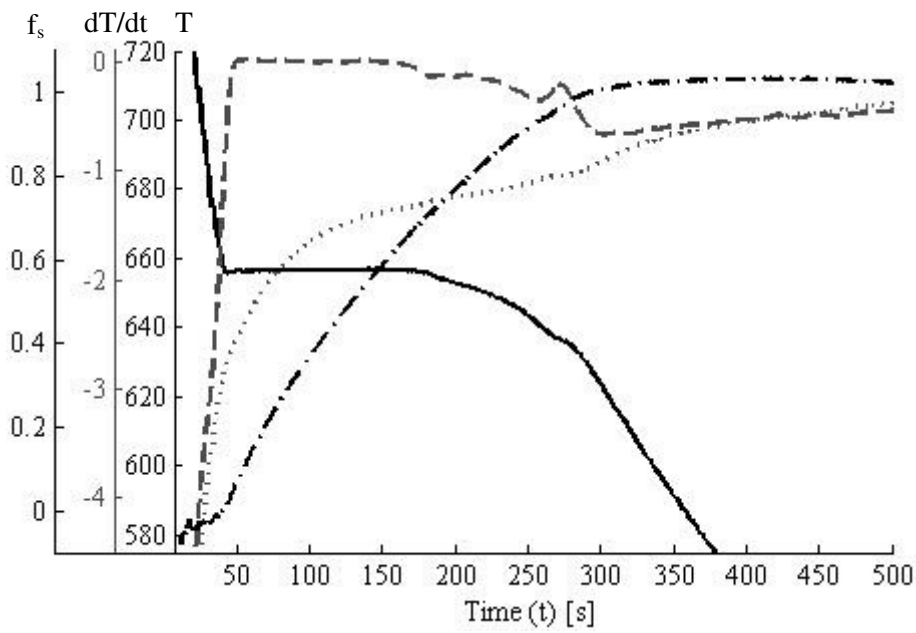
Figure 5.4: Graphs of Al 2. ___ Temperature (T), [^{0}C], --- Cooling rate (dT/dt), [^{0}C/s], … baseline (dT/dt)$_{zc}$, [^{0}C/s], _._ solid fraction (f$_s$).
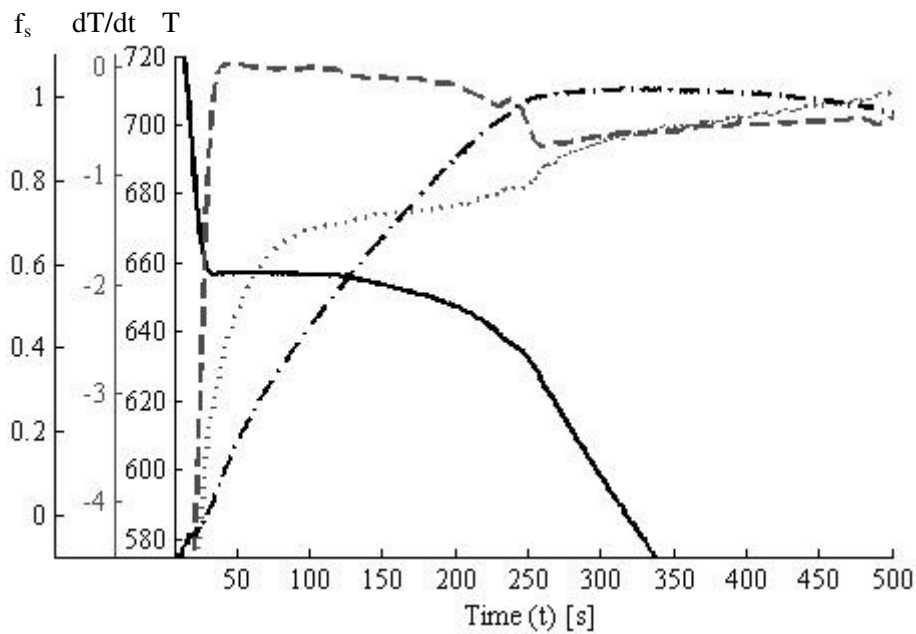
Figure 5.5: Graphs of Al 3. ___ Temperature (T), [^{0}C], --- Cooling rate (dT/dt), [^{0}C/s], … baseline (dT/dt)$_{zc}$, [^{0}C/s], _._ solid fraction (f$_s$).
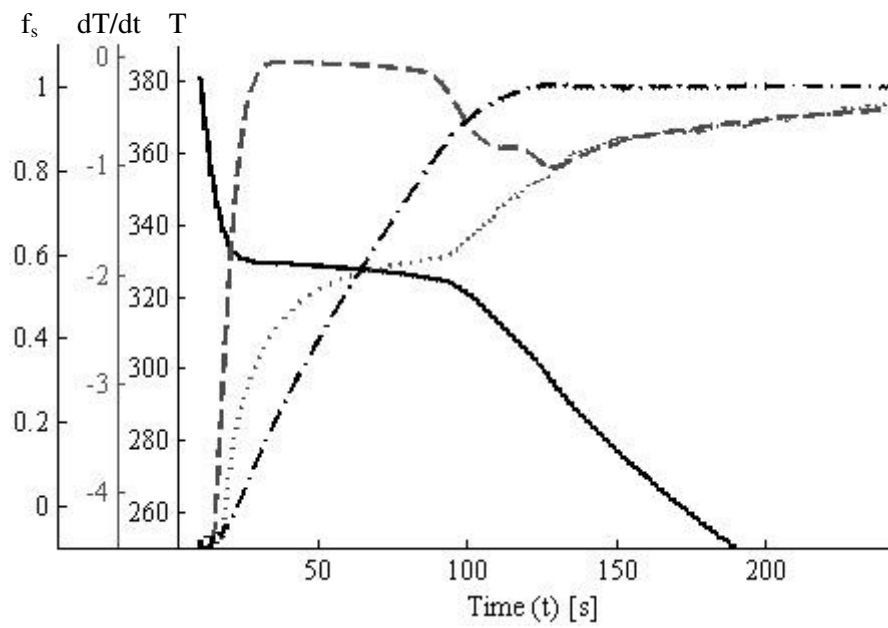
Figure 5.6: Graphs of Pb 1. ___ Temperature (T), [^{0}C], --- Cooling rate (dT/dt), [^{0}C/s], … baseline (dT/dt)$_{zc}$, [^{0}C/s], _._ solid fraction (f$_s$).
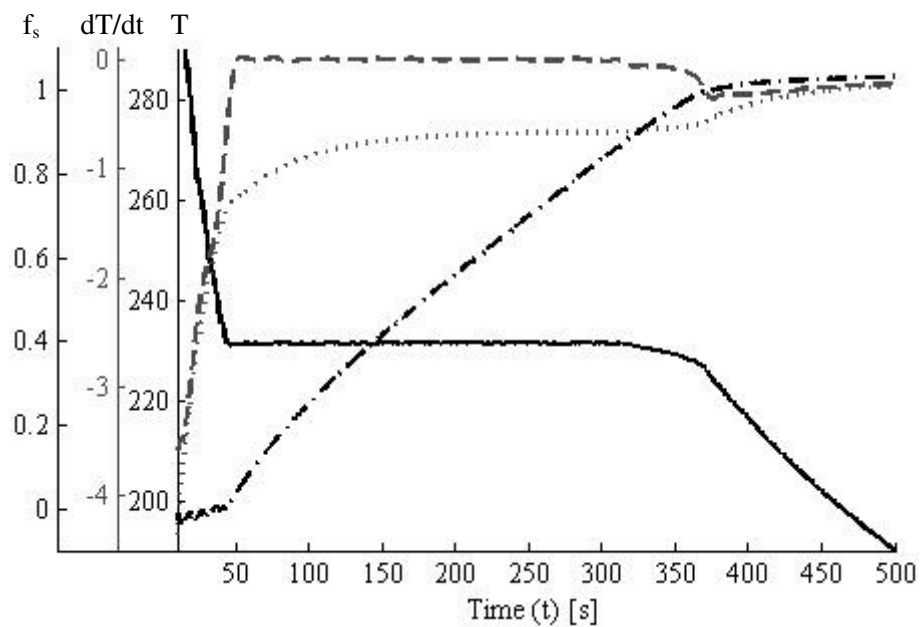
Figure 5.7: Graphs of Sn 1. ___ Temperature (T), [^{0}C], --- Cooling rate (dT/dt), [^{0}C/s], … baseline (dT/dt)$_{zc}$, [^{0}C/s], _._ solid fraction (f$_s$).
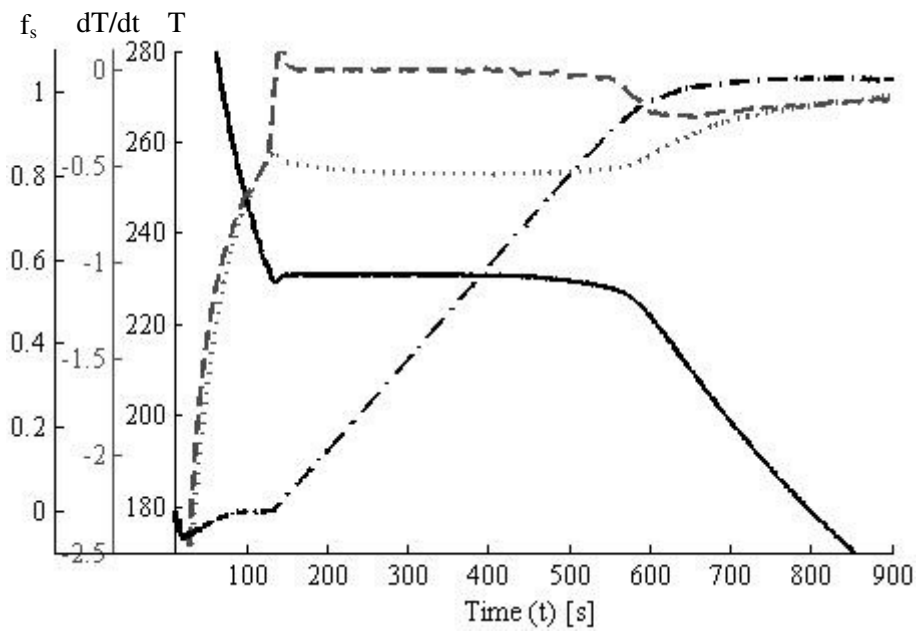
Figure 5.8: Graphs of Sn 2. ___ Temperature (T), [^{0}C], --- Cooling rate (dT/dt), [^{0}C/s], … baseline $(dT/dt)_{zc}$, [^{0}C/s], _._ solid fraction (f_s).
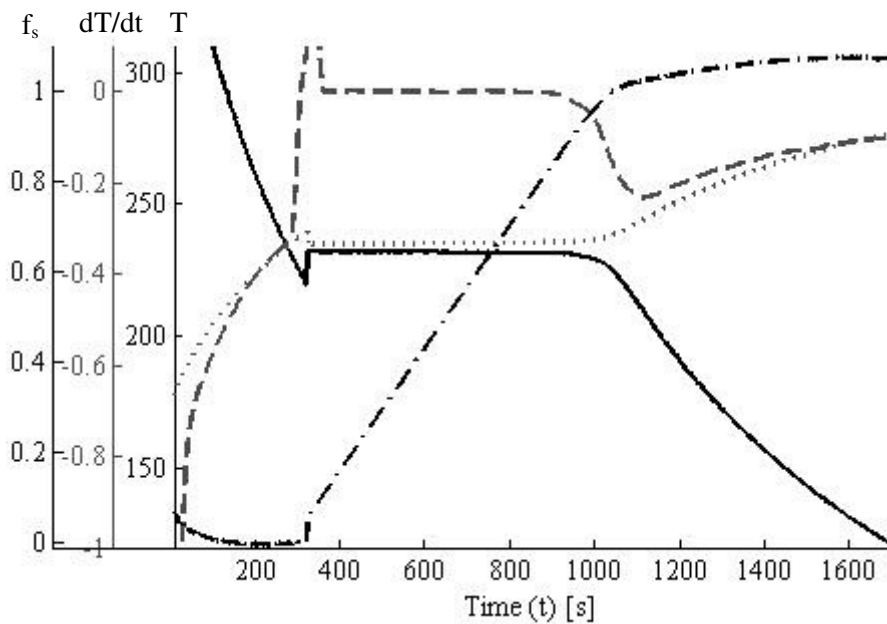
Figure 5.9: Graphs of Sn 3. ___ Temperature (T), [^{0}C], --- Cooling rate (dT/dt), [^{0}C/s], … baseline $(dT/dt)_{zc}$, [^{0}C/s], _._ solid fraction (f_s).
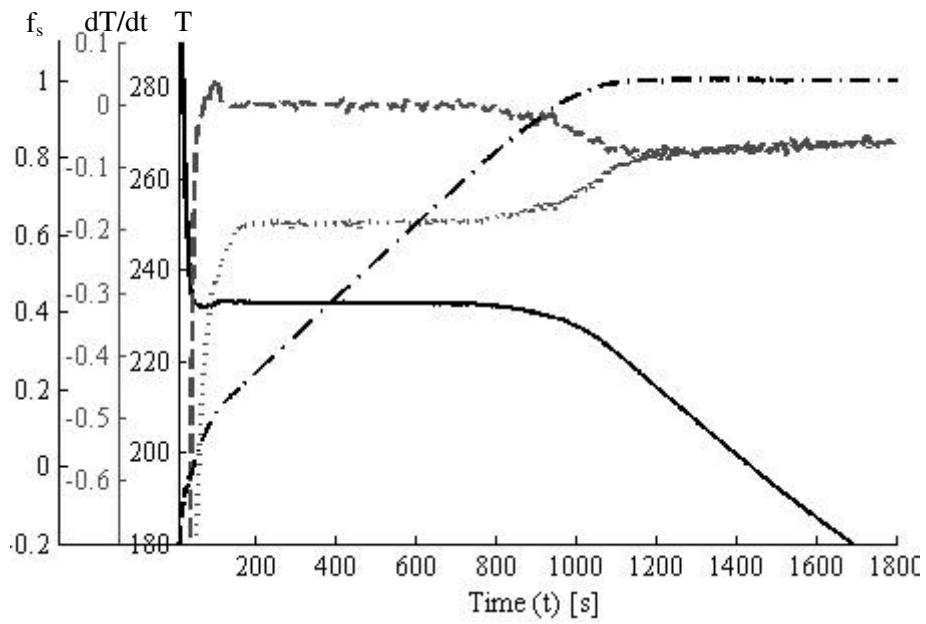
Figure 5.10: Graphs of Sn 4. ___ Temperature (T), [^{0}C], --- Cooling rate (dT/dt), [^{0}C/s], … baseline (dT/dt)$_{zc}$, [^{0}C/s], _._ solid fraction (f$_s$).
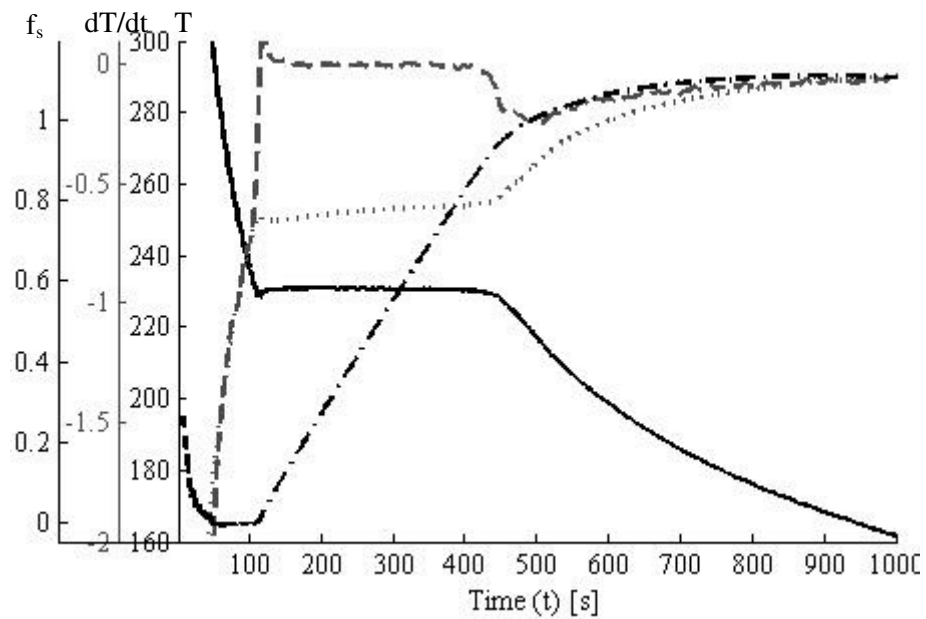
Figure 5.11: Graphs of Sn 5. ___ Temperature (T), [^{0}C], --- Cooling rate (dT/dt), [^{0}C/s], … baseline (dT/dt)$_{zc}$, [^{0}C/s], _._ solid fraction (f$_s$).
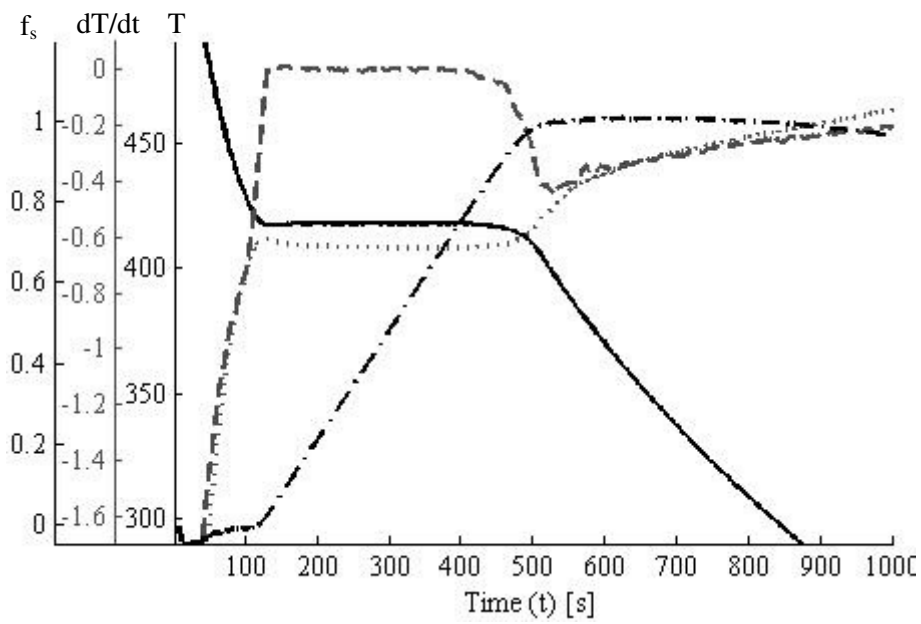
Figure 5.12: Graphs of Zn 1. ___ Temperature (T), [^{0}C], --- Cooling rate (dT/dt), [^{0}C/s], … baseline (dT/dt)$_{zc}$, [^{0}C/s], _._ solid fraction (f$_s$).
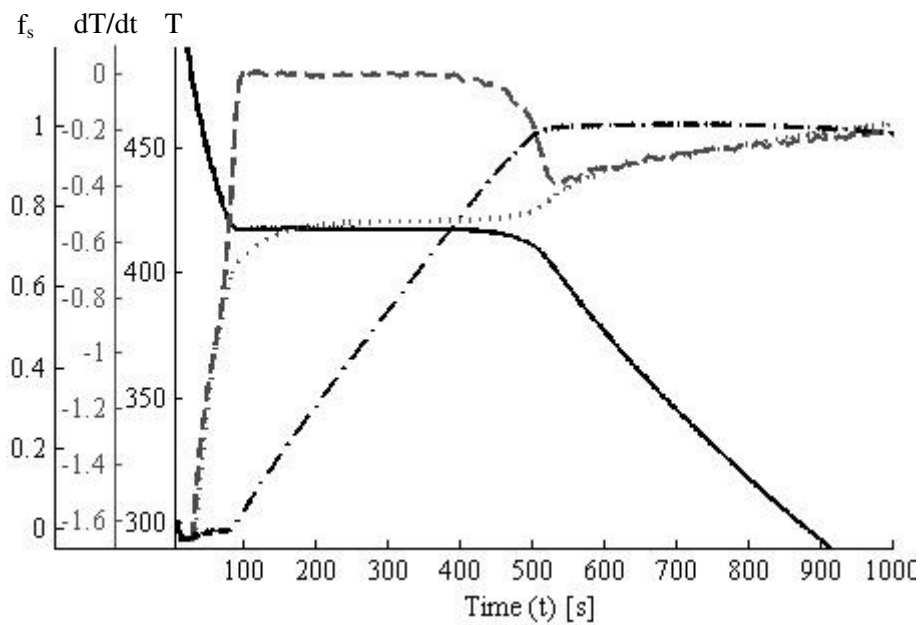
Figure 5.13: Graphs of Zn 2. ___ Temperature (T), [^{0}C], --- Cooling rate (dT/dt), [^{0}C/s], … baseline (dT/dt)$_{zc}$, [^{0}C/s], _._ solid fraction (f$_s$).
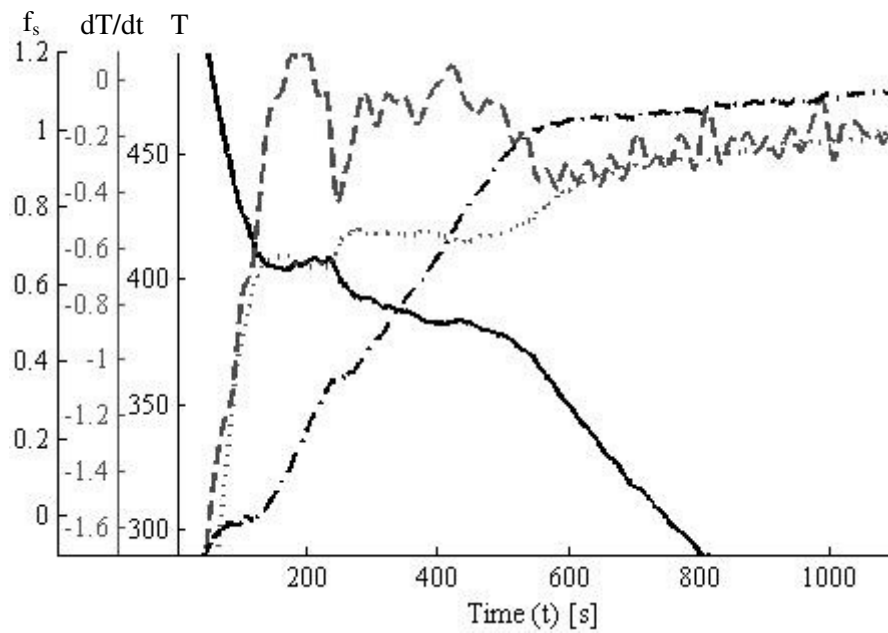
Figure 5.14: Graphs of Zn 3. ___ Temperature (T), [^{0}C], --- Cooling rate (dT/dt), [^{0}C/s], … baseline (dT/dt)$_{zc}$, [^{0}C/s], _._ solid fraction (f$_s$).

5.4 Discussion of the Results

In this study, a new model, named two-capacitive-system baseline (TCSBL) was proposed, and it was tested for the prediction of latent heat values. The percentage errors of each baseline with respect to the literal latent heats are seen in table 5.8. According to the table, TCSBL has the most significant errors in Sn4 and Sn5 experiments, which were made in outside-insulated molds. In addition, a clay bonded graphite crucible was used in Sn4 rather than sand molds. It may be said that TCSBL gives errors that are more significant in outside-insulated molds then the none insulated ones. It also gives high errors in a graphite crucible. The reason may be the cooling rate differences between solid and liquid phases. When a hot melt is poured into an outside-insulated mold, it cools very fast at the initial stage of cooling, but its cooling rate decreases after solidification. This effect makes the curve fit hard. Moreover, the determination of the end time of solidification (t$_e$) gets hard because of low temperature rate at the end stages of solidification.

Several correlation analyses were tried between errors and experimental conditions. These experimental conditions are: pouring temperature, solidification temperature interval, deviation from the melting point, curve fitting parameters etc. The only significant correlations in Sn experiments were found between the absolute values of percentage errors and absolute deviations of liquidus temperature from the literal melting point. R-square of the linear regression of the vectors in Table 5.9 is 0.81. This may be caused by impurities in the sample or measurement errors of thermocouples.

99

Table 5.9: Absolute values of percentage errors of the latent heat per specific heat (L/c) results by TCSBL method and deviations from the original melting temperature. Experiments with asterisk were insulated by the outer surface of the mold.

Exp	Measured melting temp. ($^{\circ}$C)	Deviation from Literal melting temp. ($^{\circ}$C)	L/c calculation Error (%)
Sn1	231.5	0.3	1.53
Sn2	231.0	0.8	3.50
Sn3	232.0	0.2	0.04
Sn4[*]	233.0	1.2	21.06
Sn5[*]	230.7	1.1	12.76

Table 5.10 shows the average errors of each baseline for each type of metal. Sn experiments are the most reliable for each baseline, maybe, because of low melting point. For each metal average, TCSBL is the most reliable baseline for every metal.

Table 5.10: Absolute values of the percentage errors of each metal in three baselines on the ten experiments. Outside insulated experiments (Sn4 and Sn5) are omitted.

	Al (%)	Pb (%)	Zn (%)	Sn (%)	Overall (%)
NBL	27.85	42.16	41.57	10.57	28.21
DBL	25.04	36.40	17.75	13.75	20.60
TCSBL	4.45	6.30	6.53	1.69	4.43

The standard deviations of the errors in three baselines on the ten experiments (except Sn4 and Sn5 at Table 5.8) are 35.4, 24.4, and 5.5 % for NBL, DBL, and TCSBL respectively. Standard deviations measures how much variation from the average emerges [57]. It means that the errors of TCSBL is closer than those of NBL and DBL. Therefore, it is the most precise model among the three baselines.

The most powerful advantages of TCSBL is its accurate and precise outputs. Moreover, it does not require deriving the data, and so, smoothing. Since smoothing deforms the original data in the laboratory, it is tricky for researchers. Although smoothing seems to be not ethical, there is no solution for NBL and DBL, which must use derivative in their calculations of baselines.

In view of disadvantages, TCSBL has the most complex analysis procedure of the data, especially for curve fitting. In a curve fit session of TCSBL, there are too many parameters to be computed; in addition, it contains Heaviside step function, which makes curve fitting more complicated. It is necessary to predict the range of the parameters in order to guide curve fitting. This prediction requires analysis on thermal resistances and dimensions of the metal-mold system.

CHAPTER 6

CONCLUSIONS AND FUTURE SUGGESTIONS

The main goal of this study was to produce alternative mathematical models for Newtonian thermal analysis by criticizing the widely used model: Newton's law of cooling. The findings of the simplified experiments have showed that thermal mass of the mold is one of the important determinants on the calculation of latent heat. Therefore, it is concluded that two capacitive thermal system should be modeled in order to overcome the failure of NTA. The conclusions of this study are summarized below.

1. 12 experiments made by 4 types of pure metals (aluminum, lead, tin and zinc) in several experimental conditions were applied to the thermal analysis methods in the literature. These methods are Newtonian baseline (NBL), dynamic baseline (DBL), and logarithmic relative temperature baseline (LRTBL). The latent heat calculations resulted in unsatisfactory outputs for all types of methods in general. The average percentage errors of these methods are 29%, %23 and %43 respectively. The distribution of errors through each experiment is so random that any correlation between the types of experiment and error could not be found.

2. Studies in the literature support the unreliability of the Newtonian baselines. The latent heat results are sensitively dependent to the analysis process such as curve fitting, data exclusion or smoothing. Assuming the same initial conditions for both phases is one of the possible defects of NTA. The different integration constants for liquid and solid phases should be taken into account when curve fitting is applied. Choice of the temperature interval is also important. 50 ^{0}C below or above the melting point may be preferred an ideal temperature range for thermal analysis. Not only the cooling rate function or differential equation itself, but also the cooling rate can be applied to curve fitting. However, it should be noticed that the ambient temperature should be free to be calculated by curve fitting. The real measured room temperature is a meaningless parameter because of the contributions coming from Taylor expansion.

3. Critics in the literature show that radiative contributions, thermal capacity of the mold, and temperature dependent thermal properties have significant effects on the cooling rate. Using nonlinear (quadratic or cubic) forms of Newtonian

equation for baseline is not necessary. Linear form in a narrow temperature interval is enough to produce similar results if the effect of mold's thermal capacity is blocked.

4. The effect of mold's thermal capacity may be the most significant restriction of Newtonian thermal analysis. In order to evaluate this effect, Two-capacitive system baseline (TCSBL) was proposed in this study. It is concluded that TCSBL is the most reliable baseline to calculate the latent heat among the several methods presented in the literature. Its averaged absolute error on the 12 experiments was calculated 6.53%, which is the best value among the other methods.

This study concerns with the latent heat and solid fraction computation of pure metals. However, it should be tested for different types of alloys in future researches. Moreover, the capacitive approach may be generalized to Fourier analysis, which assumes thermal gradient important. Therefore, solid fraction evolution in terms of spatial coordinates and time.

Another suggestion is about the basic assumption of TCSBL. The unique specific heat for both liquid and solid phases is assumed in this study. It may be developed for phase-dependent thermal properties in order to make detailed analysis.

REFERENCES

[1] F. P. Incropera. *Fundamentals of Heat and Mass Transfer*. 6th ed. John Wiley & Sons. pp. 260–261. (2007)

[2] D. Pitts. *Schaum's outline of heat transfer.* 2nd ed., McGraw Hill, New York, (1998).

[3] D.R Poirier and E.J. Poirier. *Heat Transfer Fundamentals for Metal Casting.* 2nd ed. with SI units, a publication of TMS, Warrendale (1994)

[4] D. Emadi, L. V. Whiting, S. Nafisi and R. Ghomashchi. *Applications of thermal analysis in quality control of solidification processes.* Journal of Thermal Analysis and Calorimetry, Vol. 81, pp. 235–242, (2005).

[5] P. Marchwica, J.H. Sokolowski and W.T. Kierkus. *Fraction solid evolution characteristics of AlSiCu alloys - dynamic baseline approach.* Journal of Achievements in Materials and Manufacturing Engineering. Vol. 47, (2011), p.116

[6] J.P. Holman. *Heat Transfer.* McGraw-Hill, New York (1992)

[7] U. Ekpoom and R. W. Heine. *Thermal analysis by differential heat analysis (DHA) of cast iron. AFS Trans.,* Vol. 85, (1981), pp. 27-38

[8] H. K. D. H. Bhadeshia. *Thermal Analysis Techniques.* www.msm.cam.ac.uk/phase-trans/2002/Thermal1.pdf. University of Cambridge, Materials Science & Metallurgy. (2002).

[9] E. Fras, W. Kapturkiewicz. *A new concept in thermal analysis of castings.* AFS Trans, 101 (1993), pp. 505–511.

[10] M. Venkataramana, V. Vasudeva Rao, R. Ramgopal Varma and S. Sunderrajan. *Instrumentation to measure heat transfer coefficient at the metal mold interface.* J. Instrum. Soc. India 37(3) pp. 157-163.

[11] L. S. Chao and W. C. Wu. Macro-micro modeling of solidification. Proc. Natl. Counc. ROC (A), Vol. 23, (1999), pp. 622-629

[12] I. Rafalski, A. Arabey, P. Lushchik and A. S. Chaus. *Computer modeling of cast alloys solidification by computer-aided cooling curve analysis (CA-CCA).* International Doctoral Seminar, Smolenice Castle, (2009).

[13] S.M. Liang, R.S. Chen, J.J. Blandin, M. Suery and E.H. Han. *Thermal analysis and solidification pathways of Mg–Al–Ca system alloys.* Materials Science and Engineering A, 480, pp. 365–372, (2008).

[14] D.H.Hou, S.M.Liang, R.S.Chen, E.H.Han and C.Dong. *Thermal analysis during solidification of Mg-4%.wtAl alloy during lost foam casting process.* Materials Science Forum Vol. 686, pp. 371-377, (2011).

[15] A. Çetin. Assessment and modelling of particle clustering in cast aluminum matrix composites. PhD Thesis, METU (2008), pp. 13-19

[16] R. H. Perry, and D. W. Green. *Perry's Chemical Engineers' Handbook. 7th ed.* McGraw-Hill, New York (1999), section 2.

[17] M. R. Chavez, A. Amaro, C. Flores, A. Juarez and C. González-Rivera. *Newton thermal analysis of gray and nodular eutectic cast iron.* Materials Science Forum, Vol. 509, pp. 153-158, (2006).

[18] W. E. Boyce and R.C. Diprima. *Elementary Differential Equations and Boundary Value Problems.* 7th ed., Wiley, New York, (2001)

[19] D. Emadi, V. Whiting, M. Djurdjevic, Witold T. Kierkus and J. Sokolowski. *Comparison of newtonian and fourier thermal analysis techniques for calculation of latent heat and solid fraction of aluminum alloys.* Association of metallurgical engineers serbia and montenegro scientific paper. (2004), pp. 91-106.

[20] A. Çetin and A. Kalkanlı. *Evaluation of latent heat of solidification of grey cast iron from cooling curves.* Canadian Metallurgical Quarterly. Vol 44, (2004), pp 01-06, 2005

[21] F. Lau, W.B. Lee, S.M. Xiong and B.C. Liu. *A study of the interfacial heat transfer between an iron casting and a metallic mould.* Journal of Materials Processing Technology 79, (1998), pp. 25–29.

[22] J. N. Silva, D. J. Moutinhoa, A. L. Moreirab, I.L. Ferreirac and O.L. Rochaa. *Determination of heat transfer coefficients at metal–mold interface during horizontal unsteady-state directional solidification of Sn–Pb alloys.* Materials Chemistry and Physics, 130, (2011), pp. 179– 185.

[23] C.A. Santos, J.M.V. Quaresma and A. Garcia. *Determination of transient interfacial heat transfer coefficients in chill mold castings.* Journal of Alloys and Compounds 319, (2001), pp. 174–186.

[24] L. A. Dombrovsky and T.N. Dinh. *The effect of thermal radiation on the solidification dynamics of metal oxide melt droplets.* Nuclear Engineering and Design 238, (2008), pp. 1421–1429.

[25] C. O'Sullivan. *A simple experiment to study cooling by convection and radiation.* Department of Physics, National University of Ireland Cork, (2006).

[26] M. Vollmer. *Newton's law of cooling revisited.* Eur. J. Phys. 30 , pp. 1063–1084, (2009).

[27] Q. Shan and E. F. Schubert. *Thermal model of packaged LEDs and RC circuit analogue.* http://www.ecse.rpi.edu/~schubert/Course-Teaching-modules/ , last visited on 17th of August 2013.

[28] S. H. Strogatz. *Nonlinear dynamics and chaos.* Perseus Books, New York, (1994).

[29] M. D. Weir, F. R. Giordano, J. R. Hass. *Thomas' Calculus with Second Order Differential Equations.* 11th ed., Pearson Addison Wesley, (2006)

[30] *General information about thermocouples (in Turkish).* www.elimko.com.tr, last visited on 14th of March 2013

[31] *Smoothing.* http://en.wikipedia.org/wiki/Smoothing , last visited on 11th of April 2013

[32] *Filtering and smoothing data.* www.mathworks.com/help/curvefit/smoothing-data.html, last visited on 11th of April 2013

[33] *Curve fitting.* http://en.wikipedia.org/wiki/Smoothing , last visited on 2nd of May 2013

[34] *Goodness of Fit.* http://en.wikipedia.org/wiki/Goodness_of_fit, last visited on 2nd of June 2013

[35] *Evaluating Goodness of Fit.* www.mathworks.com/help/curvefit/evaluating-goodness-of-fit.html, last visited on 2nd of May 2013

[36] D. Sparkman. *Thermal Analysis sampling cups.* MeltLab Systems – Using Thermal Analysis in the foundry. (2009).

[37] L.A. Dobrzański, M. Król, T. Tański and R. Maniara. *Effect of cooling rate on the solidification behaviour of MC MgAl6Zn1 alloy.* Journal of Achievements in Materials and Manufacturing Engineering, Vol. 37, (2009), p. 67

[38] F.J. Bradley, C. Jun and M.H. Zmerli. *Numerical Simulation of the Solidification of Eutectic Ductile Iron Casting Alloys.* Numerical Methods in Thermal Problems. Vol. 6, (1989), pp. 322-323.

[39] H. M. Şahin, K. Kocatepe, R. Kayıkcı and N. Akar. *Determination of unidirectional heat transfer coefficient during unsteady-state solidification at metal casting–chill interface.* Energy Conversion and Management 47, (2006), pp. 19–34.

[40] T. G. Kim and Z.H. Lee. *Time-varying heat transfer coefficients between tube-shaped casting and metal mold.* Int. J. Heat Mass Transfer. Vol. 40, No. 15, (1997), pp. 3513-3525.

[41] A. Dioszeg and I. L. Svensson. *On the problems of thermal analysis of solidification.* Materials Science and Engineering A 413–414, (2005), pp. 474–479.

[42] A. E. Çetin. *Matlab 7 for everyone (in Turkish).* 1st ed., Alfa, Ankara, (2006)

[43] *Fit curves and surfaces to data using regression, interpolation, and smoothing.* www.mathworks.com/help/curvefit/product-description.html, last visited on 2nd of May 2013

[44] D. Larouche, C. Laroche, M. Bauchard. *Analysis of differential scanning calorimetric measurements performed on a binary aluminum alloy.* Acta Materialia. Vol. 51, pp. 2161, (2003)

[45] L.A. Dobrzanski, R. Maniara, J. Sokołowsk, and W. Kasprzak. *Effect of cooling rate on the solidification behavior of AC AlSi7Cu2 alloy.* Journal of Materials Processing Technology 191, (2007), pp. 317–320.

[46] Y.C. Chiang, J.J. Chieh, H.C. Chen, and S.L. Chen. M*odified RC thermal circuit model applied to cold storage system with multi-loop heat pipes.* ASHRAE Transactions, Vol. 111, Issue 1, (2005), p387

[47] J. A. Hines. *Determination of Interfacial Heat-Transfer Boundary Conditions in an Aluminum Low-Pressure Permanent Mold Test Casting.* Metallurgical and Materials Transactions B, Vol. 35b, p. 299, (2004).

[48] L. Battezzati, M. Baricco, F. Marongiu, G. Serramoglia and D. Bergesio. *Melting and Solidification Studies by Advanced Thermal Analysis of Cast Iron.* Metallurgical Science and Technology, pp. 16-20, (2000).

[49] C. A. Santos, C. A. Siqueiraa, A. Garcia, J. M. V. Quaresma and J. A. Spim. *Metal–mold heat transfer Coefficients during horizontal and vertical unsteady-state solidification of al–cu and sn–pb alloys.* Inverse Problems in Science and Engineering, Vol. 12, No. 3, pp. 279–296, (2004).

[50] Y. Chen, L.S. Chao and L.S. Lin. *Prediction of thermal properties in a solidification process.* Materials Transactions, Vol. 48, No. 9, pp. 2304-2311, (2007).

[51] J. W. Gibbs and P. F. Mendez. *Solid fraction measurement using equation-based cooling curve analysis.* Scripta Materialia 58, pp. 699–702, (2008).

[52] A. Loizaga, A. Niklas, A. I. Fernandez-Calvo1 and J. Lacaze. *Thermal analysis applied to estimation of solidification kinetics of Al–Si aluminium alloys.* International Journal of Cast Metals Research, vol. 22, No 5, pp. 345-352, (2009).

[53] S. Farahany, A. Ourdjini, M. H. Idris and S. G. Shabestari. Computer-aided cooling curve thermal analysis of near eutectic Al–Si–Cu–Fe alloy. Journal of Thermal Analysis and Calorimetry, (2013).

[54] W. Kurtz, D.J. Fisher. *Fundemantals of solidification.* 1st ed., Trans Tech Publications, Switzerland, (1984).

[55] J. D. Meiss. *Differential dynamical systems.* SIAM, USA, (2007).

[56] J. O. Barlow, D.M. Stefanescu. *Computer-aided cooling curve analysis revisited.* Transactions of the American Foundrymen's Society, V 104, p 349-354, (1997).

[57] *Standard deviation.* www.en.wikipedia.org/wiki/Standard_deviation, last visited on 12nd of Dec 2013.

CURRICULUM VITAE

PERSONAL INFORMATION

Surname, Name: Erbaş, Kadir Can
Nationality: Turkish (TC)
Date and Place of Birth: 16/12/1977, Burdur
Marital Status: Single
Phone: 05333944877
Fax: -

EDUCATION

Degree	Institution	Year of Graduation
M.S.	METU, Physics Dept.	2008
B.S.	METU, Physics Education Dept.	2001
High School	Burdur Republic High School	1994

PROFESSIONAL EXPERIENCE

Year	Place	Enrollment
2011-present	METU, Physics Dept.	Research Assistant
2010-2011	TED, Ankara College	Physics Teacher
2003-2006	Yuce Science High School	Physics Teacher

PUBLICATIONS